

Review

Inferring earthquake physics and chemistry using an integrated field and laboratory approach

André Niemeijer^{a,b,*}, Giulio Di Toro^{b,c}, W. Ashley Griffith^d, Andrea Bistacchi^e, Steven A.F. Smith^b, Stefan Nielsen^b

^a Faculty of Geosciences, Utrecht University, Budapestlaan 4, 3584 CD Utrecht, The Netherlands

^b Istituto Nazionale di Geofisica e Vulcanologia, Via di Vigna Murata 605, 00143 Roma, Italy

^c Dipartimento di Geoscienze, Università degli Studi di Padova, Via Gradenigo 6, 35131 Padova, Italy

^d Department of Geology and Environmental Science, University of Akron, OH, USA

^e Dipartimento di Geologia, Università di Milano Bicocca, Piazza della Scienza 4, 20126 Milano, Italy

ARTICLE INFO

Article history:

Received 11 February 2011

Received in revised form

22 February 2012

Accepted 29 February 2012

Available online 9 March 2012

Keywords:

Earthquakes

Field

Laboratory

Fault geometry

Integrated study

ABSTRACT

Earthquakes are the result of a combination of (1) physico-chemical processes operating in fault zones, which allow ruptures to nucleate and rock friction to decrease with increasing slip or slip rate, and (2) of the geometrical complexity of fault zones. In this review paper, we summarize recent experimental findings from high velocity (conducted at about 1 m/s slip rate, or typical seismic slip rates) rock friction experiments with an emphasis on potential dynamic weakening mechanisms (melt lubrication, nano-powder lubrication, etc.) and how these mechanisms might be recognized by means of microstructural and mineralogical studies in exhumed fault zones. We discuss how earthquake source parameters (coseismic fault strength, weakening distances, energy budgets, etc.) might be derived from the field and laboratory experiments. Additionally, we discuss what needs to be considered in terms of fault zone geometry and morphology (focusing on fault surface roughness) in order to develop models of realistic fault surfaces and present theoretical considerations for microphysical modeling of laboratory data at seismic slip rates, with an emphasis on the case of melt lubrication. All experimental data and, in the case of melt lubrication, microphysical models indicate that faults must be very weak ($\mu < 0.1$) during coseismic slip. Moreover, experiments have shown that the slip weakening distance during coseismic slip is on the order of a few tens of centimeters at most under natural conditions, consistent with inferences from field observations. Finally, we discuss open questions, future challenges and opportunities in the field of earthquake mechanics.

© 2012 Elsevier Ltd. All rights reserved.

1. Introduction

Traditionally, earthquake mechanics have been investigated by the interpretation of seismic waves or by monitoring of active faults at the Earth's surface (e.g. Lee et al., 2002). However, these methods can only be used to infer relative stress changes during a seismic event and thus yield incomplete information about the earthquake source (e.g. the dynamic strength and energy budget remain poorly constrained, e.g. Kanamori and Brodsky, 2004). In addition, the physical and chemical processes that are active during the seismic cycle, which might explain why a certain mechanical evolution is observed, cannot be investigated with these methods.

In recent years, several drilling programs (e.g. the Nojima Fault in Japan, Boullier et al., 2001; the Chelungpu Fault in Taiwan, Ma et al., 2006; and the San Andreas Fault in the U.S.A., Ellsworth et al., 2000) have been undertaken to probe active faults. In addition to gaining direct information on fault composition and the possibility to extract samples for use in laboratory experiments, fault drilling allows for real-time monitoring of *in-situ* parameters such as strain rate and pore fluid pressure, and for sampling high-quality seismological data via downhole seismometers. However, the costs of fault drilling projects are typically high, the fault zone volume sampled is very small and the maximum depth that can currently be drilled is limited (3 km or so). Some similar data come from active faults found in deep mines (e.g. McGarr et al., 1975; Reches, 2006; Lucier et al., 2008; Heesakker et al., 2011a,b), but these datasets are even more scarce.

An alternative multi-disciplinary approach to understanding earthquake mechanics is to combine field geology, microstructural

* Corresponding author. Faculty of Geosciences, Utrecht University, Budapestlaan 4, 3584 CD Utrecht, The Netherlands.

E-mail addresses: a.r.niemeijer@uu.nl, niemeijer@geo.uu.nl (A. Niemeijer).

observations, laboratory experiments and numerical modeling (a possible work-flow is outlined in Fig. 1). Field studies on exhumed fault zones (block A in Fig. 1) can establish whether seismic slip has occurred, based on the presence of pseudotachylites for example (Sibson, 1975). Once this is established, the dominant deformation mechanisms within and surrounding the main slipping zones can be determined with the aid of careful microstructural and (micro) chemical analysis (block B in Fig. 1). Quantitative analysis of fault zone geometry, morphology and architecture using methods such as laser-scanning (Light Detection And Ranging; LIDAR), differential GPS and photogrammetry is necessary to provide input for large-scale numerical models (block D in Fig. 1). Experimental studies (block C in Fig. 1) that investigate the physical properties of the fault rocks, preferably under conditions that are close to those encountered in nature (i.e. σ_n up to ~ 200 MPa, slip velocities of 10^{-6} – 1 m/s, “ambient” temperatures up to 400 °C and the presence of (hydrothermal) fluids at elevated pressure), can be used to constrain or calibrate microphysical or empirical constitutive equations for use in large-scale numerical models (block D in Fig. 1). At the same time, experimental microstructures can be compared

to natural microstructures to verify that the active deformation mechanisms are similar. An ideal final step is to integrate data from experiments and natural exposures of faults to realize numerical models capable of generating artificial seismograms that can be directly compared to observations of actual earthquakes (block D in Fig. 1). We are still some way from realizing such a complex numerical model, but significant progress has been made in recent years (e.g. Dunham et al., 2011a,b). In the following sections, we summarize and discuss progress that has been made in each of the four panels depicted in Fig. 1, with an emphasis on the recognition of dynamic weakening mechanisms in the laboratory, potential seismic slip indicators in the field, and their use in inferring earthquake source parameters, and on the difficulties associated with extrapolation of laboratory data to natural conditions and upscaling to a realistic fault including geometrical complexity.

2. Dynamic weakening mechanisms in the laboratory

In the past two decades, the development of high velocity friction apparatuses has inspired a large number of experimental

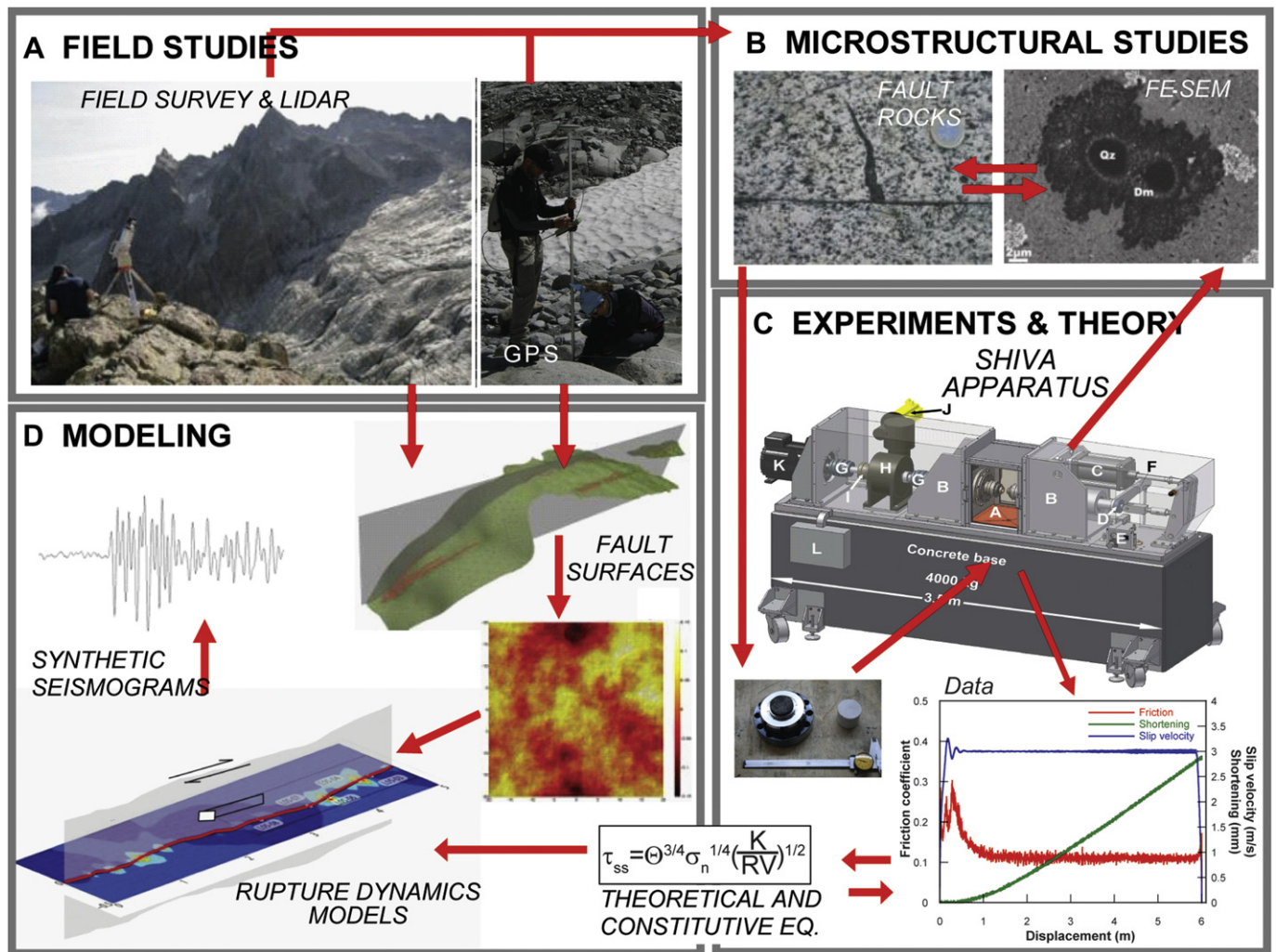


Fig. 1. Schematic diagram illustrating a multi-disciplinary integrated approach to understanding the earthquake machine: (a) Field studies of exhumed fault zones in order to verify and characterize the occurrence of ancient seismic slip and to determine the operating deforming mechanisms through (b) detailed microstructural and (micro)chemical analysis and to map the 3-dimensional geometry of the fault zone in detail and over a large range of scales to serve as input for (d) large-scale numerical models. (c) Systematic laboratory experiments to determine the microphysico-chemical processes that control the evolution of friction with slip combined with microstructural and (micro)chemical analyses of the experimental products to verify the operation of the same deformation mechanisms as in nature. Finally, the experimental results can be used to develop and test a microphysically based model which can then be used as input for (d) the large-scale numerical model, allowing dynamic simulations of the seismic cycle, producing as one of the output artificial ground motion records which can be compared with observations of real earthquakes.

studies on the frictional properties of cohesive rocks and gouges at seismic slip velocities (on average 1 m/s, Heaton, 1990). These studies have shown that, independent of rock type and presence or absence of fluids, the resistance against shear, expressed by the sliding coefficient of friction (=shear stress/effective normal stress), decreases dramatically above a certain threshold sliding velocity (see Fig. 2 and Di Toro et al., 2011). A dramatic drop in friction with increasing displacement is observed in a large majority of high velocity friction experiments, but the details of the evolution of friction and level of steady-state friction vary significantly with rock type and are probably dependent on the deformation mechanisms responsible for the observed weakening. Observations during and after the experiments in combination with theoretical considerations suggest that the following mechanisms might be responsible for the dramatic dynamic weakening: flash heating and weakening, melt lubrication, thermal decomposition, silica gel formation, thermal pressurization, fluidization, and (nano)powder lubrication (e.g. Rice, 1999; Tsutsumi and Shimamoto, 1997; Di Toro et al., 2004; Han et al., 2007a, 2010; Brantut et al., 2008; Goldsby and Tullis, 2011). Of these, melt lubrication has been unequivocally demonstrated in the laboratory, whereas the others have been inferred. Part of the reason for this is that different weakening mechanisms operate contemporaneously during high velocity sliding, depending on the thermal and microstructural evolution of the slipping zone (e.g. De Paola et al., 2011a; Niemeijer et al., 2011). The thermal evolution is controlled mainly by the applied normal stress, acceleration, slip rate and accumulated slip, whilst the microstructural evolution is controlled by wear rate, chemical reactions (triggered by the temperature rise in the slipping zone), and, in some cases, by preferential alignment of grains and shear localization. It follows that it is extremely difficult to truly isolate the different weakening mechanisms in a single experiment, especially during the initial stages of sliding (see Fig. 4 for the case of melt lubrication).

Furthermore, microstructural features and unstable phases that are produced during high speed sliding might be very short-lived, leaving little evidence in the microstructure after the experiment (e.g., Tisato et al., in press; Tullis and Goldsby, 2003).

2.1. Melt lubrication

The first experimental observations indicating melting of rock during fast slip include Friedman et al. (1974), Erisman et al. (1977) and Spray (1987, see also Fig. 3a and b). In the first two studies, melting was inferred from the presence of glass phases in deformed samples after the experiment. In contrast, Spray (1987) observed a “cherry red glowing interface” in an experiment on metadolerite using a friction welding apparatus at 5 MPa normal stress and 0.24 m/s mean slip velocity (experiments were done using a solid cylinder so that the slip velocity varied from 0 to ωr from the center to the periphery of the sample, with ω the angular velocity and r the radius). Since these first observations, several experimental studies have investigated the effects of melt production at high slip rates on the friction of mostly igneous rocks with low quartz content (Tsutsumi and Shimamoto, 1997; Lin and Shimamoto, 1998; Hirose and Shimamoto, 2005a,b; Di Toro et al., 2006a,b; Del Gaudio et al., 2009). In these experiments, melt is produced during rapid slip and friction evolves from an initial peak (point a in Fig. 4) followed by a drop to a minimum (point b in Fig. 4) and a steady rise to a second peak (point c in Fig. 4, see also Tsutsumi and Shimamoto, 1997; Hirose and Shimamoto, 2005a; Del Gaudio et al., 2009; Niemeijer et al., 2011). When enough melt has accumulated to form a through-going continuous layer (see movies in the auxiliary material and Fig. 5) friction drops dramatically, following a decay that can typically be fit satisfactorily with an exponential equation of the form (e.g. Hirose and Shimamoto, 2005b):

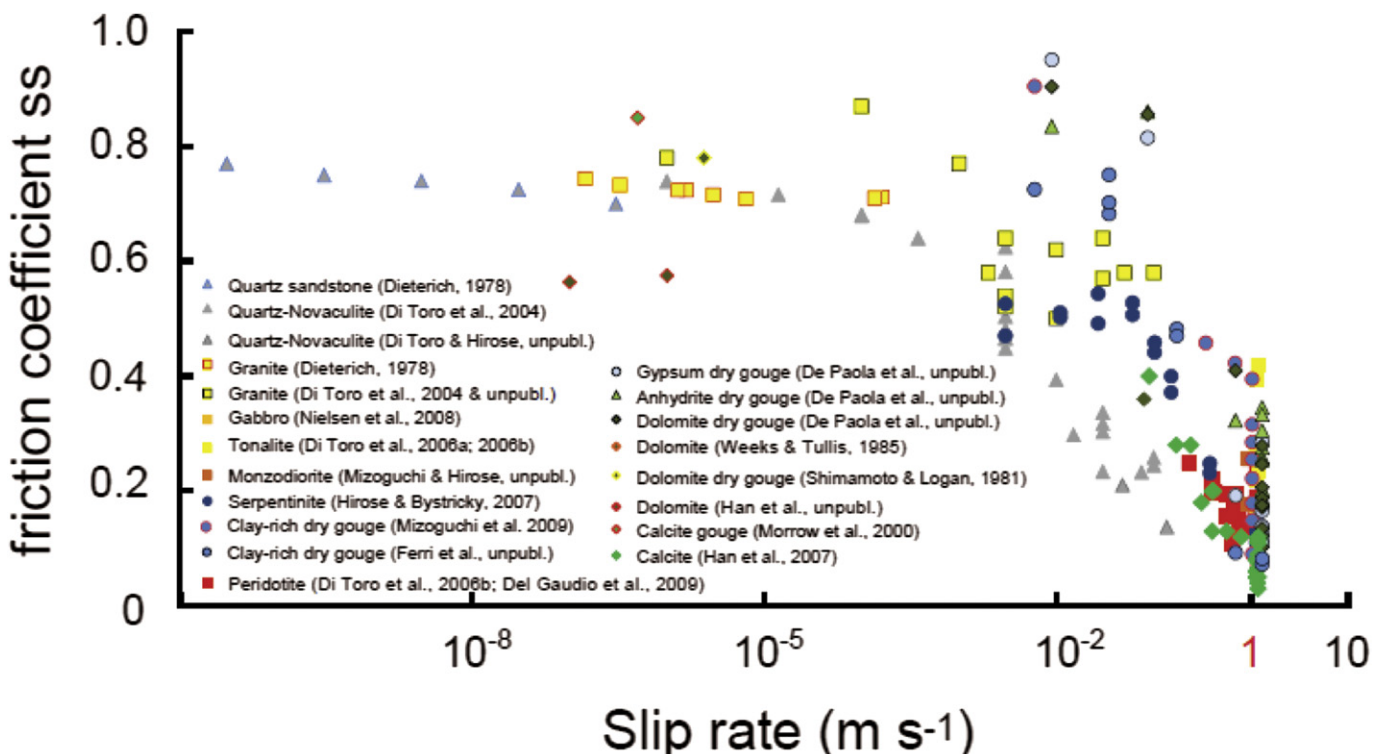
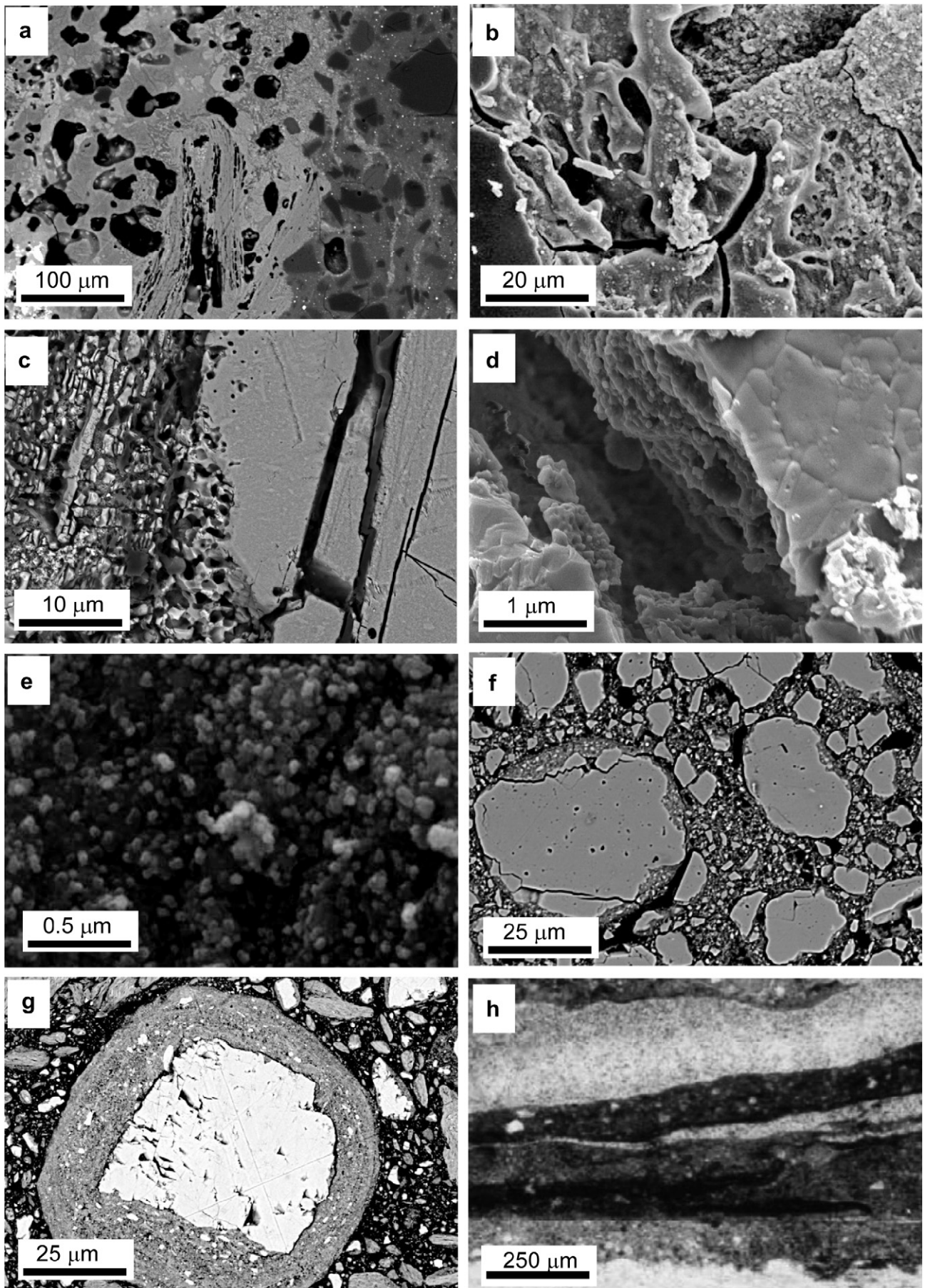


Fig. 2. Plot of steady-state friction coefficient as a function of slip velocity for a large variety of rock types, experimental conditions and apparatuses, showing that all rock types are extremely weak at high (seismic) slip velocities (1 m/s). Figure from Di Toro et al. (2011).



$$\mu = \mu_{ss} + (\mu_p - \mu_{ss}) \exp \left\{ \ln(0.05) \cdot \left[\frac{d - d_p}{d_w} \right] \right\} \quad (1)$$

where μ_{ss} is the steady-state friction coefficient (=shear stress over effective normal stress, ignoring cohesion), μ_p is the friction coefficient at the onset of exponential weakening (which is not necessarily the peak friction), d is the displacement, d_p is the displacement at the onset of weakening (displacement at point c in Fig. 4) and d_w is an exponential slip weakening distance over which friction decays to 95% of the difference between the peak and steady-state friction (hence $\ln(0.05)$). Eq. (1) can only be used to fit the exponential decay of friction but not to fit the restrengthening that occurs during the final stage of deceleration of the experiments. Two examples of the evolution of friction with displacement from experiments on identical gabbroic rocks and their corresponding slip weakening distances are shown in Fig. 6. Note that Eq. (1) can be used to empirically fit the data with all parameters free, or by imposing values of μ_p , μ_{ss} and d_p , which may yield slightly different results for the slip weakening distance. The initial evolution of friction is remarkably similar in both cases, after which the results start to diverge considerably. The difference in both the slip weakening distance and the level of steady-state friction can be explained by the difference in sample size. It has been established that steady-state melt lubrication in the laboratory involves a balance between the melt production rate (determined by the heat production) and the rate at which melt can escape the slipping zone by squeezing out of the unconfined cylinders (e.g. Nielsen et al., 2008). For a smaller sample, the distance that the melt needs to travel before being squeezed out is shorter, and this results in a less efficient lubricating effect of the melt. In addition, the slip weakening distance will be shorter in the case of the small sample. Because the slip rate of the center of the sample is zero, the heat production rate due to sliding (and thus temperature rise) is negligible and temperature only increases due to heat diffusion from the periphery towards the center of the sample. Therefore, in the case of a smaller sample, the central part will be heated faster and a balance between melt production and squeezing will be established earlier than for larger samples. Obviously, this sample size effect poses a serious problem if we want to extrapolate experimental results to natural conditions, and a microphysical model such as that of Nielsen et al. (2008, 2010a,b) is necessary to achieve this.

Supplementary video related to this article can be found at doi: 10.1016/j.jsg.2012.02.018.

2.2. Flash heating and weakening

Flash heating is suggested to be a general weakening mechanism for most rocks at the early stages of slip, once a critical slip rate (usually in the range of 0.01–0.1 m/s) is overcome (e.g. Kohli et al., 2011; Goldsby and Tullis, 2011; Tisato et al., in press). Hirose and Bystricky (2007) reported dynamic weakening in experiments using solid cylinders of serpentinite at a slip velocity of 1.1 m/s and normal stresses up to 24.5 MPa. They measured an

increase in humidity during slip and suggested this may reflect dehydration of serpentine. The bulk temperature along the sliding surface calculated for their experimental conditions was only 200 °C, well below the dehydration temperature of serpentine (~500 °C). However, the flash temperature calculated for the surface asperities was as high as 1200 °C, so Hirose and Bystricky (2007) explain the observed dynamic weakening by flash weakening occurring at asperities (i.e. thermal softening, see also, Rice, 1999, 2006; Rempel and Rice, 2006; Rempel, 2006; Rempel and Weaver, 2008; Beeler et al., 2008). It must be noted that the slip weakening distances observed in the experiments of Hirose and Bystricky (2007) are several orders of magnitude larger than that inferred from models (0.1–1 m vs. 4–40 μm, see Beeler et al., 2008), but this might be partly explained by the fact that the models assume a fully localized fault, whereas a considerable gouge layer (~100 μm thick) was observed after the experiments. A similar dynamic weakening in serpentinite at slip velocities of 0.1–0.4 m/s and 5 MPa normal stress was observed recently by Kohli et al. (2011). Furthermore, they observed the presence of talc at raised sites (i.e. asperities) along the sliding surface, indicating that temperatures at those sites reached at least 500–700 °C. In contrast to the results of Hirose and Bystricky, these authors report a slip weakening distance of 1–2 mm which is still much larger than that inferred from models (Rice, 2006; Beeler et al., 2008). In another recent study, Goldsby and Tullis (2011) report results of high velocity friction experiments on several rocks (quartzite, novaculite, albite rock, granite and gabbro) at 5 MPa normal stress (except for novaculite where normal stress was 70 MPa) and observed strong weakening in all materials tested. The obtained mechanical data fit remarkably well with the model expectations (e.g. Rice, 2006; Beeler et al., 2008 and others) and previous plate-impact experiments on novaculite (Yuan and Prakash, 2008). Again, the observed slip weakening distance was on the order of 3 mm. However, in their experiments, Goldsby and Tullis (2011) observed a marked hysteresis in friction, i.e. friction during the initial acceleration from slow slip rates to the peak value is higher than that obtained during deceleration from the peak velocity, similar to the hysteresis observed by Kohli et al. (2011). Both explain this hysteresis by the mode of deformation: at the initial slow sliding deformation is distributed but localizes when velocity is increased to a value above the weakening velocity. This localization of slip takes up to ~3 mm to accomplish, explaining the observed long slip weakening distance. In contrast, when velocity is stepped down, the increase in friction occurs over a distance of only 3–4 μm, consistent with model expectations.

Results from recent experiments using SHIVA in combination with a high speed camera (Niemeijer et al., 2011) confirm that flash heating and subsequent weakening probably occurs during initial slip, at least in gabbroic samples (see Fig. 5 and high speed movies in auxiliary material). It must be noted that in these experiments, the initial flash weakening occurs over a very short time-interval (<20 ms) and what can be observed on the outside of the sample is probably related to the subsequent strengthening by the

Fig. 3. Microstructures of experimental slipping zones. (a) Experimental pseudotachylite produced by frictional melting of tonalite. A large biotite grain (pale gray in colour) in the wall rock to the left undergoes to selective melting resulting in lattice breakdown, biotite dehydration and formation of vesicles (black in color). The Fe-rich melt from the biotite is mingled in the friction melt (20 MPa normal stress, 1.3 m/s slip rate and 3 m of slip, BSE-SEM image, Di Toro et al., 2006a,b). (b) Silica–gels decorating the sliding surface of deformed novaculite (112 MPa normal stress, 3.2 mm/s slip rate, 1.7 m of slip SEM image, Goldsby and Tullis, 2002: photo courtesy of David Goldsby). (c) Decarbonation products and porous microstructure in deformed Carrara marble (100% calcite). The slip surface is located 50 μm to the left (10 MPa normal stress, 6.5 m/s slip rate, slip 13.45 m, BSE-SEM image). (d) Sliding surface of dolomitic marble. The sliding surface has a pavement of euhedral grains about 100 nm thick of Mg-rich calcite. The pavement covers a 25–40 μm thick layer made of nanoparticles of periclase and lime (10 MPa normal stress, 6.5 m/s slip rate, slip 19.5 m, BSE-SEM image). (e) Sliding surface on limestone made of nanoparticles of probable calcite. Experimental conditions aimed at investigate flash heating and weakening (3 and 5 MPa normal stress, 0.3 m/s slip rate, slip 4 cm, SE-SEM image, Tisato et al., in press). (f) Cortex aggregates in wet dolomitic gouges (1.6 MPa normal stress, 1.3 m/s slip rate, slip 42.11 m, BSE-SEM image, De Paola et al., 2011a). (g) Clay clast aggregate (CCA) produced by shearing a clay-bearing fault gouge from the Vajont landslide under room humidity conditions (1.1 MPa normal stress, 1.31 m/s slip rate, slip ~30 m SEM-BSE image, Ferri et al., 2010). (h) Slipping zone produced by shearing gouges from the Nojima Fault Zone (0.62 MPa normal stress, 1.03 m/s slip rate, slip 27 m). Optical microscope image, parallel Nicols, Mizoguchi et al., 2009a,b).

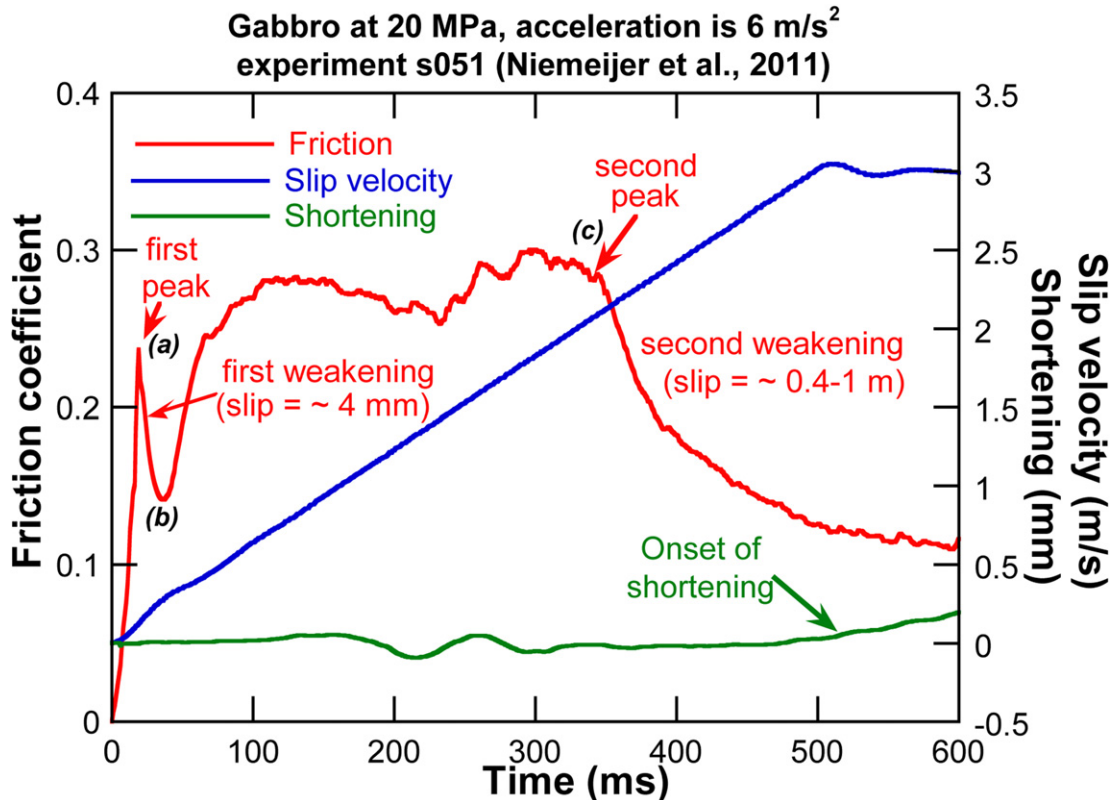


Fig. 4. Plot of the evolution of friction (=shear stress/effective normal stress) with displacement during the initial acceleration of a high velocity experiment on gabbroic rock samples (Niemeijer et al., 2011). Note the sharp weakening after ~ 35 ms (≈ 4 mm slip) and subsequent strengthening affected by vibrations of the machine (better visible in shortening). Also note that these data were acquired at 25 kHz and subsequently averaged with a 500 record interval (20 ms, see also Niemeijer et al., 2011).

migration of melt patches than to flash heating and weakening. In the models of Beeler et al. (2008), Rice (2006) and others, weakening occurs by thermal softening of contacting asperities. The velocity at which this weakening occurs then depends on the type of mineral(s) involved, on the temperature of mineral breakdown (dehydration, decarbonation, melting, etc.) and on the initial asperity size distribution. Typically, a single value for the asperity size is used in the models for flash weakening, although it is well known that asperity sizes varies across the sliding surface and evolve with sliding distance. In addition, a gouge layer is typically formed after only a small amount (few hundreds of micrometers) of displacement and it is unknown how this affects flash weakening (Tisato et al., in press, Fig. 3b). The details of the process remain thus rather enigmatic, partly also because of the difficulties in investigating flash weakening in high velocity rotary shear experiments due to relatively low data acquisition rates (this was just recently addressed by Goldsby and Tullis, 2011 or Niemeijer et al., 2011, see also Fig. 4), the small amount of reaction products produced (which are difficult to detect with standard analytical techniques and often unstable, Tisato et al., in press) and apparatus vibrations during initial sliding. To obtain small displacements of few centimeters at most at (sub-)seismic velocities (0.01–0.3 m/s), the samples have to be abruptly accelerated and decelerated. This typically results in vibrations of the apparatus that significantly affect the mechanical data. At the same time, the small slip impedes the achievement of larger bulk temperatures in the slipping zone and the production of reaction products detectable with standard analytical techniques (Tisato et al., in press). If larger displacements are imposed, other weakening mechanism might operate (see Fig. 4). A systematic experimental study aimed at understanding the details of initial sliding by varying the normal stress, acceleration and peak slip

velocity, should significantly improve our understanding of the various input parameters for the models of flash weakening which will allow extrapolation to natural conditions.

2.3. Carbonate decomposition and nanopowder lubrication

Han et al. (2007a, 2010) showed that decarbonation of both calcite and dolomite marble occurred when samples were deformed at moderate normal stress (~ 10 MPa) and relatively high slip velocity (>0.1 m/s). In these experiments, the total slip was of the order of meters, so longer than those reported in Section 2.2. They measured an increase in CO₂ concentration that accompanied strong dynamic weakening and concluded that thermal decomposition of the carbonates occurred. Observations of the slip surfaces after the experiments demonstrated the presence of very fine-grained ($<1\ \mu\text{m}$) powders of lime (CaO) and portlandite (Ca(OH)₂) (Fig. 3c and d). Experiments run on pre-decarbonated samples also showed strong weakening, so it was concluded that the weakening was not caused by increased fluid pressure due to the release of CO₂ but rather by nanopowder lubrication, a well-known phenomenon in tribology (e.g. Heshmat, 1991, 1995; Wornyoh et al., 2007). Han et al. also performed a number of slide-hold-slide tests which demonstrated that the nanopowders coating the sliding surface rapidly restrengthen during short periods (as short as 4 s) of no sliding.

The microphysics of nanopowder lubrication is not completely clear, but it has been suggested that when the grain size is extremely small ($<1\ \mu\text{m}$), rolling of grains dominates over sliding between grains (Chang et al., 2006; Han et al., 2010; Rapoport et al., 2003). Recent high velocity rotary shear experiments demonstrated that dynamic wear of initially intact rock samples of Sierra White Granite produces a similar powder lubrication effect (Reches and Lockner,

a

Initial evolution of shear stress and mean gray value of a box profile (see b, c & d) over sliding surface in a high speed movie of experiment s050 (Niemeijer et al., 2011).

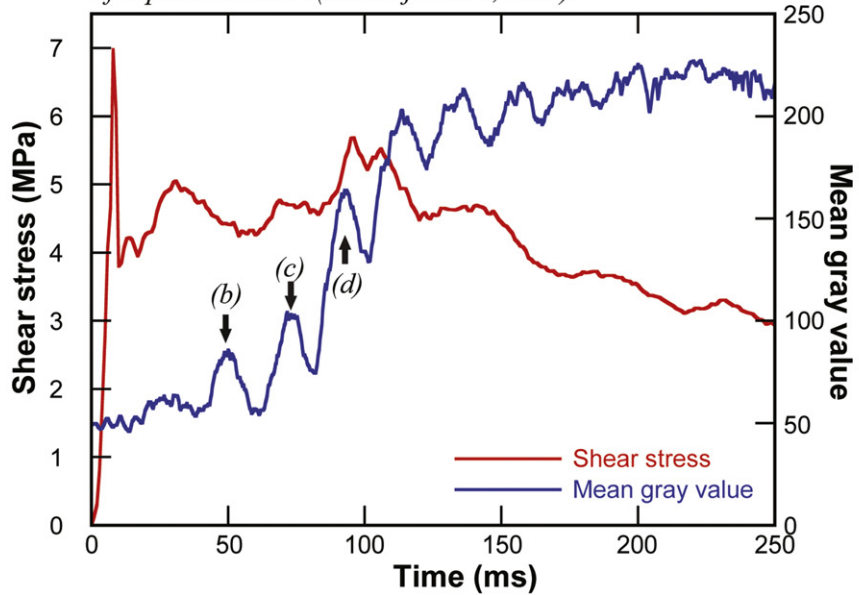
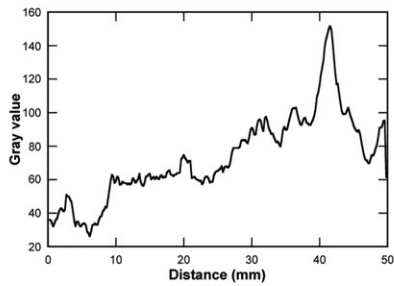
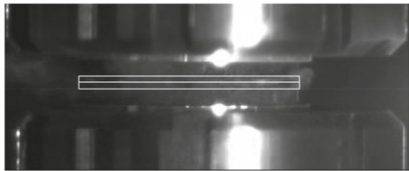
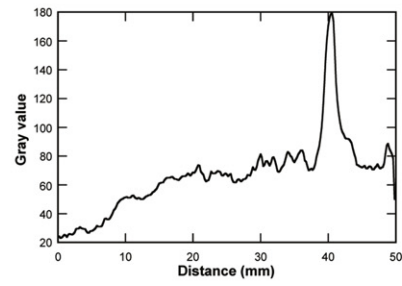
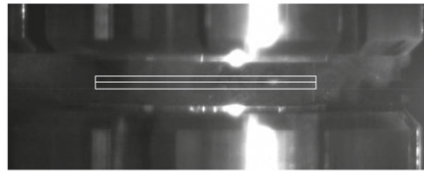
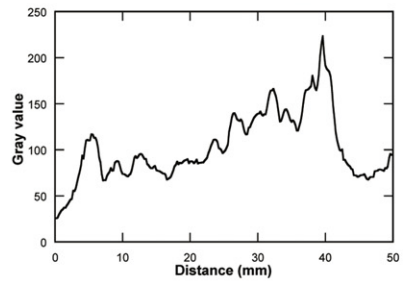
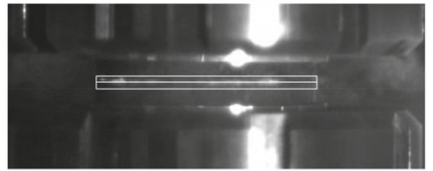
**b****51 ms****c****74 ms****d****93 ms**

Fig. 5. Image analysis of the evolution of the initial sliding surface observed during experiment s051 (Niemeijer et al., 2011) using a high speed movie (recorded at 10 kHz). (a) Plot of the evolution of shear stress during the initial stage of the experiment (acceleration to 3 m/s was completed after 100 ms) and the average gray level of a box profile covering the sliding interface (shown in the snapshots in b–d). Note the oscillations in gray level which are probably related to vibration of the machine and the saturation of the gray level values when shear stress drops exponentially. (b) Snapshot of a high speed video after 51 ms and corresponding gray level of a line profile over the sliding interface. Note the peak at ~ 40 mm distance. (c) Snapshot of a high speed video after 74 ms and corresponding gray level of a line profile over the sliding interface. Note the emergence of a second peak at ~ 5 mm distance. (d) Snapshot of a high speed video after 93 ms and corresponding gray level of a line profile over the sliding interface. Note the emergence of a second peak at ~ 5 mm distance.

2010). In this study, at relatively low normal stress (<10 MPa), a decrease in wear rate was observed that coincided with a decrease in friction (Reches and Lockner, 2010), which suggests that a critical gouge layer thickness had been reached so that the wear loss along the (open) sample boundaries was balanced by the wear rate. Clearly, more experimental work on the details of the (nano)powder lubrication effect is needed, for instance on the effects of sample roughness on the production of (nano)powders.

2.4. Silica–gel lubrication

Goldsby and Tullis (2002) and Di Toro et al. (2004) demonstrated dynamic weakening at relatively low slip rates (as low as 1 mm/s) in experiments using cylinders of Cheshire quartzite (>95 wt% quartz)

and Arkansas novaculite (>99 wt% quartz). The first study was done at normal stresses up to 100 MPa and a slip rate of 3.2 mm/s, while the second study investigated normal stresses up to 5 MPa and slip rates up to 150 mm/s. In contrast to most high velocity experiments, the observed velocity and slip dependence of friction could not be attributed to thermally-activated reaction and weakening mechanism, since the maximum temperatures measured (with thermocouples) and estimated (numerical modeling) were below 150 °C (Goldsby and Tullis, 2002; Di Toro et al., 2004). Instead, the dynamic drop in friction was attributed to amorphization of silica and gel formation via shearing and comminution in the presence of moisture (mechanically-induced reaction, for discussion about mechanically vs. thermally induced reactions, see Di Toro et al., 2011, Fox, 1975, Fisher, 1988). The gel layer behaves like

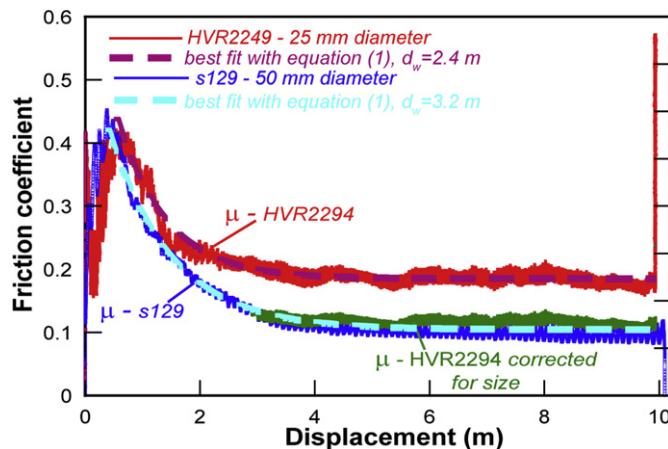


Fig. 6. Plots of the evolution of friction of two high velocity experiments, which were performed on solid cylindrical samples of gabbro of identical composition under identical experimental conditions of slip velocity, acceleration and normal stress (1.3 m/s, 3.25 m/s² and 10 MPa respectively), but using different sample sizes, 25 mm diameter cylinders for the experiment performed with the HV-1, now at Kochi, Japan (Shimamoto and Tsutsumi, 1994; Tsutsumi and Shimamoto, 1997) and 50 mm diameter for the experiments with the Slow to High Velocity Apparatus (SHIVA) in Rome, Italy (Di Toro et al., 2010; Niemeijer et al., 2011). Both the absolute value of friction and the displacement over which friction drops (the slip weakening distance) are different for the different sample sizes as a result of 1) a difference in the distance over which the melt has to travel before being squeezed out of the sample and 2) a larger variation in slip velocity across the slipping surface for solid cylindrical samples.

a thixotropic fluid, the time-dependent analogue to time-independent shear-thinning of a fluid (Goldsby and Tullis, 2002; Shaw, 1980). If a thixotropic fluid is sheared at a constant velocity, shear stress (viscosity) eventually reaches a constant value, which depends on the sliding velocity, as a result of a dynamic balance between the reformation and breakdown of the structural elements within the fluid. Similar mechanical results were reported by Hayashi and Tsutsumi (2010) in experiments using chert and quartz gouges. In this paper, the presence of hydrated amorphous silica, i.e. silica gels, was confirmed after the experiment using micro Fourier transform infrared spectroscopy. The authors noted that the formation of a hydrated amorphous silica layer involves the reaction of silicon oxide to hydrated silica which requires a large activation energy. The reaction is probably promoted even at relatively low sliding velocities by mechano-chemical effects, i.e. by high contact stresses at asperities or by comminution producing fine-grained particles (Fox, 1975; Fisher, 1988).

In addition to silica gel formation in highly siliceous rocks, Roig Silva et al. (2004) showed similar weakening in experiments on solid samples of Tanco albite rock (68.6 wt% SiO₂) and Westerly granite rock (69.2 wt% SiO₂) at a normal stress of 5 MPa. In addition, they found no weakening for a sample of gabbro rock (50 wt% SiO₂) and showed that steady-state friction at constant velocity and displacement decreases with increasing SiO₂-content. These observations suggest that weakening due to the formation of an amorphous silica gel formation might be quite common in silica-bearing rocks. However, experimental results on weakening by silica gel formation to date remain limited to either high normal stress and low slip rate (112 MPa and ≤ 3.2 mm/s, Goldsby and Tullis, 2002) or low normal stress and high slip rate (5 MPa and ≤ 150 mm/s, Di Toro et al., 2004). It has yet to be confirmed how important weakening via silica gel lubrication is at conditions of high slip rate and normal stress. In fact, experiments on Arkansas novaculite at 20 MPa and 1 m/s resulted in the production of frictional melting and melt lubrication (Di Toro et al., 2006b). However, these tests were done at room humidity conditions, whereas the presence of free water, as is the case in natural fault zones, might

buffer the increase in temperature, reducing the possibility of bulk melting and melt lubrication and possibly increasing the importance of silica gel lubrication. Further work is necessary to establish the possible activation of silica gel lubrication during earthquakes.

2.5. Moisture drainage

Experimental work by Mizoguchi et al. (2006, 2009a) using silica-poor rocks such as gabbros also showed significant dynamic weakening, although frictional heating was limited due to low normal stress and/or low slip velocity. In addition, strong fault strength recovery (healing) was reported from slide-hold-slide experiments. The observed healing was larger for experiments in which the normal stress was removed during the periods of no slip ("unconfined" test, see Mizoguchi et al., 2009a), and the healing rates were an order of magnitude larger than typical values for conventional low velocity experiments (e.g. Beeler et al., 1994; Karner et al., 1997; Karner and Marone, 2001; Tenthorey and Cox, 2006), and about twice as large as values obtained for experiments in which solution-transfer processes were active (Niemeijer and Spiers, 2006; Niemeijer et al., 2008). The observation of the large strength recovery and the absence of quartz suggest that a weakening mechanism other than silica gel formation was operating in these experiments. Mizoguchi et al. suggested that the observed weakening was the result of moisture drainage at the contact scale during frictional heating, followed by cooling and water absorption during hold periods resulting in strength recovery. It should be noted that an artificial gouge layer up to 50 µm thick was produced in all the experiments. It is unknown whether the moisture-related weakening/strengthening mechanism could operate under natural conditions where normal stresses and fluid-content are typically much higher.

2.6. Dynamic weakening in gouges

In addition to the experiments above, that used cylinders of rock on rock, many high velocity experiments have been performed at low normal stress (typically <2 –3 MPa) using artificial gouge layers sandwiched between two 'wall rocks' (Mizoguchi et al., 2009b; Boutareaud et al., 2008, 2010; Brantut et al., 2008, 2011; Ferri et al., 2010; Kitajima et al., 2010; Ujiie and Tsutsumi, 2010; De Paola et al., 2011a). Interpretation of these experiments is complicated by: 1) the varying contribution to friction of an outer confining sleeve (typically Teflon®); 2) the use of solid cylinders as wall rocks, resulting in variable slip velocity and frictional heating from the center to the edge of the sample, and; 3) decomposition of Teflon® (~ 260 °C) due to heating along the sample-teflon sleeve interface. This may release aggressive gases (mostly C₂F₄) into the gouge layer inhibiting or promoting chemical reactions and modifying the gouge microstructures.

2.6.1. Dynamic weakening in gouge: thermal pressurization and devolatilization

Many rock-forming minerals contain volatiles (H₂O, CO₂) that might be released by dehydration or decarbonation reactions at elevated temperature. As these volatiles are released, they might become trapped leading to an increase in pore fluid pressure, a decrease in effective normal stress and thus a decrease in shear strength. Similarly, when fluids are heated, they expand much more than rocks and thus the pore pressure increases. Experimentally, it is very difficult to measure in-situ pore fluid pressures in gouge samples, especially during high velocity experiments. However, numerous authors have reported evidence that the release of pore fluid, either by dehydration or by heating of the pore fluid, occurred during their experiments.

In a study on natural fault gouges obtained from outcrops of the Nohima Fault (SW Japan) that slipped during the 1995 Kobe earthquake, dramatic weakening was observed at a slip velocity of 1.03 m/s and 0.62 MPa normal stress, as well as for artificial quartz gouge sheared under the same conditions (Mizoguchi et al., 2009b). Although the authors did not reach conclusions about the active deformation mechanisms responsible for the weakening, they did conclude that the crucial factor was the heat production rate (the product of shear stress and slip velocity). Microstructural observations after the experiments demonstrated a localized zone of slip as thin as 30 μm along the wall rock–gouge interface, as well as flow structures similar to those observed in samples taken from the fault gouge that was interpreted to have slipped seismically during the Kobe earthquake.

De Paola et al. (2011a) observed two separate steady-state friction levels during experiments on dolomite and Ca-bearing dolomite gouges. The first and lowest steady-state friction level followed dynamic weakening and was interpreted to reflect a combination of flash weakening, thermal pressurization and, probably to a lesser extent, nanopowder lubrication (Fig. 3f). The second, slightly higher, steady-state friction level appeared after ca. 15–20 m of displacement and was accompanied by release of CO₂ from the gouge layer. The authors interpreted this small increase in friction as an indication that trapped CO₂ was lowering the frictional strength of the gouge during the first steady-state friction level (i.e. thermal pressurization). Similarly, pore fluid pressure increase as a result of dehydration of kaolinite was invoked as the dynamic weakening mechanism by Brantut et al. (2008) based on the observation of partial amorphization and dramatic grain size reduction of the kaolinite in a localized slipping zone (1–10 μm thickness). X-ray diffraction analysis indicated the presence of dehydrated kaolinite. In experiments on gypsum, pressurization due to dehydration of gypsum in addition to the water to vapor transition was demonstrated by Brantut et al. (2011). Microstructural and X-ray diffraction analysis showed a progressive increase in the thickness of a dehydrated layer containing bassanite (2CaSO₄·H₂O) and in the extreme case anhydrite (CaSO₄). Thermodynamic considerations suggest that endothermic dehydration reactions might buffer the temperature of fault zones during seismic slip (Brantut et al., 2011), thereby potentially inhibiting the activation of other weakening mechanisms such as melt lubrication.

2.6.2. Dynamic weakening in gouge: fluidization

Here, we consider fluidization to describe a transformation from a solid-like state to a fluid-like state and can be associated with either high particle velocity or high pore fluid pressure. As such, it is difficult to study in the laboratory, but some microstructural features such as flow structures might be used as indicators that gouge was fluidized (Fig. 3h from Mizoguchi et al., 2009b).

Boutareaud et al. (2008) showed that so-called clay clast aggregates (CCA's, central clasts surrounded by a variable-thickness outer cortex of fine-grained clays) were produced experimentally during fluidization of water-saturated clay-bearing fault gouges collected from the Usukidani Fault (SW Japan) at a normal stress of 0.6 MPa. In later studies, CCA's were reported from high velocity friction experiments on fault gouge from the Punchbowl Fault, CA, U.S.A. (Kitajima et al., 2010, σ_n of 0.2–1.3 MPa), on smectite-rich gouges from the slip zone of the 1963 Vajont landslide (Ferri et al., 2010, σ_n of 1.0 MPa), and from kaolin-bearing fault gouges from the Median Tectonic Line, Japan (Boutareaud et al., 2010, σ_n of 0.6–1.2 MPa). In all cases, dramatic dynamic weakening was accompanied by significant dilatancy (Ferri et al., 2010), suggesting that pressurization of the gouges by water released from the clays was occurring. CCA's were observed independent of the initial saturation conditions (i.e. room humidity or water saturated) in

most studies (Boutareaud et al., 2008, 2010; Kitajima et al., 2010), with the outer cortex typically having a thickness less than 15 μm. The clast mineralogy varied and mimicked the bulk mineralogy, i.e. clasts were quartz, feldspar, calcite or even aggregated (and foliated) clays. Boutareaud et al. (2010) demonstrated that a critical slip velocity may be required before abundant CCA's are formed in the gouge layer. They did, however, also report CCA's forming at slip velocities of only 0.09 m/s, raising some doubt as to whether they can be used as an unequivocal indicator of high slip speeds.

Interestingly, Ferri et al. (2010) did not find any CCA's in samples that were deformed in the presence of free fluid. However, it was inferred that in the water-saturated case, the free fluid formed a through-going continuous layer at one of the wall rock-gouge interfaces, effectively totally lubricating the sliding surface. Similarly, in the study of Boutareaud et al. (2010) CCA's were reported for velocities of 0.9 m/s and higher only under saturated conditions. In combination with their calculations of a lower temperature for saturated conditions than that for dry conditions for a given sliding velocity, this suggests that a critical temperature might be required to produce CCA's. The authors related the critical temperature required for the production of abundant CCA's to the water liquid–vapor transition. It was inferred that thermal pressurization occurred as a result of this transition. Sub-rounded clasts that survived the initial comminution process were capable of deforming by grain rolling as a result of the dilatancy and were then wrapped by nanometric particles present in the gouge matrix. Electrostatic forces and capillary forces were proposed to control the aggregation process, whereas short-range capillary forces kept the aggregated particles bounded to the central clast. In this view, clay particles are especially prone to being aggregated, owing to their surface charge.

It must be noted that all experiments to date that produced CCA's were conducted at low normal stress and on clay-rich fault gouges and it remains unclear whether CCA's can be produced at higher normal stresses and/or in fault gouges of different mineralogy.

3. Estimation of earthquake source parameters from laboratory experiments

Laboratory experiments that reproduce earthquake slip rates can be used to determine numerous earthquake source parameters comparable to those derived from seismological and field observations (see Section 5 and Beeler, 2006 for a review). However, there are several caveats that complicate a direct comparison with seismological-derived data. First of all, in seismology only relative shear stress (i.e. traction) levels can be determined and the effective normal stress on the fault is poorly known. Moreover, the stress values are averaged across the fault, although faults are highly inhomogeneous and both friction and stress will vary across the fracture surface. Also, the initial stress level in experiments is typically zero and any measured initial peak friction is essentially a failure stress where the sample starts to rotate, whereas the static initial stress level in nature will vary between zero and the yield stress of the fault (static friction). Finally, the samples used in the experiments consist of a single, flat and smooth sliding surface, without the complex roughness and geometry which characterize natural faults (see Section 6).

3.1. Rate-and-state friction (RSF) equations

A well-developed body of studies has been available which describes experimental results on rock friction at relatively low slip rates (e.g. Dieterich, 1978, 1979; Ruina, 1983; Mair and Marone, 1999; Marone, 1998; Marone and Kilgore, 1993). Their mathematical formalization, known as rate-and-state friction (RSF), occurs in terms of a set of differential equations governing one or more

hidden, empirical state variables. In a rock against rock contact interface, given the presence of natural roughness, it is speculated that friction evolution is controlled by the renewal of contact asperities. However, the classical RSF formulation can also simulate the behavior of more complex interfaces, where a powder layer separates the two blocks, following a proper rescaling of the governing parameters (e.g. Marone and Kilgore, 1993; Sammis and Steacy, 1994). In these cases, the interpretation of the friction evolution is more complicated. The RSF formalism remains an empirical representation of experimental results, which makes its extrapolation to conditions not covered by the experiments somewhat speculative. In particular, the operation of time-dependent and/or thermally-activated processes during deformation requires understanding of the underlying kinetics to reliably extrapolate experiments to natural conditions (e.g. Bos et al., 2000; Niemeijer and Spiers, 2006, 2007; Giger et al., 2008). Time-dependence of friction in the RSF formulation is modeled through the somewhat enigmatic state variable which has no physical basis. However, classical RSF equations have been widely used in models of fault slip nucleation and propagation both for quasi-static, slow slip (e.g. Kuroki et al., 2004; Yoshida and Kato, 2003; Liu and Rice, 2005; Rubin, 2008) and dynamic slip (e.g. Rice and Tse, 1986; Dieterich, 1992; Fukuyama and Madariaga, 1998; Bizzarri and Cocco, 2003) and the temporal distribution of aftershocks (e.g. Dieterich, 1994; Harris and Simpson, 1998; Ziv and Rubin, 2003).

While the validity of the classical RSF formulation has been clearly verified for relatively slow slip velocities in many experimental studies, it is unlikely to hold for more extreme conditions where both normal stress and slip velocity are relatively high, as expected during the dynamic phase of seismogenic slip on crustal faults. Indeed, while RSF allows for total reversibility of friction with velocity, this is obviously not the case if conditions of slip promote phase transitions due to the high release of mechanical work and heating. As a consequence, the effect of slip velocities in the seismic range (>1 m/s) has been thought for some time now to induce previously unknown and perhaps dramatic effects on the frictional evolution, although it was not easy to verify this experimentally before the development of high velocity rotary shear apparatuses. Prior to this, some speculative modifications or extensions of the classical RSF such as the effects of pore fluid pressure (e.g. Segall and Rice, 1995) were proposed and included in fault rupture modeling under dynamic conditions (Zheng and Rice, 1998; Nielsen and Carlson, 2000).

3.2. Modeling high velocity friction

As discussed in Section 2, most of the weakening reactions during high velocity experiments are thermally triggered during intense heating in the vicinity of the sliding interface. A comparison of experiments performed on novaculite (100% quartz) in different machines and varying conditions (silica–gel lubrication, Goldsby and Tullis, 2002; Di Toro et al., 2004; melt lubrication, Di Toro et al., 2006b), suggests that it is the combination of normal stress and slip rate (or work rate MW m^{-2}) rather than the combination of normal stress and slip (MJ m^{-2}) that controls the activation of different weakening mechanisms (Fig. 7). In the case of steady-state friction coefficient vs. work, melt lubrication and silica–gel lubrication data overlap (Fig. 7a) but when the same friction data are plotted vs. work rate, the different weakening mechanisms separate in two different regimes: silica–gel lubrication at low work rate and melt lubrication for large work rate (Fig. 7b). Work rate controls the heat flux (i.e. temperature increase) and wear rate (i.e. the amount of new surface produced which will be prone to chemical reactions): both temperature increase and the formation of new surface area control the kinetics of the reactions occurring in

the slipping zone and are thus possibly related to the weakening mechanism. As a first approximation, a model describing many frictional processes occurring under high slip velocity should include temperature as a key variable. In such a model, shear work provides a principal heat source, while heat diffusion and, in the advanced stages of the process, latent heat absorbed by phase transitions act as heat sinks or thermal buffers which limit the rise of temperature. These basic ideas were applied in order to describe the expected thermal evolution of a sliding interface in the presence of melt (Fialko and Khazan, 2005; Nielsen et al., 2008, 2010a,b), decarbonation (Sulem and Famin, 2009) and dehydration (Brantut et al., 2010).

In the case where the melting temperature is reached, the formation of a pervasive melt layer is observed in crystalline rocks both on some ancient fault outcrops (see Sections 4 and 5) and in laboratory experiments (see Section 2, Figs. 4 and 6). Melting temperatures are reached only at high slip rates because diffusion has no time to achieve a consistent heat loss. It was proposed that the advanced stages of frictional evolution (after the onset of pervasive melting across the sliding interface) are controlled by the shear resistance of a thin melt layer whose temperature, viscosity and thickness vary as slip evolves (Fialko and Khazan, 2005; Nielsen et al., 2008). The analysis of this case is quite complex, as it involves the solution of the Stefan problem of thermal diffusion in the presence of an advancing melt/solid interface, while accounting for shear heating and extrusion of a melt mass with variable viscosity and temperature. Using a series of assumptions, it is possible to build an analytical model and derive an expression for the steady-state friction (i.e. under a constant or slowly varying slip rate) as a function of velocity and normal stress (Nielsen et al., 2008; for an example of the predicted shear stress and shortening, see Fig. 8a). This model predicts that friction does not increase linearly with normal stress, but rather according to a power law where the exponent is smaller than 1 (theoretically predicted value is $\frac{1}{4}$). The model also predicts that friction decreases with increasing slip rate (i.e. rate-weakening behavior). Both predictions appear compatible with experimental observations, although the exponent for the normal stress dependence seems to underestimate the actual observations (for recent experiments under a wide range of normal stress the exponent appears closer to $\frac{1}{2}$ than $\frac{1}{4}$, see Fig. 8b and Niemeijer et al., 2011). For simplicity, the model assumes that the melt layer is sandwiched between two parallel planar faces, permitting the analysis of shear and extrusion mechanics in a closed mathematical form. In fact, the rock faces on either side of the melt are quite rough on the small scale (Hirose and Shimamoto, 2005a) and the typical asperity elevation is not small compared to the average melt thickness (an indicative value is about 100 μm , Nielsen et al., 2010a). It follows that the assumption of planarity is a rather rough simplification, a likely cause of the misfit observed for the exponent value.

In an attempt to include some effects of the small-scale interface roughness in the model, Nielsen et al. (2010a) describe the evolution of the phase boundary in a polymimetic rock undergoing fast melting. They show that the rugosity is determined by the melting rate, which is controlled by the heat production rate. A higher heat production rate induces faster melting, which results in a relatively smooth melt/solid interface. Since heat production rate is proportional to slip rate, this has an interesting consequence (though this aspect needs to be further explored both in the field and experimentally); it may be possible to estimate the average slip rate during an ancient earthquake from observations of microstructures and small-scale roughness in the corresponding fossil fault (see Section 5). In general, frictional melt fundamentally differs from classical RSF in its irreversible nature and in its strong non-linear dependence on the conditions of normal stress and sliding

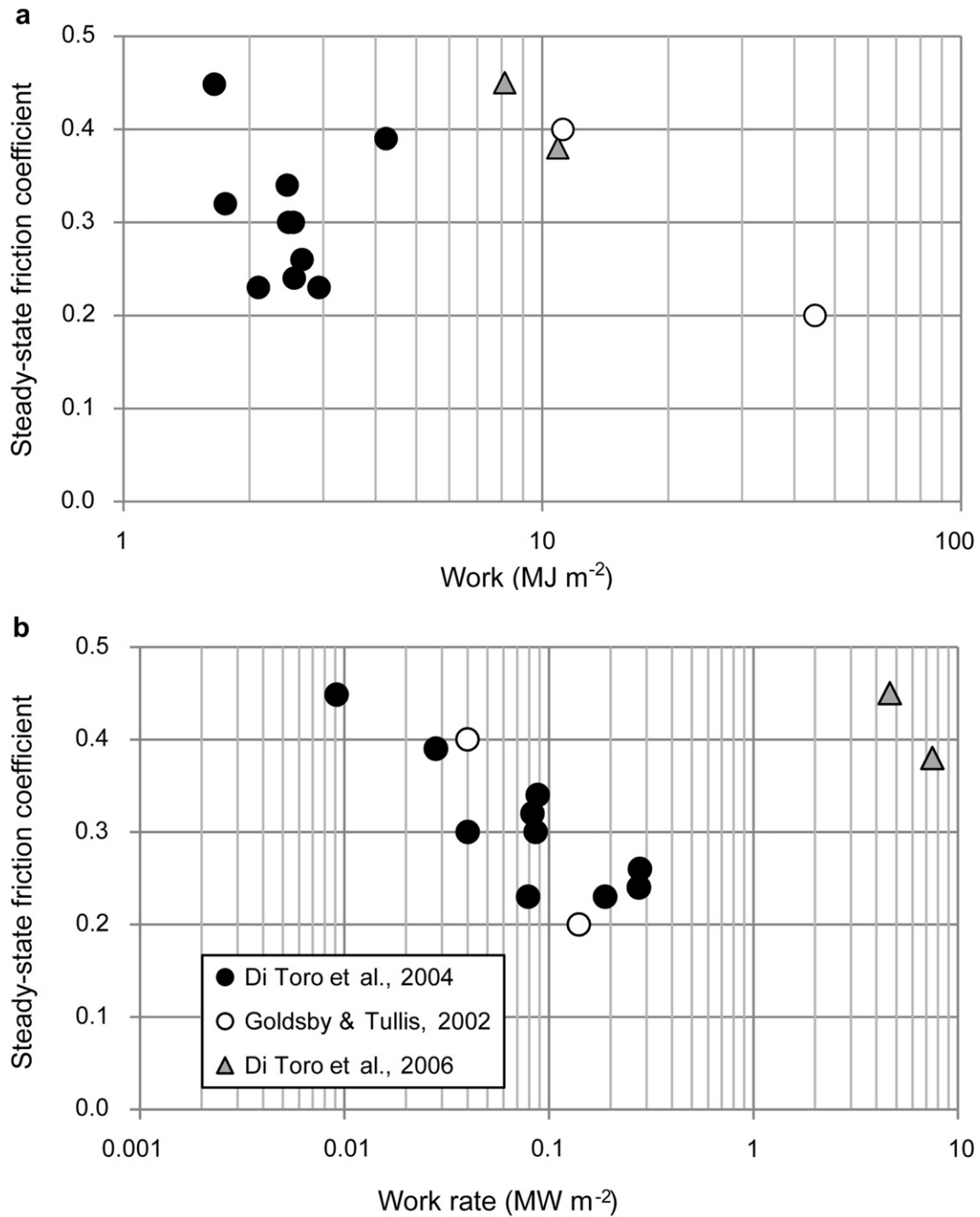


Fig. 7. Steady-state friction coefficient of novaculite vs. the work per unit fault surface (top) and vs. work rate per unit fault surface (bottom). (a) In the case of steady-state friction vs. work, gel lubrication occurs at higher work per unit fault surface in the experiments performed by Goldsby and Tullis (2002) than in the experiments performed by Di Toro et al. (2004). This is because of the higher applied normal stress (up to 112 MPa) imposed in the experiments performed by Goldsby and Tullis (2002) with respect to that (5 MPa) imposed by Di Toro et al. (2004); slip distance was almost the same (about 2 m). One data for gel lubrication overlaps with the work done to produce melt lubrication in novaculite. In the latter case, normal stress was 15 MPa and slip 3 m (Di Toro et al., 2006b). The work per unit fault surface does a poor job in discriminating the different weakening mechanisms. (b) In the case of steady-state friction coefficient vs. the work rate, the data from Goldsby and Tullis (2002) obtained at about 112 MPa and 3.2 mm/s overlap with those obtained at 5 MPa 0.1 m/s from Di Toro et al. (2004). In both cases silica gel lubrication is the weakening mechanism and the data for silica gel lubrication is distinct from the data where friction melting was observed. The latter was obtained at about 15 MPa normal stress and 1.3 m/s slip rate. A comparison between diagrams (a) and (b) suggests that is the work rate (or power density), rather than mechanical work, that allows to discriminate between the weakening mechanisms.

velocity, generally described in the form of power laws. Will it prove to be the case also for high velocity sliding friction in the absence of melt? The evolution of frictional melt is indirectly controlled by temperature, through a series of thermally-activated processes involving melt production and the growth and persistence of a sufficient melt layer to insure lubrication. Several other

processes involving phase transitions other than melting are observed to occur under seismic slip conditions and it is clear that they are also related to thermally-activated phase transitions (Brantut et al., 2008; Han et al., 2007a,b, 2010; Kitajima et al., 2010). Given the common importance of temperature evolution in these processes, we may speculate that the characterization of friction

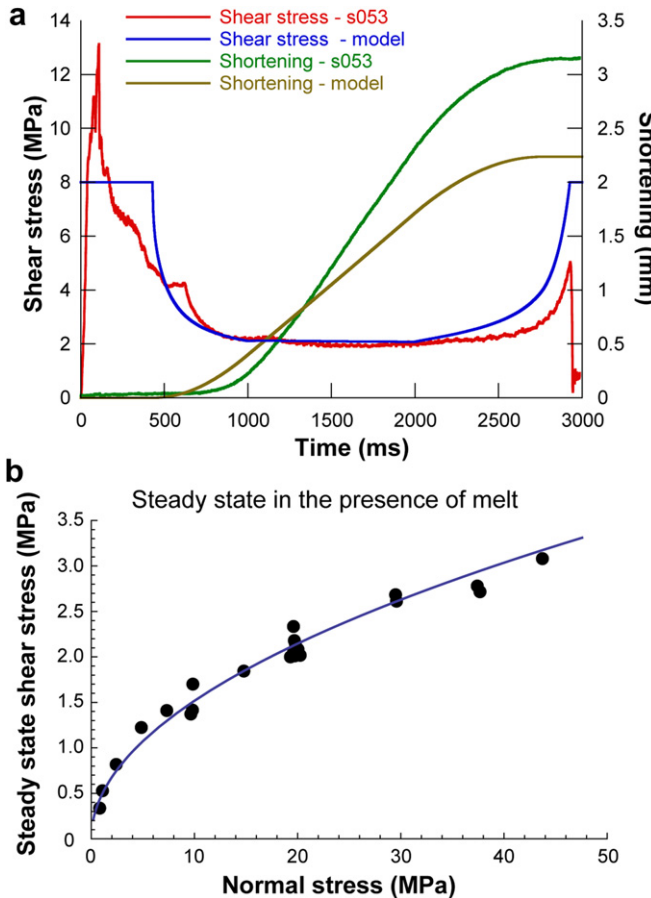


Fig. 8. (a) Plots of shear stress and shortening as measured in experiment s053 on a gabbroic sample at 20 MPa normal stress, a velocity of 3 m/s and an acceleration and deceleration of 3 m/s^2 (Niemeijer et al., 2011) and the results of the melt lubrication model of Nielsen et al. (2010b). (b) Plot of steady-state shear vs. normal stress for gabbro sliding at 3 m/s (Niemeijer et al., 2011) showing the non-linear dependence of shear stress on normal stress when melt lubricates the experimental fault. The data can be fit by a $\sigma_n^{0.5}$ dependence (blue line).

observed and modeled in the presence of melt (in terms of the non-linear, power law dependence of its parameters) will, to some extent, also apply to non-melting processes. The dependence of shear stress on normal stress is of particular importance, since this will determine the power and thus heat production during the seismic slip event. This assumption should be tested as more HVRF experiments are performed on non-crystalline rocks (e.g. carbonates) where melting is less likely to occur and is indeed only observed experimentally in extreme cases.

3.3. Determination of seismological parameters directly from laboratory results

Despite the difficulties in extrapolating experimental results to natural conditions mentioned above, it might be worth to determine parameters such as slip weakening distance, dynamic stress drop and breakdown work in the laboratory (see for an excellent review, Beeler, 2006), and to investigate their dependence on rock type, normal stress, slip velocity and acceleration/deceleration. Unfortunately, the slip weakening distance is the only parameter that has received considerable attention in previous experimental studies. Nonetheless, this parameter is poorly defined and different authors use different approaches to determine its value. In seismology, the slip weakening distance is defined as the distance over which traction reaches a minimum value (e.g. Beeler, 2006; Tinti

et al., 2009; Cocco et al., 2009). However, in experiments it is often not straightforward to obtain a slip weakening distance in a consistent, reproducible manner. For example, Di Toro et al. (2011) defined a thermal weakening distance as the distance over which friction falls $1/e$ (or 68% reduction of the stress drop from the peak to the steady-state), whereas Hirose and Shimamoto (2005b) and Mizoguchi et al. (2009a) define the slip weakening distance as the distance over which the reduction of the stress drop is 95%. Using $1/e$, which corresponds to a significant stress drop, slightly simplifies the mathematical expressions of the dynamic weakening (see Di Toro et al., 2011, suppl. information).

As an example for these kinds of problems, in Fig. 9 we show two friction evolution curves for two experiments using gabbro and marble. Here, the evolution of friction with displacement is fit well by Eq. (1) for the gabbro data, defining a slip weakening distance of 0.78 m, but the equation does not fit the marble data as well. In fact, it seems that there might be two different distances over which friction decreases in the case of marble. As a comparison, we inverted the marble data using rate-and-state friction (RSF) using Dieterich's slowness equation and two state variables (see e.g. Marone, 1998 and Niemeijer et al., 2010) and obtained a reasonable fit with two characteristic slip weakening distances of 0.13 and 1.767 m. The inversion was done by assuming an instantaneous velocity-step from the velocity at the peak friction (0.65 m/s in this case) to the steady-state velocity (6.5 m/s). Although it is interesting to see that it is possible to use RSF to fit the experimental data, the physical significance of two characteristic slip distances remains unclear and a detailed discussion is beyond the scope of the present contribution.

Tsutsumi and Shimamoto (1997) already recognized that the slip weakening distance from high velocity friction experiments, d_w , differs from the characteristic slip distance from slow slip rate experiments, d_c , determined by fitting data with the empirical rate-and-state friction equations (e.g. Dieterich, 1979; Ruina, 1983). Whereas the characteristic slip distance, d_c , is typically described as a material parameter, related to the asperity distribution of the sliding contacts, the slip weakening distance, d_w , can be directly associated with mechanical (such as powder lubrication) and

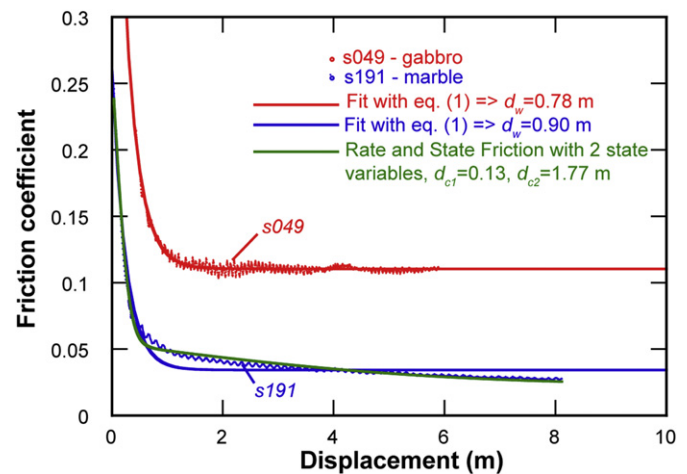


Fig. 9. Plot of the evolution of friction with displacement for two experiments exhibiting different dynamic weakening mechanisms: melt lubrication (gabbro, experiment s049) and nanopowder lubrication (Carrara marble, experiment s191). The exponential decay that is typically observed in high velocity experiments fits the gabbro data very well, but shows significant misfit with the marble. Instead, the data can be inverted for a two state variables rate-and-state friction equation (using Dietrich's slowness equation and assuming a velocity-step from the velocity at peak, 0.65 m/s to the velocity at steady-state, 6.5 m/s) with $a = 0.004486$, $b_1 = 0.075792$, $b_2 = 0.014029$, $d_{c1} = 0.107 \text{ m}$ and $d_{c2} = 2.02 \text{ m}$, indicating that perhaps two weakening mechanisms are operating on two different length scales.

thermal weakening (such as frictional melting) processes and hence with the heat budget of the fault (see e.g. Beeler, 2006). Since the power and the heat production rate per unit fault surface during seismic slip is proportional to the product of the shear stress and the slip velocity, and shear stress depends on normal stress (see also Section 6), d_w should vary with both and cannot be seen as a material property. Indeed, experimental studies have shown that the slip weakening distance is a strong function of normal stress and slip velocity, independent of the actual weakening mechanism that is operating (Hirose and Shimamoto, 2005b; Beeler, 2006; Mizoguchi et al., 2007; Han et al., 2010; Kitajima et al., 2010; Di Toro et al., 2011; Niemeijer et al., 2011). In Fig. 10, we show a plot of the slip weakening distance (in this case, the thermal weakening distance, defined as the distance over which friction falls to $1/e$ of its peak value, which translates to $1/3$ of d_w) from a suite of experimental studies covering various rock types as a function of the product of normal stress and the square root of slip velocity. It is striking to note that in the case of friction melting, the data (black dots in Fig. 10) can be fit by a log-linear relation. The dependence of d_w on $(\sigma_n \sqrt{v})^{-1}$ during the decay of shear stress from the peak value to steady-state can be explained as follows. In the case of melt lubrication, we may assume that dynamic weakening is achieved when a given temperature rise ΔT has occurred on the fault (for example, a temperature rise such that a pervasive melt layer is formed). The temperature rise is due to frictional work on the fault plane, which is produced at a rate τv . If we assume that during the initial slip transient the product of shear stress and slip rate τv can be equated to a constant value, then the temperature rise on the

fault can be equated (by solving the heat diffusion with constant heat inflow, Carslaw and Jaeger, 1959) to the square root of time t_{th} such that $\Delta T = \tau v(t_{th})^{0.5}/\rho c \sqrt{k\pi}$ where t_{th} is the time necessary to achieve weakening. Under the approximation that the velocity v is constant we may write the weakening distance as $d_w = v t_{th}$, which implies that

$$d_w \propto (\tau \sqrt{v})^{-2}. \quad (2)$$

For Mohr-Coulomb type friction ($\tau = \mu \sigma_n$), Eq. (2) would imply a weakening distance inverse to the square of the normal stress. However, in the case of melt-lubricated faults, the stress during the weakening phase is not constant and only the initial peak stress appears to follow Mohr-Coulomb friction. According to both experiments and theoretical models, once sliding has started the shear stress adopts a non-linear dependence on normal stress in the form of a power law during both transient and steady-state regimes. For example, the steady-state sliding stress for melt lubrication in gabbro experiments shows a power law with an exponent close to $a = 0.5$ (Niemeijer et al., 2011), while a value of $a = 0.25$ is predicted by theoretical models (Nielsen et al., 2008, 2010b). It follows that the inverse square dependence of d_w implied by a linear dependence on normal stress cannot apply to the case of frictional melt (Nielsen et al., 2010b; Niemeijer et al., 2011), where the normal stress dependence is quite complex. If we empirically fit the dependence of d_w on both normal stress and velocity for experiments performed under constant sliding velocity on gabbro samples (Nielsen et al., 2010b; Niemeijer et al., 2011) we find that

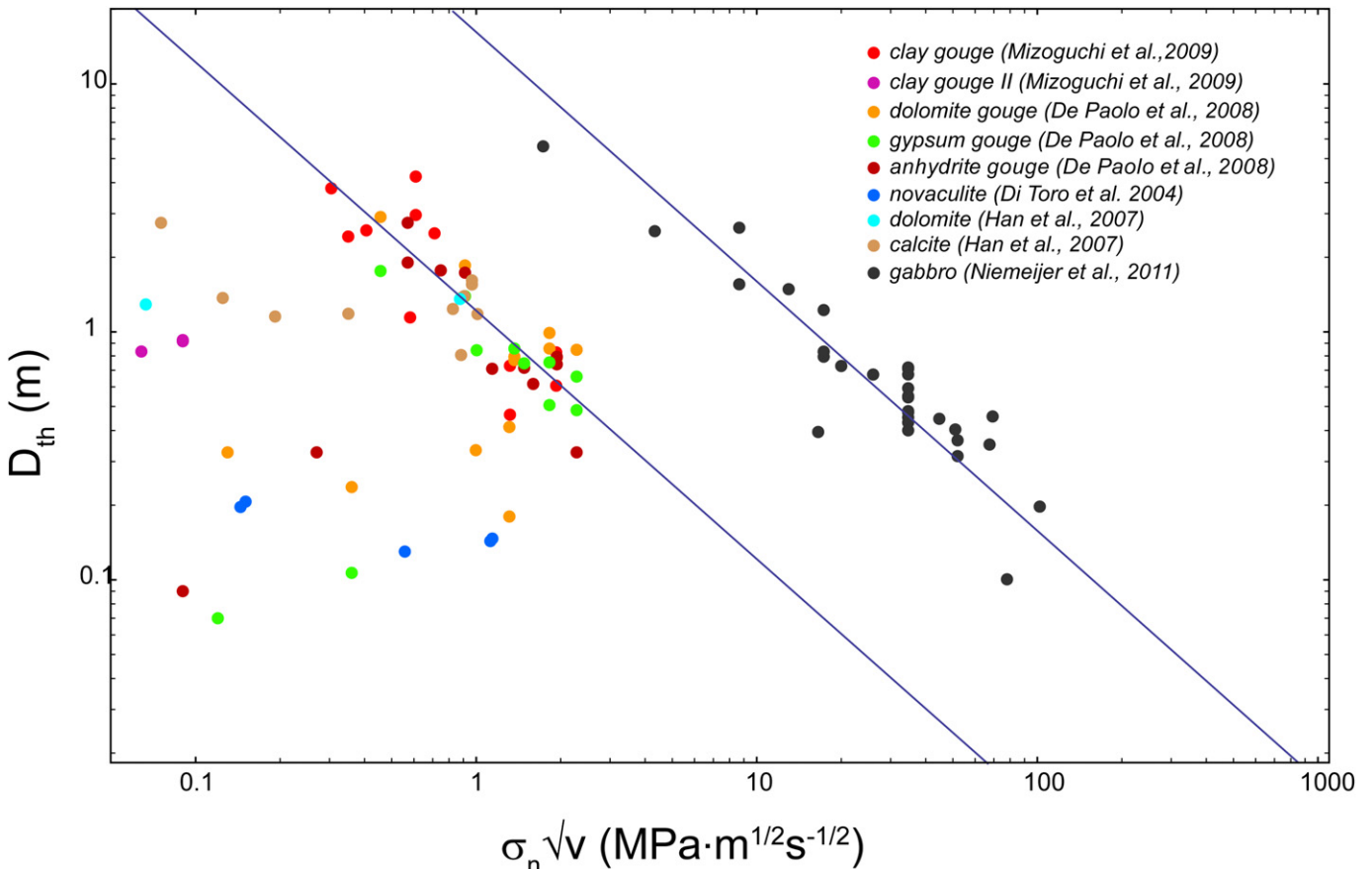


Fig. 10. Log-log plot of the thermal weakening distance (defined as the distance over which friction falls to $1/e$ of the peak value, d_w is 3 times this distance) as a function of the product of normal stress and the square root of the velocity, equivalent to the power supplied to the sample for a variety of rock types. An inverse linear relation (in log-log space) seems to the data pretty well. Note that the data for gabbro extend to conditions equivalent to those occurring in natural earthquakes (i.e. at a velocity of 1 m/s and 100 MPa normal stress).

$$d_w \propto (\sigma_n \sqrt{v})^{-a} \quad (3)$$

with $a = 1$. For thermally-activated weakening mechanisms other than melting, discussed in Section 2, no microphysical model exists to date that relates the shear stress with normal stress and only some experimental results are available.

For carbonates, Han et al. (2010) used a $1/\sigma_n^2$ dependence to fit their slip weakening distance data, similar to the fit used by Brantut et al. (2008) for clay-bearing gouges, but for a narrow normal stress range (0.3–1.3 MPa). Both these fits are consistent with a Mohr-Coulomb-type dependence of shear stress on normal stress, implying that for these experiments, deformation can still be considered "brittle". However, it is unclear what the value of the exponent would be if a general power law had been used to fit their data. De Paola et al. (2011a) reported a power of -1.4 for experiments on dolomite gouges, but since they infer that thermal pressurization occurred during the first steady-state stages in their experiments, it is not clear how d_w evolves with effective normal stress. Moreover, it is not obvious if these relations will hold at higher normal stresses, so without a microphysical model, scaling and extrapolation of the experimentally obtained slip weakening distances to natural conditions remains problematic and requires knowledge about the potential dynamic weakening mechanism(s).

Few studies discuss the other seismological parameters that can potentially be extracted from high velocity experiments, such as

breakdown work (fracture energy) or stress drop. Mizoguchi et al. (2007) estimated a "fracture energy" (breakdown work in our terminology, W_b) of 1–3 MJ/m² from their high velocity friction curves on fault gouge samples from the Nojima Fault that ruptured during the 1995 Kobe earthquake, which is the same order of magnitude as the seismological estimate. In addition, they showed that there was no systematic dependence of the breakdown work on normal stress. Similar results were obtained by Brantut et al. (2008), who reported values of 3.8–5.8 MJ/m² and no dependence on normal stress. Note that these experiments were performed on fault gouges sandwiched in between cylinders with a Teflon sleeve as the confining medium so that normal stress was limited to <2 MPa. In contrast, recent experiments performed on rings of gabbro up to ~50 MPa normal stress, showed indications that the breakdown work depends on normal stress as well as on the maximum slip velocity and acceleration (Fig. 11, Niemeijer et al., unpublished data). Note, however, that there is only a normal stress dependence visible when the breakdown work is normalized with respect to the total work expended in the experiment (compare Fig. 11a and b). Moreover, the value of the breakdown work is on the low end (1–3 MJ/m²) compared to seismological estimates of large earthquakes worldwide (1–100 MJ/m², e.g. Rice, 2006; Tinti et al., 2005). Slightly higher values for W_b (up to 5 MJ/m²) were reported by De Paola et al. (2011a) for experiments on dolomite gouges, in agreement with W_b estimates for the 1997 Colfiorito earthquake

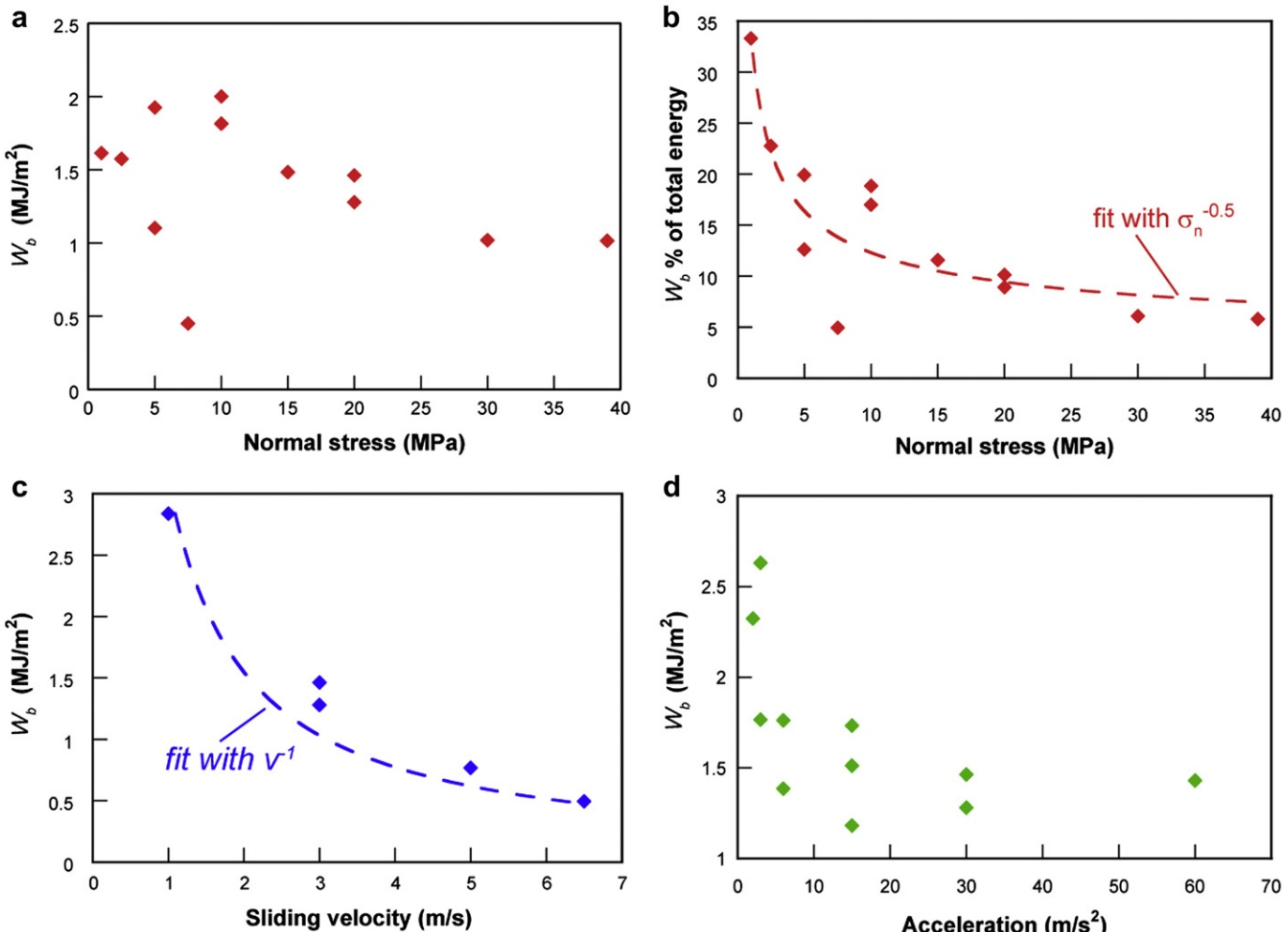


Fig. 11. : Plots of the breakdown work (W_b) determined from friction evolution curves for experiments on gabbroic rocks under a wide range of experimental conditions (Niemeijer et al., 2011). (a) Breakdown work as a function of normal stress. (b) Relative amount of breakdown work as a function of normal stress. (c) Breakdown work as a function of sliding velocity. (d) Breakdown work as a function of acceleration.

that propagated in similar rock types. They also reported a power law dependence of the breakdown work on the slip weakening distance with a power of 0.47. From this, we can infer that in their case, the breakdown work decreases with normal stress as a power law with a power of -0.66 . So extrapolating their experimental data obtained at less than 2 MPa to natural conditions would imply a much smaller breakdown work for the conditions of the Colfiorito earthquake. It should be noted that observations and modeling indicate that the effective normal stress was low during this earthquake due to near-lithostatic pore pressures (e.g. Chioldini and Cioni, 1989 and Miller et al., 2004), but at the same time the effective normal stress during the high velocity experiments of De Paola et al. (2011a) was unknown.

Part of the discrepancy between some of the experimental data and seismological estimates could be explained by the simple experimental configuration compared to natural earthquakes, where several other factors such as off-fault damage and fault roughness could affect the breakdown work and slip weakening distance. In addition, the high stress drops associated with thermal weakening in high velocity experiments does not compare well with seismological estimates, which suggest that the stress drop should be rather small. However, at this time only limited experimental results are available that cover a wide enough range of normal stresses to systematically investigate stress drops.

4. Indicators of seismic slip in fault zone rocks

In the following sections, we discuss possible indicators of seismic slip which might be observed in exhumed fault zone rocks, now exposed in outcrops or sampled in boreholes. We follow the definition of Cowan (1999), who defined seismic events as those that involve particle velocities (i.e. slip velocities) on the order of $0.1\text{--}1\text{ m/s}$, occurring over relatively short time periods (less than a few seconds to tens of seconds). These slip velocities, together with rupture propagation, are expected to produce the seismic wave radiation of typical earthquakes (Heaton, 1990) and therefore non-volcanic tremor and slow earthquakes are not included in this definition.

As such, indicators of seismic slip in the field should provide evidence for both high particle velocities in the slipping zone and short-duration slip events. We stress that friction-induced melts (pseudotachylite, Section 4.1) are currently the only unequivocal and widely accepted indicator of seismic slip in fault zone rocks (Cowan, 1999), but in recent years a number of other structures and microstructures have been proposed as potential indicators of seismic rupture speeds, some of which are discussed below. These have been proposed principally on the basis of field observations of exhumed fault zones, and rock deformation experiments carried out using rotary shear apparatuses, and must be rigorously tested using further observations.

4.1. Pseudotachylite

The term “pseudotachylite” was first used by Shand (1916) to describe dense aphanitic black rocks which occur in vein networks crosscutting a granitic intrusion from Parijs, Orange Free State, South Africa, associated with the Vredefort Dome meteoric impact structure. The term is motivated by the true tachylites (sic) being black glassy volcanic rocks. Initially, Shand (1914) assigned a primary igneous origin to these rocks, but, after a more detailed investigation, he suggested a different melt origin for these rocks, defined as “explosive” in his 1916 seminal paper. Nowadays, it is clear that pseudotachylites are formed by melting of rock during “catastrophic” events such as impacts (Shand, 1916; Reimold, 1998), “superfaults” (Spray, 1997), very large landslides (Erisman, 1979; Erisman et al., 1977; Masch et al., 1985; Lin et al., 2001) and

earthquakes (Sibson, 1975; Lin, 2008; Di Toro et al., 2009) and subsequent solidification. Only those produced during earthquakes, also called “tectonic pseudotachylites” (Magloughlin and Spray, 1992) will be considered in the following.

Tectonic pseudotachylites have been reported from thrust, strike-slip and normal faults and occur in a variety of host rocks, but mostly in crystalline, metamorphic or igneous rocks (for a review, see Sibson and Toy, 2006; see also Fig. 12a). They typically occur as fault or injection veins and can often be recognized by their dark color (e.g. Sibson, 1975; Di Toro and Pennacchioni, 2005). Where pseudotachylites occur as fault veins, they often are situated on the border of cataclastic horizons, have sharp boundaries and commonly overprint cataclasites (Di Toro and Pennacchioni, 2005). Thick pseudotachylite veins can be found in dilatational jogs along non-planar sections of the fault (Di Toro and Pennacchioni, 2005).

An ongoing debate in the literature concerns the apparent scarcity of pseudotachylites in exhumed fault zones (the so-called “local heat flow paradox”, Fialko and Khazan, 2005). A simple calculation of the bulk temperature rise expected at stresses typical of seismogenic depths ($>50\text{ MPa}$), seismic slip rates (1 m/s) and total slips (tens of centimeters to meters), indicates temperatures well above the melting point of most minerals, suggesting that pseudotachylites should be widespread in nature ($\sim 1300\text{--}1400\text{ }^{\circ}\text{C}$, see e.g. McKenzie and Brune, 1972; Sibson, 1980). Their apparent scarcity has led some authors (e.g. Sibson, 1973; Lachenbruch, 1980; Sibson and Toy, 2006; Brantut et al., 2010, 2011) to claim that pseudotachylites are rare because they are not often produced (perhaps because other dynamic weakening mechanisms operate before melting occurs or because slip is not confined to a thin slipping zone as assumed in the above-mentioned calculation), whereas other authors prefer the explanation that it is difficult to preserve pseudotachylites during exhumation (e.g. Di Toro et al., 2009). Indeed, other authors suggest it is not an uncommon rock type at all, but that they might be easily missed given that their thickness is usually $<1\text{ cm}$ (e.g. Spray, 1995; Di Toro et al., 2006b; Griffith, et al., 2008; Kirkpatrick and Shipton, 2009). This interpretation is supported e.g. by the case of the thin pseudotachylites only recently found at Bear Creek (Sierra Nevada, California), after about 30 years of detailed structural geology surveying of the area (Griffith et al., 2008; Kirkpatrick et al., 2008, 2009). The same applies, at a larger scale, to the European Alps. This area has been mapped with the highest detail since the end 19th century–early 20th century. However, pseudotachylites have only been found in the last 25–30 years, and are being recognized more and more.

A second point of discussion involves whether pseudotachylites are produced by melting or by comminution (e.g. Wenk, 1978), but it has been well established that comminution occurs before and/or during melting, so that both are linked when producing pseudotachylites (Spray, 1995). Numerous field studies focus on analyzing the composition, structure and geochemistry of pseudotachylites (e.g. the role of water) and it is beyond the scope of this paper to discuss these here (for extensive reviews see Lin, 2008; Di Toro et al., 2009 and Snook et al., 1998 and the two Special Volumes dedicated to pseudotachylites published by Tectonophysics in 1992 and 2005).

4.2. Clay Clast Aggregates (CCA) and other types of rounded, aggregate grains

Microstructures resembling Clay Clast Aggregates (CCA) produced in the laboratory (see Section 2.6 and Fig. 3f and h) have been reported from the slip zones of natural clay-bearing faults, from the basal detachments of large rockslides, and from the slip zones of active normal faults in limestone from the central Apennines of Italy. Examples include:

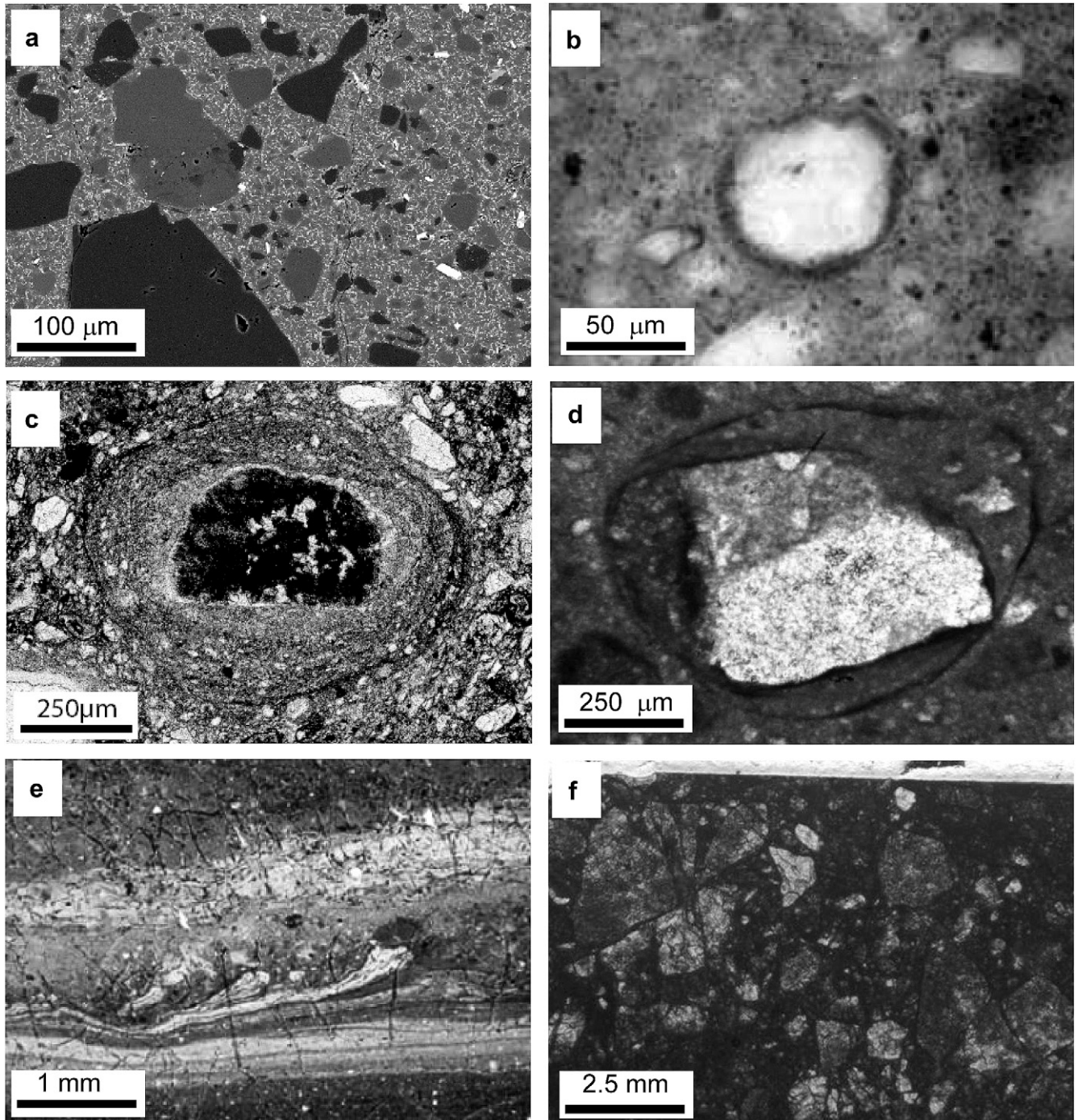


Fig. 12. Microstructures of natural slipping zones. (a) Natural pseudotachylite from the Gole Larghe Fault Zone, Italian Southern Alps (SEM-BSE image, Di Toro and Pennacchioni, 2004). (b) Natural Clay Clast Aggregate (CCA) from the slipping zone of the Chelungpu Fault, retrieved from 1111 m depth (FZA1111, TCDP Hole A), Taiwan (optical microscope image, crossed polars, gypsum plate, Boutareaud et al., 2010). (c) Armoured carbonate grain found within the basal detachment horizon of the Heart Mountain landslide, Montana, USA (optical microscope image, parallel polars, from Fig. 3d of Anders et al., 2010), (d) Clast-cortex grain from the principal slipping zone of the Tre Monti normal fault, Italian Apennines (optical microscope image, parallel polars, Smith et al., 2011). (e) Fluidal microstructures in the gouge of the slipping zone of the Nojima Fault, Japan (optical microscope image, parallel polars, Mizoguchi et al., 2009a,b). (f) Pulverized dolomite grains at few millimeters from the slipping zone of the Foiana Fault, Italian Southern Alps (optical microscope image, parallel polars, courtesy of Michele Fondriest).

- 1) “Snowballed” smectites found in exhumed fault gouges from the Alpine Fault, New Zealand (Fig. 5e in Warr and Cox, 2001). The clasts in this case contain rims of smectite surrounding central clasts of quartz, and are believed to be representative of relatively shallow levels of deformation (≤ 5 km, $T \leq 120$ °C). In the same samples an ultrafine-grained matrix derived from altered pseudotachylite glass was interpreted as evidence of older

seismic slip and progressive exhumation from deeper levels ($T \leq 320$ °C). Warr and Cox (2001) did not discuss the possible formation mechanisms of “snowballed” smectite rims, nor did they directly relate them to possible seismic slip speeds.

- 2) *Clay Clast Aggregates* found in the clay-bearing principal slip zone of the Chelungpu thrust Fault, at a depth of ~1.1 km, responsible for the 1999 Mw 7.6 Chi-Chi earthquake in Taiwan

- (Boullier et al., 2009, Fig. 12b). The CCA's were found in a 2 cm-thick isotropic gouge layer, and consist of rounded clasts enclosed in rims of fine-grained (<1 µm) clay about 5 µm thick.
- 3) "Armoured" carbonate grains present within the detachment surfaces and sliding zones at the base of catastrophic landslides, like the Heart Mountain rockslide in Wyoming and Montana (Beutner and Gerbi, 2005; Anders et al., 2010; Goren et al., 2010) and the Palisades rockslide in southeastern Idaho (Anders et al., 2000, Fig. 12c). These rockslides accommodated several tens of kilometers of movement and are interpreted as catastrophic events that occurred in a few to tens of minutes (Goren et al., 2010). At Heart Mountain, the sliding zone is defined by a layer of 'microbreccia' up to 3.5 m thick, predominantly located within the Bighorn dolomite, a moderately to highly calcareous dolomite (Beutner and Gerbi, 2005; Anders et al., 2010). Inside the microbreccia, abundant armoured carbonate grains up to 1 cm in diameter are present, with a central clast of volcanic or carbonate material surrounded by a spherical outer cortex of fine-grained mixed material (Anders et al., 2010). The armoured grains are interpreted as forming during fluidization of the microbreccia associated with catastrophic, high speed (10–100 m/s) emplacement of the rockslide and thermally driven decomposition of the carbonates (Beutner and Gerbi, 2005; Anders et al., 2010; Goren et al., 2010).
- 4) Carbonate Clast-Cortex Grains reported from the principal slip zone of the seismically active Tre Monti normal fault in the central Apennines of Italy, exhumed from <1 km depth and <100 °C (Smith et al., 2011, Fig. 12d). The Tre Monti Fault cuts Mesozoic limestones, and the principal slip zone consists of ca. 100% calcite. Sub-rounded to angular clasts of calcite or reworked carbonate cataclasite are surrounded by an outer cortex of ultra fine-grained (2–3 µm) calcite. The outer cortex can be simple, containing only one recognizable lamination, or more complex, containing a series of internal laminations with complex geometry (e.g. Fig. 12d). The clast-cortex grains, up to 3 mm in diameter, are restricted to an ultracataclastic slip layer <10 mm in thickness, immediately adjacent to the principal slip surface, and are not found elsewhere within the fault core or host rocks.

These examples suggest that rounded, rimmed, aggregate-type grains can be found in nature and might be indicators of high slip speeds and localized fluidization of thin slipping layers. Many questions relating to the formation of aggregate-type grains and their significance remain, which includes the effects of normal stress (i.e. depth) on their formation and preservation, whether they form only above a critical slip velocity and whether they form in a wide range of lithologies.

4.3. Fluidized fault rocks

Fluidized fault rocks are (usually) cohesive, ultrafine, matrix supported aphanitic rocks found in the fault core and injected into the wall rocks (Lin, 1996; Otsuki et al., 2003; Ujiie et al., 2007; Brodsky et al., 2009; Meneghini et al., 2010; Smith et al., 2008). They might be distinguished from fine-grained cataclasites by the observation that clasts suspended in the matrix are usually rounded and randomly dispersed, suggesting preferential abrasion and wearing of the grain corners. In addition, "fragmented counterparts" – clast fragments that can be recognized as being derived from the same starting clast – are rarely identified (Otsuki et al., 2003; Monzawa and Otsuki, 2003; Smith et al., 2008). Fluidized fault rocks often lack any indication of slip localization, and, of course, have flow structures such as folding and fluttering

structures and undulating surfaces but no evidence of a melting stage (otherwise, they should be defined as pseudotachylites, see Section 4.1). According to this definition, fluidized fault rocks are a particular type of ultracataclasite (*sensu* Sibson, 1977).

Fluidized rocks in fault zones have been found in subduction-zone thrusts (Brodsky et al., 2009; Meneghini et al., 2010; Ujiie et al., 2007), strike-slip settings (Otsuki et al., 2003), and associated with both high- and low-angle normal faults (Smith et al., 2008, 2011). Fluidized fault rocks have been found associated with pseudotachylites (which suggests a coseismic origin, Otsuki et al., 2003; Meneghini et al., 2010), and with calcite/laumontite-bearing veins (which suggests the presence of fluids, Ujiie et al., 2007; Smith et al., 2008, 2011). Fluidal microstructures that resemble those found in nature such as folding and fluttering structures (Mizoguchi et al., 2009b) and include also clay clast aggregates (CCA's) and folding structures (Kitajima et al., 2010) have been produced in high velocity friction experiments conducted on clay-rich gouges (see Fig. 3). Fluidization is a deformation mechanism by which granular materials acquire the ability to flow like gas molecules, transmitting stress through intergranular collisions. Although the process of formation is not well known, it is expected that rock fluidization occurs because of rock pulverization in the presence of fluids, which leads to granular flow of a low viscosity material (few Pa s) resulting in a very low shear resistance during seismic faulting (Brodsky et al., 2009). In particular, the presence of injection veins filled by "fluidized fault rocks" has been claimed for evidence of thermal pressurization as a driving mechanism for the intrusion of the fluidized granular material in the wall rocks (Ujiie et al., 2007).

4.4. Pulverized fault zone rocks

In recent years, fault rocks that appear to have been penetratively fragmented *in-situ* without accommodating significant shear strain have been reported from surface outcrops along various sections of the San Andreas Fault (Wilson et al., 2005; Dor et al., 2006a; Rockwell et al., 2009; Yuan et al., 2011), Garlock Fault (Rockwell et al., 2009), San Jacinto Fault (Dor et al., 2006b), north Anatolian Fault (Dor et al., 2008), and the Arima-Takatsuki line in Japan (Mitchell et al., 2011). These fault rocks, that have been termed 'pulverized rocks', are fundamentally different from other types of breccia and cataclasite in that they appear to have been very heavily and penetratively fractured without accumulating any relevant shear strain. Important characteristics of pulverized rocks include: 1) a lack of macroscopic shear planes and a friable outcrop nature; 2) high microfracture densities, but little evidence that microfractures accommodated shear displacements – most microfractures appear to be tensile; 3) preservation of still recognizable primary rock structures and microstructures; 4) pervasive grain size reduction, down to the micron scale, and; 5) little evidence for weathering products, suggesting that pulverized rocks predominantly reflect mechanical (rather than chemical) processes (Fig. 12f). Most examples of pulverized rocks to date have been documented in granitic lithologies, although Dor et al. (2009) found pulverized sandstones along the Mojave section of the San Andreas fault, and Agosta and Aydin (2006) report a possible case of pulverized rocks in limestone along the Venere Fault Zone, central Italy. In general, these rocks appear to be a relatively shallow phenomenon formed in the upper 1–3 km of the Earth's crust (e.g. Lewis et al., 2005). Pulverized rocks along the San Andreas Fault and Arima-Takatsuki line are found at distances of up to several hundred meters from the fault core (Rockwell et al., 2009; Mitchell et al., 2011). In the latter case, the authors found that microfracture density in the pulverized granites decreased exponentially with distance from the fault core, with 1D scanline microfracture

densities adjacent to the fault core up to 80 microfractures per mm. An important characteristic of pulverized rocks is related to their distribution: they appear to be asymmetrically distributed with respect to the principal fault surface, which is probably due to a preferential rupture direction, leading to an asymmetry in shaking intensities (e.g. Dor et al., 2006b; Mitchell et al., 2011). If the wall rocks located on either side of the principal fault are in different lithologies, pulverized rocks are typically found in the lithology with the highest seismic velocities (Ben-Zion and Shi, 2005; Mitchell et al., 2011).

Using a split Hopkinson pressure bar, Doan and Gary (2009) and Yuan et al. (2011) demonstrated experimentally that pulverization of granite at room pressure and temperature occurs during shock loading at high strain rates ($>150\text{ s}^{-1}$), although they did not report on the microstructural characteristics of the pulverized samples, and it remains to be determined whether the micromechanisms of fracturing in these experiments replicate those found in nature.

Theories to explain the formation of pulverized rocks must account for both the structural and microstructural characteristics, the large thickness around the fault core (up to hundreds of meters) and also the apparent asymmetric distribution around the principal fault surface (see Yuan et al., 2011 for discussion). Brune (2001) suggested that normal stress vibrations created during earthquakes by sliding on a rough fault may be responsible for rock pulverization, although it is difficult to envisage why this would produce asymmetric damage. More recently, Ben-Zion and Shi (2005) have proposed that dynamic ruptures along faults separating different lithologies (bi-material interfaces) may result in a preferred rupture propagation direction, and a strong reduction in normal stress (implosion) near the propagating rupture tip on the side of the fault with the highest seismic velocities, thus potentially producing damage asymmetry. According to the authors, since moderate to large earthquakes nucleate at depth, where rock pulverization should not occur, successive earthquakes maintain the same rupture bottom to top direction when they propagate to the surface. Repeated earthquakes propagating in the same direction are expected to lead to a marked asymmetry in rock damage at shallower depth (<3 km), consistent with geological observations of pulverized rocks. Understanding the global distribution of pulverized rocks has the potential to offer important insights into possible preferred rupture directions along major fault zones, and as a consequence has implications for seismic hazard evaluation. Although some geophysical studies of fault zone trapped waves seem to indicate that pulverized rocks are present in the upper 1–3 km of the crust (e.g. Lewis et al., 2005), it will be important to understand in more detail the depth and spatial distribution of pulverized rocks, and also the physics of the fracturing processes that contribute towards their formation.

4.5. Mineralogical and geochemical signatures of frictional heating

A promising direction in studies of ancient seismicity along faults is to search for mineralogical or geochemical signatures of frictional heating during earthquakes. Because thermal diffusivity in crustal rocks is typically low, and the duration of an individual slip pulse is a few seconds or less, most of the heat produced during earthquake slip is restricted to a narrow band, a few mm thick, within and immediately adjacent to the slipping zone (e.g. Lachenbruch, 1980; Sibson, 2003; Rice, 2006). As discussed in Section 2.1, temperature rises within the slip zone are sometimes sufficient to trigger melting of host rocks and formation of frictional melts (e.g. pseudotachylites) that can be recognized in exhumed faults (e.g. Sibson, 1975). In other cases, the temperature rises may promote thermal decomposition or dehydration of certain mineral phases and the formation of breakdown products that can be

identified in the rock record (see experiments discussed in Section 2, Brantut et al., 2008; De Paola et al., 2011a; Ferri et al., 2010; Han et al., 2007a; Kuo et al., 2011).

Candidates of breakdown products indicating a transient temperature rise that might potentially be identified include lime (CaO), magnetite (Fe_3O_4) and periclase (MgO). Lime, however, is an unlikely mineral to be preserved in the geological record because it is highly reactive and back-reacts quickly (in seconds to minutes) in an atmosphere containing CO_2 and H_2O to form portlandite ($\text{Ca}(\text{OH})_2$) and calcite (e.g. Agrinier et al., 2001). Unlike lime, magnetite is potentially stable over geological time periods, and may be identifiable as a signature of past earthquakes in the slipping zones of faults that cut Fe-bearing carbonates (e.g. Hirono et al., 2006). Similarly, other metal-bearing carbonates such as dolomite [$\text{MgCa}(\text{CO}_3)_2$] and ankerite [$\text{Ca}(\text{Fe}, \text{Mg}, \text{Mn})(\text{CO}_3)_2$] breakdown at elevated temperatures to form breakdown phases such as periclase (MgO , unstable), magnetite (Fe_3O_4), magnesioferrite (MgFe_2O_4) and Mg-rich calcite ($\text{Ca}_{(1-x)}\text{Mg}_x\text{CO}_3$, e.g. Samtani et al., 2002; Galai et al., 2007; De Paola et al., 2011b).

Several other mineralogical and geochemical phenomenon may record high-temperature pulses restricted to thin slipping zones, although the following are perhaps more challenging, time consuming, or costly to detect in the rock record:

- 1) Ujiie et al. (2008) proposed that fluid inclusions trapped in calcite can re-equilibrate and undergo permanent 'stretching' induced by transient heat pulses associated with seismic slip events. This stretching leads to an increase of fluid inclusion homogenization temperatures, which may be detectable using detailed analysis within the slip zones of exhumed faults. They reported a distribution of homogenization temperatures consistent with frictional heating in a carbonate-bearing subduction thrust complex exhumed from 4 to 6 km in Japan, and validated their results using experiments conducted on a heating–cooling fluid inclusion stage. Based on a comparison between the natural and experimental results, Ujiie et al. (2008) suggested that stretching of fluid inclusions in calcite may detect relatively small temperature rises in slip zones of only 50–150 °C.
- 2) O'Hara (2004) studied the vitrinite reflectance of coals from three faulted areas in the USA and Wales. Vitrinite reflectance increases with increasing temperature and duration of the heat pulse, and, because it does not degrade over time, maxima in vitrinite reflectance generated by ancient thermal events may be preserved in the rock record. He found that spikes in vitrinite reflectance data from the three areas correlated spatially with faults and zones of intense brittle deformation, and proposed that such spikes were due to transient frictional heating during seismic slip. He estimated that the temperature anomalies that produced the spikes were on the order of 425–475 °C in two of the cases, and 580–680 °C in another case. In a recent contribution, Sakaguchi et al. (2011) determined the vitrinite reflectance in two fault zones from the Nankai trough that were sampled in deep boreholes. They estimated that the two fault zones experienced peak temperatures over 350 °C indicating that seismic slip propagated at least once to the up-dip end of the subduction interface and into the toe of the accretionary wedge.
- 3) Ishikawa et al. (2008) analyzed the major and trace element compositions, along with isotope ratios, of cores recovered from the Chelungpu Fault following the 1999 M7.6 Chi-Chi earthquake in Taiwan. The cores crossed three active fault zones in shales at depths of between 1.1 and 1.25 km. At least one of these fault zones is thought to be part of the slipping zone of the 1999 earthquake. They found that, with respect to

the country rock, the three fault zones were markedly enriched in Sr, depleted in Li, Rb, Cs, and show a low $^{87}\text{Sr}/^{86}\text{Sr}$. All of these elements are generally known to be fluid-mobile elements, with significant mobilization occurring at fluid temperatures $>300\text{--}350\text{ }^{\circ}\text{C}$. Model calculations by Ishikawa et al. (2008) suggest that fluid–sediment interaction at temperatures of $350\text{ }^{\circ}\text{C}$ can adequately explain the observed enrichment and depletion patterns found in the fault zones. The current temperature in the fault zones was measured as $46\text{--}49\text{ }^{\circ}\text{C}$, indicating that high fluid temperatures must have been achieved either by frictional heating during earthquake slip, or by the influx of a pulse of hot fluids arriving from depth. The authors favor the former because a) the hydraulic diffusivity of the fault zones is too low to allow migration of a fluid pulse, and b) frictional heating is consistent with an increase in magnetic susceptibility and formation of ferromagnetic grains observed in the fault gouges.

We conclude this section highlighting the similarities between artificial fault materials from experiments that reproduce seismic slip rates and displacements (in most cases the normal stress is well below that expected in nature) with those found in exhumed natural faults (compare, for instance, Figs. 3a with 12a, 3f with 12c and d, 3h with 12e and 3g with 12b). We kept the experimental microstructures separated from the natural microstructures, because in several cases the similarity is ambiguous. But we emphasize that microstructural similarity between experiment and nature, which implies that the same (micro)physico-chemical processes were operating, remains the starting point for any extrapolation of mechanical data obtained in the laboratory to natural conditions as will be discussed in the next sections.

5. Estimating earthquake source parameters from exhumed faults

Typically, seismology can retrieve five main earthquake parameters from the analysis of seismic waves: the seismic moment M_0 , the static stress drop $\Delta\tau_s$, the radiated energy E_R , the rupture speed V_r , and the seismological fracture energy E_F (Kanamori and Rivera, 2006). The latter is sometimes called breakdown work W_b (Cocco and Tinti, 2008). In Fig. 13 and in its caption we introduce definitions of stress drops and earthquake energy sinks from the seismological literature (Kanamori and Rivera, 2006; Abercrombie and Rice, 2005; Cocco and Tinti, 2008) and compare the earthquake energy budget at a point of a fault (Fig. 13a) with the global earthquake energy budget for a fault with unit area (Fig. 13b). In the case of the shear stress evolution at a single point along a fault (Fig. 13a), this diagram is similar to those obtained in high speed rock friction experiments (see Section 2), though experiments do not reproduce the dynamic stress field associated to the tip of the propagating rupture (Reches and Dewers, 2005; Beeler, 2006). A discussion on the “single point” vs. “areal” representation of these processes is also given in Section 6.

It is noteworthy that fundamental information, including the absolute value of shear stress acting on the fault, energy partitioning during an earthquake, and data concerning the physical processes acting on the fault during seismic slip, are out of the range of seismological investigations (Ma et al., 2003; Andrews, 2005).

We distinguish between the earthquake energy budget at a point of a fault (Fig. 13a) from the average earthquake energy budget for a fault per unit area (Fig. 13b, Abercrombie and Rice, 2005; Kanamori and Rivera, 2006; Cocco and Tinti, 2008). The latter considers the whole fault and coseismic slip is averaged over the entire fault length. The total earthquake available energy per

unit fault surface (area of AELO in Fig. 13b) includes the elastic strain energy and gravitational energy that will be released during the earthquake and it is unknown (Dahlen, 1977; Scholz, 2002). The total energy is partitioned into radiated energy, fracture energy and frictional energy. The frictional energy (area below JHGEF in Fig. 13b) cannot be determined by seismic wave inversion analysis. The fracture energy (area of JABCKH in Fig. 13b) is determined from seismic moment, corner frequency and radiated energy estimates (Abercrombie and Rice, 2005). Though the determination of the fracture energy is model dependent, its estimate is more robust than the individual estimate of the slip weakening distance and dynamic stress drop (Cocco and Tinti, 2008). The radiated energy (area of DEGHK in Fig. 13b) is determined from seismic wave inversion analysis, though it remains difficult to constrain (Abercrombie et al., 2006; Venkataraman et al., 2006). According to the energy partitioning reported in Fig. 13b, the area of ABC (the excess work done to achieve the yield strength due to an increase in stress prior to dynamic slip) and of EFG (energy exchanged during fault strength recovery or coseismic healing) are balanced by the area of CDK.

In the case of the energy budget at a point of a fault, the mechanical work done is partitioned into work against gravity, radiated energy, heat Q , and fracture surface energy U_s (Kostrov and Das, 1988, Fig. 13a). To include radiated energy, the shear stress curve should be coupled to rupture and elasto-dynamic models including radiation and non-local interaction (Beeler, 2006). Instead, we introduced the breakdown work W_b which differs from the seismological fracture energy because it is related to the energy effectively dissipated (and measured) on the fault surface (Cocco and Tinti, 2008). According to this interpretation, W_b is the natural equivalent of the area comprised between the traction curve and the minimum shear stress during the weakening stage in the shear stress vs. slip experiments described in Section 2. The fracture surface energy is the energy adsorbed during phase transitions (e.g. solid to melt) and required to create new surfaces in the slipping zone and in the wall rocks: it is one of the possible energy sinks of the seismological fracture energy and of the breakdown work (Kanamori and Heaton, 2000; Kanamori and Rivera, 2006; Cocco et al., 2006; Rice, 2006).

In this section, we summarize recent results from studies of exhumed faults and information retrieved from drilling of active faults (for a review, see Boullier, 2011). Most of the information about seismic source parameters described below was retrieved from field observations and interpretations of pseudotachylite-bearing faults from the Gole Larghe Fault Zone that cuts the Adamello tonalites (Italian Southern Alps, Di Toro and Pennacchioni, 2004, 2005; Di Toro et al., 2005a; Pennacchioni et al., 2006). One of the reasons is that pseudotachylites remain the most certain indicator of ancient seismic ruptures in the upper crust to date (Cowan, 1999). The relatively simple geological framework, combined with the high-quality and 3-dimensional nature of the exposures, allow for a detailed investigation of earthquake source processes that can readily be compared to experimental observations (e.g. Di Toro et al., 2006a).

5.1. Seismic rupture velocity and directivity

Seismic inversions can constrain rupture directivity (the direction of propagation of the seismic rupture), and also rupture velocity (e.g. Cirella et al., 2009; D'Amico et al., 2010), but given the long recurrence times of most large earthquakes (>100 years), the number of historically recorded events along a given fault is rather small and the statistics of earthquake directivity cannot yet be determined (Bakun et al., 2005). However, rupture directivity is of paramount importance in earthquake hazard evaluation. In the

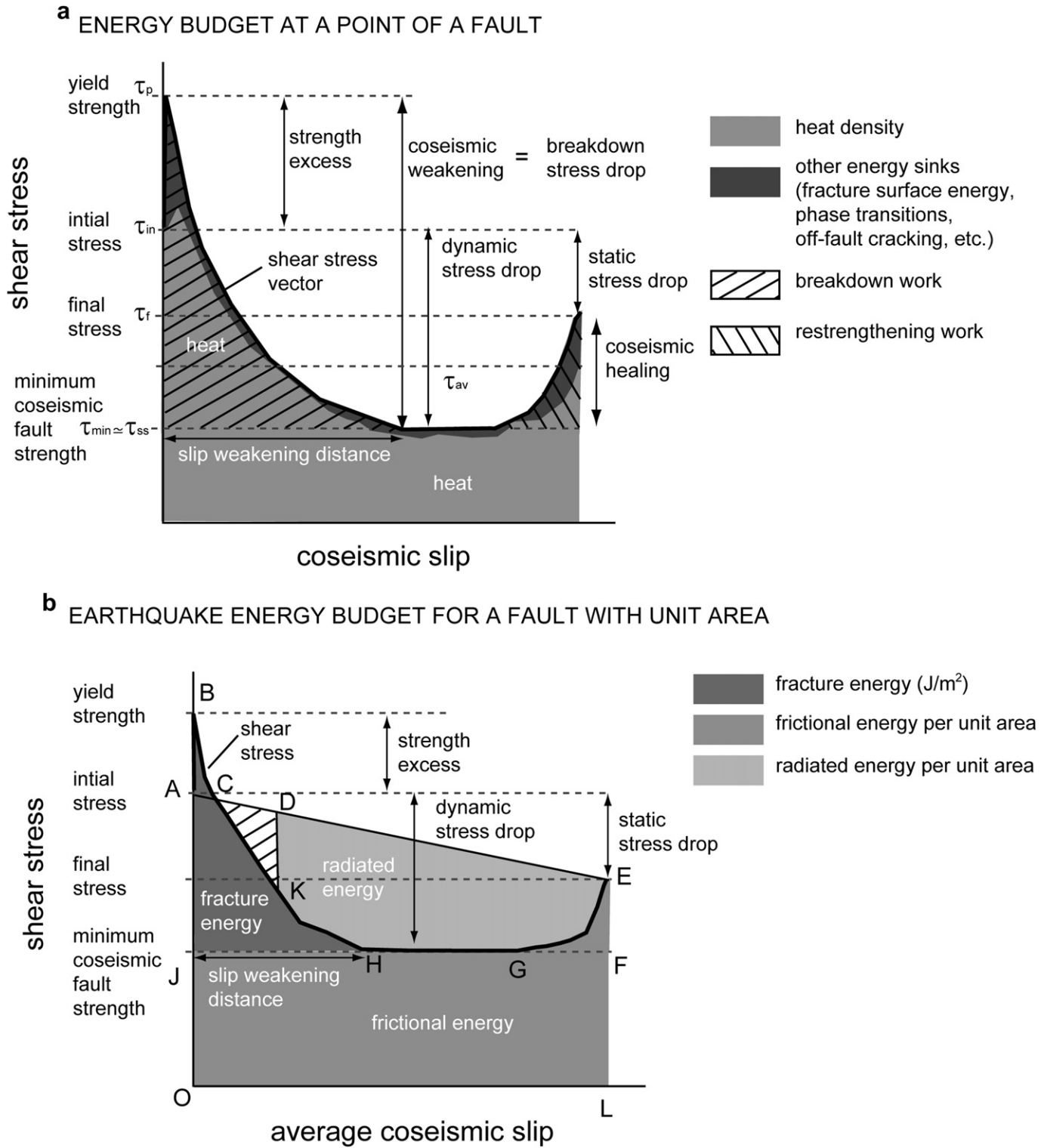


Fig. 13. Schematic diagrams of the shear stress (actually, traction) evolution during seismic slip and of the earthquake energy budget at a point of a fault and over the entire fault. (a) Energy budget at a point of a fault. This diagram is similar to those obtained in high speed rock friction experiments (though experiments do not reproduce the dynamic stress field associated to the tip of the propagating rupture, Beeler, 2006). The diagram reports the definition of breakdown work (W_B), surface fracture energy (U_S), heat (Q), initial shear stress (τ_i), final shear stress (τ_f), peak shear stress (τ_p), average shear stress (τ_{av}), breakdown stress drop ($\Delta\sigma_B$), the dynamic stress drop ($\Delta\sigma_d$), the static stress drop ($\Delta\sigma_s$), the slip weakening distance (d_w) and the total displacement (d). Before the initiation of sliding (the rupture tip is approaching the point on the fault), stress increases from τ_i to τ_e (elastic deformation) which switches to plastic before shear stress overcomes τ_p (yielding of the rock) and decays towards a minimum shear stress τ_m over a weakening slip distance d_w . The shear stress coincides with coseismic fault strength once the yield strength is achieved at the passage of the rupture front. The minimum shear stress might be similar in magnitude to the steady-state shear stress. We also report the average shear stress: this value might be obtained by thickness/displacement ratios in pseudotachylite-bearing faults (see Section 4.2). Depending on the slip rate vs. time curve (not reported here), shear stress recovers towards a final shear stress τ_f . The breakdown work is the area limited by the shear stress curve and the minimum shear stress (i.e. it includes the surface fracture energy). If coseismic healing occurs as shown here, energy is also dissipated in fault restrengthening work. The frictional work per unit area (area below the shear stress curve) is partitioned in heat density and fracture surface energy per unit area. The heat exchanged in seismic

case of unilateral rupture propagation, the radiated wave field is amplified in the direction of propagation, leading to increased strong ground motions (Somerville et al., 1997; Rowshandel, 2006; Boatwright, 2007; Spudich and Chiou, 2008).

Fault rocks at depth may record rupture directivity during slip events. This is because the presence of a dynamic crack (the propagating seismic rupture) embedded in an elastic medium (the wall rocks) subject to a remote “regional” stress field induces a perturbation in the stress field in the proximity of the crack tip. The stress perturbation, resulting in dramatic increases and rotations of the stress tensor, depends mainly on fracture length, stress drop, energy dissipated during fracturing, extension of the weakening zone behind the rupture tip, rupture directivity, and speed (Freund, 1998). The stress perturbation results in reactivation of pre-existing fractures and production of new, coseismic fractures. If it is possible to link a particular fracture pattern to a single seismic rupture, information on rupture directivity and velocity can be retrieved from an outcrop. This can be done for some of the Gole Larghe Fault Zone pseudotachylyte-bearing faults.

Pseudotachylytes often form continuous layers, decorating the main fault (fault vein), but also intrude the wall rocks along secondary fractures (injection veins; Sibson, 1975). When there is no reworking or alteration, it is sometimes possible to associate a single fault vein, and injection veins radiating from it, to a single seismic event. Particularly the pattern of injection veins is important when studying directivity. At least two mechanisms (possibly concurrent) produce injection veins during rupture propagation: (1) hydrofracturing, due to volume expansion related to the transition from solid to melt (an increase in volume of about 12–15% is expected in the case of granitoid rocks, Maddock et al., 1987; Swanson, 1992), and (2) the intense stress field perturbation at the rupture tip propagating at kilometers per second (Di Toro et al., 2005b). Since frictional melt production occurs after the rupture propagated through a point on a fault, we might expect that the nucleation and orientation of the secondary fractures departing from the main fault is mainly controlled by the stress perturbation at the rupture tip, while their growth in length and aperture is controlled by the amount and viscosity of the friction melt and by the elastic properties of the wall rocks. Given a Mode II crack propagating along a fault, theoretical (Poliakov et al., 2002; Kame et al., 2003; Rice et al., 2005) and experimental (Rosakis et al., 2000; Samudrala et al., 2002; Griffith et al., 2009a) studies predict the possible patterns of secondary fractures that a seismic rupture may leave in its trail, which are always asymmetric. Dynamic crack propagation induces an intense (depending on the rupture velocity V_R) tensional stress perturbation to one side of the fault and a corresponding compressive perturbation in the opposite block. Since rocks are about ten times weaker in tension than in compression, this may result in a strong asymmetry of the newly formed cracks with respect to the main fault. Moreover, the orientation of the newly formed fractures is related to the rupture speed, as the angle between the fracture and the fault increases from about 30° to about 90° from a quasi-static propagation to a crack propagating at about the Rayleigh wave speed (0.92 the V_s speed). It follows that the asymmetry in distribution and

orientation of pseudotachylyte-bearing injection veins can be used to reconstruct rupture directivity, rupture velocity and fracture energy (Di Toro et al., 2005b).

In the Gole Larghe Fault Zone, the asymmetric distribution of pseudotachylyte-bearing fractures shown in Fig. 14 is compatible with (1) a dominant eastward propagation direction during repeated seismic ruptures, (2) subsonic fracture propagation velocities (close to Rayleigh wave velocity) and, (3) fracture energy E_F values ranging from 8 to 67 MJ m⁻² (see also Section 5.4, Di Toro et al., 2005b).

5.2. Coseismic fault strength and stress drop

Interpretation of geophysical and seismological data suggests that a variety of coseismic processes can be explained by a low dynamic friction coefficient during earthquake rupture. For example, the absence of a heat flow anomaly around the San Andreas Fault (Lachenbruch and Sass, 1980), the local heat flow paradox, the type of rupture propagation (Beeler and Tullis, 1996; Zheng and Rice, 1998), or the increase of radiated energy with earthquake size (Mayeda and Walter, 1996; Malagnini et al., 2010). As discussed in detail in Section 2, several dynamic weakening mechanisms have been proposed to explain this (Tullis, 2008; Wibberley et al., 2008; Di Toro et al., 2011), although the dynamic friction coefficient cannot be easily retrieved from seismic inversion data (Guatteri and Spudich, 1998; Scholz, 2002). Instead, it is possible to determine frictional strength during seismic slip by applying the first principle of thermodynamics to seismic faulting (Sibson, 1975). Assuming that most frictional work during faulting is converted into heat (i.e. the energy associated with the creation of new surfaces is negligible, see Section 5.4), it is possible to determine the average shear stress during seismic slip τ_{av} (i.e. the average shear stress includes the peak and minimum shear stress, Fig. 13) from the amount of melt (pseudotachylytes, Sibson, 1975) or the amount of reaction products found in faults (such as carbonate decomposition products or clay dehydration products, Hirono et al., 2007; Hamada et al., 2009; Hirono and Hamada, 2010). In the case of pseudotachylyte-bearing faults, from Sibson (1975):

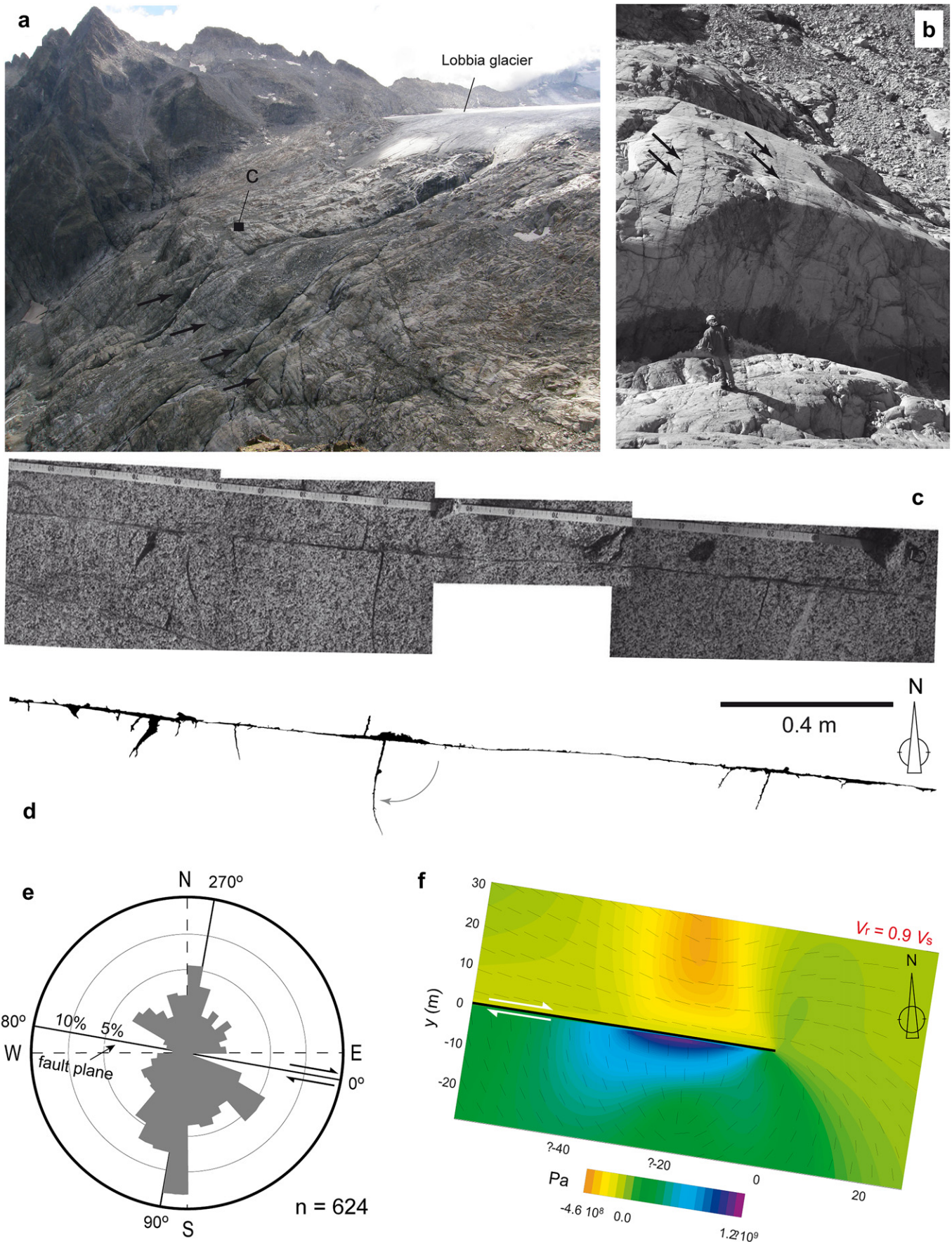
$$\tau_{av} = \rho c_p (T_i - T_{hr}) w_{av} / d \text{ [Pa]} \quad (4)$$

where ρ is rock density, c_p is the specific heat [J K⁻¹ kg⁻¹] at constant pressure, T_i is the highest temperature achieved by the melt, T_{hr} is the ambient host rock temperature, w_{av} is the average thickness of the pseudotachylyte (it should include also the melt injected in the wall rocks, Di Toro et al., 2005a), d is the coseismic slip. If we include in Eq. (4) the latent heat of fusion H (Wenk et al., 2000), the presence of survivor clasts (with a volume fraction $\varphi = V_{clast}/V_{pt}$), and superheating of the frictional melt (Di Toro et al., 2005a), we obtain:

$$\tau_{av} = \rho [(1 - \varphi)H + c_p (T_i - T_{hr})] w_{av} / d \text{ [Pa]} \quad (5)$$

Eqs. (4) and (5) were used in pseudotachylyte-bearing faults (Sibson, 1975; Wenk et al., 2000; Di Toro et al., 2005a, 2006b; Barker, 2005; Andersen et al., 2008; Nielsen et al., 2010a) and

faulting determines the increase in temperature in the slipping zone and wall rocks. Fracture surface energy includes effects due to the formation of new grain surfaces during fracturing, phase transitions (e.g. solid to melt), off-fault cracking, etc. According to this schematic model, most of the surface fracture energy is produced at the initiation of slip (i.e. just behind the rupture tip). This diagram does not include radiated energy. To include radiated energy, the shear stress curve should be coupled to rupture and elasto-dynamic models including radiation and non-local interaction which is not considered here (Beeler, 2006). (b) Average earthquake energy budget for a fault per unit area (modified from Abercrombie and Rice, 2005; Kanamori and Rivera, 2006). This budget considers the whole fault and coseismic slip is averaged over the entire fault length. The total earthquake available energy per unit fault surface (area of AELO, Dahlen, 1977) includes the elastic strain energy and gravitational energy that will be released during the earthquake. The total energy is partitioned into radiated energy, fracture energy and frictional energy. The frictional energy (area below JHGFE) cannot be determined by seismic wave inversion analysis. The fracture energy (area of ABCKH) and radiated energy (area of DEGHK) can be determined by seismic wave inversion analysis to some extent (in the limit of the resolution of the data). According to this energy partitioning, the area of ABC (the excess work done to achieve the yield strength due to an increase in stress prior to dynamic slip) and of EFG (energy exchanged during fault healing) is balanced by the area of CDK.



their robustness has recently been confirmed in high velocity experiments performed on gabbro at normal stresses exceeding ~15 MPa (Niemeijer et al., 2011). Nevertheless, Eqs. (4) and (5) should be applied with some caution in nature. In fact, as discussed in detail in Di Toro et al. (2005a), defining both fault rock thickness and net displacement can be a problem. Pseudotachylite thickness is highly variable along fault strike, so an average thickness, calculated over a length of several meters along a continuous exposure, should be used, and the melt injected in the wall rocks must be included. Only large exposures allow the average thickness of several pseudotachylite-bearing faults to be measured: if there is little scatter in the measured average thickness and the average thickness increases slightly with measured fault slip the data are robust enough to estimate the average shear stress. Such outcrops are uncommon and just a few have been studied: the Fort Foster Brittle Zone (Swanson, 1988, 2006) and the Gole Larghe Fault Zone (Di Toro and Pennacchioni, 2005).

At the same time, constraining the amount of coseismic slip that produced the frictional melt (now pseudotachylite) might be impossible because of pre- or post-seismic displacements, or because of the occurrence of multiple seismic events along the same fault. Eqs. (4) and (5) can be applied only in the case of faults that ruptured only once during their evolution (this is not uncommon in pseudotachylite-bearing faults, Sibson, 1975; Swanson, 1988, 2006; Allen, 2005). The occurrence of single-jerk episodes should be confirmed by detailed field and microstructural studies (for a discussion see Pittarello et al., 2008). But even in this case, the determination of the displacement requires the presence of structural markers (so that separation can be determined) and a lineated fault surface which allows the definition of the slip vector. Moreover, the maximum temperature achieved in the slipping zone needs to be determined, which is a difficult task since frictional melting is a non-equilibrium process and, as a consequence, conventional methods used in igneous petrology to determine the temperature of a melt starting from the rock's composition cannot be applied (Spray, 1992, 2010). As a matter of fact, frictional melts might be superheated and their maximum temperature spans, depending on the rock type, from 750 °C to 1500 °C (see also Di Toro et al., 2009; Spray, 2010; Lin, 2008). Lastly, a critical assumption is that most frictional work is converted into heat and that the energy expended for producing new cracks is negligible. This seems to be the case in the Gole Larghe Fault Zone, exhumed from 10 km depth (Pittarello et al., 2008: see Section 5.4), the Punchbowl Fault exhumed from 1 to 3 km depth (Chester et al., 2005) and in the Chelungpu Fault, drill holes down to 2 km depth (Ma et al., 2006), but it might not always be the case and it might be that a relevant part of the earthquake energy budget goes into plastic deformation of the wall rocks (Andrews, 2005).

In the case of the Gole Larghe Fault Zone, from Eq. (4) using $\rho = 2700 \text{ kg m}^{-3}$, $\varphi = 0.2$, $H = 3.28 \times 10^5 \text{ J kg}^{-1}$, $c_p = 1180 \text{ J kg}^{-1} \text{ K}^{-1}$ and $(T_i - T_{hr}) = 1200 \text{ K}$, τ_{av} was estimated to range between 12.9 and 41.8 MPa (Di Toro et al., 2006b). Since the normal stress at the time of seismic faulting was estimated to be between 110 and 200 MPa (Di Toro et al., 2005a), this results in an average friction coefficient of <0.25. Such low dynamic friction during seismic slip

in the presence of melts is consistent with theoretical and experimental analyses (Nielsen et al., 2008; Di Toro et al., 2009). It follows that at intermediate crustal depths, low fault strength and melt lubrication can occur during seismic faulting.

A similar approach was applied in slipping zones where reaction products were found (Hirono et al., 2007). Frictional heating during coseismic slip triggers various endothermic reactions and, if the amount of reactions products can be measured, it is possible to estimate the average shear stress. A further advantage of the method would be that endothermic reactions, by adsorbing heat (which is usually larger for dehydration or decarbonation than the latent heat of fusion), buffer the temperature rise in the slipping zone and superheating effects would be less pronounced than in the case of frictional melting (Brantut et al., 2011). Though the idea is straightforward and the approach promising, in practice, determining coseismic shear stress from the amount of reaction products is not a simple task for several reasons: 1) reaction kinetics (which is determined by the temperature evolution, the activation energy, etc.) and reaction mechanisms control the amount of reaction products, so that determining the average shear stress from the amount of reaction requires numerical modeling and strong assumptions (Hirono et al., 2007; Hamada et al., 2009; Hirono and Hamada, 2010) and 2) in the case of reactions triggered during frictional sliding, the activation energy might be much smaller than that determined for reactions under static conditions (Di Toro et al., 2011; Kuo et al., 2011), leading to more reaction products than expected for a given temperature (which is related to the heat production and thus the coseismic shear stress). In other words, an overestimation of the activation energy would result in an overestimation of the coseismic shear stress. Nevertheless, Hirono and Hamada (2010) estimated the shear stress at a point of the Chelungpu Fault during the 1999 Chi-Chi earthquake. This resulted in an estimate of a shear stress of ~9 MPa at 1 km depth. This value is in agreement with experimental results from high velocity experiments (Sone and Shimamoto, 2009; Mizoguchi et al., 2008).

An alternative method to determine the fault strength, or at least the static stress drop during earthquakes, was applied by Griffith et al. (2009b). In this case, the authors selected strike-slip faults exposed end-to-end in the granodiorites from the Bear Creek area (Sierra Nevada, USA), where the occurrence of thin pseudotachylites indicated ancient seismicity. The presence of rhombochasm (rhombohedral dilational jogs filled by randomly oriented epidote crystals and interpreted as the result of slip occurring in single events) distributed along the fault length allowed the estimation of coseismic slip distribution. In the case of a circular crack of radius R in an elastic medium, it is possible to estimate the static stress drop from the average slip d (Kanamori and Anderson, 1975):

$$\Delta\sigma = \frac{7}{16}G \frac{\Delta d}{R} \quad (6)$$

where G is the shear modulus. Using Eq. (6) and considering elliptical to circular cracks, Griffith et al. estimated stress drops of the order of 90–250 MPa for these faults exhumed from 4 to 15 km

Fig. 14. The Gole Larghe Fault Zone and rupture directivity. (a) View of the Gole Larghe Fault Zone at the base of the Lobbia Glacier, looking to the East. (b) Deep creeks cutting the outcrop surface allow a 3-dimensional view of the Fault Zone. (c and d) Photomosaic and drawing of a pseudotachylite-bearing vein network. Most injection veins are towards the South. (e) Rose diagram of the angle of the injection veins measured clockwise from the east side of the fault veins. The angular reference frame is relative to the fault plane orientation (the 0°–180° direction). The fault plane strike is close to the east–west direction (dashed lines indicate the geographic reference frame). The sense of the shear is dextral for all faults. Most veins intrude the southern wall rock. (f) Tensile stress field during rupture propagation in the vicinity of a fracture tip for $V_R = 0.9 V_S$. The fracture tip is shown as a black line. The diagram is a zoom box, around the fault tip, of the original model. The model assumes pre-stress and constitutive parameters based on the Gole Larghe Fault at the time of seismicity. Fracture propagation is from west to east on a vertical dextral strike-slip fault. Colour shows stress magnitude (in Pa), from orange (negative, compression) to blue (positive, tension); thin black segments indicate the local direction of planes of maximum tension (on the southern side of the rupture). For this rupture velocity, the maximum tension planes are oriented nearly orthogonal to the fault plane, which is consistent with orientation of most pseudotachylite-filled tension cracks observed in the southern bounding block along the Gole Larghe Fault (d–f).

depth. Such large static stress drops (at least when compared to typical stress drops of 1–10 MPa for moderate to large magnitude earthquakes, e.g. Hanks, 1977) determined for small faults (<15 m in length), are actually in the range of the stress drops estimated for microearthquakes along the San Andreas Fault at SAFOD (Imanishi and Ellsworth, 2006).

5.3. Seismic slip rates and weakening distance

Coseismic slip rates (Heaton, 1990) and the slip weakening distance d_w (the distance after which traction drops to its minimum, termed d_c in seismology, Ide and Takeo, 1997) can be estimated based on seismic wave inversion, though the determination of both parameters remains strongly model dependent (Fukuyama et al., 2003; Cocco et al., 2009). Although extremely challenging, and currently possible only in the case of frictional melting, useful constraints may come from field studies.

5.3.1. Seismic slip rates

A method to determine seismic slip rate from exhumed pseudotachylite-bearing faults was proposed by Nielsen et al. (2010a). When frictional sliding and melting occurs, microscale roughness at the melt-wall rock contacts becomes more accentuated due to varying microstructural and mineralogical properties of the wall rocks (grain size, indentation hardness and individual melting point of the rock-forming minerals, Spray, 1992) and by Gibbs–Thomson effects (preferential melting of the wall rock grains with a high surface-to-area ratio such as the grains sticking out from the wall rocks into the melt (Hirose and Shimamoto, 2003)). On the other hand, the increase in temperature in the slipping zone will be more abrupt if more power (shear stress times slip rate) is dissipated on the fault surface and the melting rate will be higher accordingly.

Due to wall rock heterogeneity and Gibbs–Thomson effects, at steady-state, the roughness of the melt-wall rock contacts is expected to decrease with increasing melting rate and temperature gradient perpendicular to the fault surfaces (Fig. 15; Nielsen et al., 2010a). For this reason, Nielsen et al. (2010a) proposed that the ratio of melt thickness w_{SZ} to roughness w_0 depends on the sliding velocity v and that this ratio can be used as a slip-rate gauge:

$$\frac{w_{SZ}}{w_0} \approx \frac{a}{v} \quad (7)$$

where the characteristic velocity a may be estimated based on laboratory tests at different velocities for a given rock type. Ideally, Eq. (7) may be used to estimate v independent of the shear stress and other ambient conditions by inspection of fault rock samples. However, since the structure of a natural fault is highly non-symmetric and heterogeneous, also at the microscale (see Section 6.1), an accurate characterization may require multiple samples and measures.

5.3.2. Slip weakening distance

The slip weakening distance d_w is a crucial parameter in earthquake physics, as it describes the evolution of shear stress with increasing slip which controls seismic radiation and rupture propagation (e.g. Kanamori and Brodsky, 2004; Beeler, 2006). Two methods have been proposed to determine the slip weakening distance, both applicable in the case of pseudotachylite-bearing faults. The first method uses Eqs. (4) and (5) to estimate the shear stress based on pseudotachylite-bearing fault thickness vs. displacement ratios, and exploits a relatively large catalogue of faults with a wide range of separations (see Di Toro et al., 2006b; Nielsen et al., 2010a; Niemeijer et al., 2011).

By using data collected from the Outer Hebrides Fault Zone by Sibson (1975) and Hirose (published in Nielsen et al., 2010b), and assuming that slip on all faults took place under similar average conditions of slip rate and lithostatic load, data from faults with different slip amounts illustrate a progressive frictional decay with increasing slip (Fig. 16). This field data suggest a $d_w \leq \sim 0.1\text{--}0.4$ m and a residual shear stress of a few tens of MPa at 10 km depth and in the presence of frictional melts. These estimates are consistent with those extrapolated from experimental work (Di Toro et al., 2011; Niemeijer et al., 2011), and predicted by theory (Nielsen et al., 2010b).

The other method stems from microstructural observations of the evolution, with increasing slip, of fault micro-roughness and thickness in frictional melting experiments (Hirose and Shimamoto, 2003, 2005b). As described in Section 2, for a given slip rate and applied normal stress, experiments show that a steady-state friction coefficient is achieved after an exponential decay or transient (Fig. 6). If different experiments are stopped during the transient

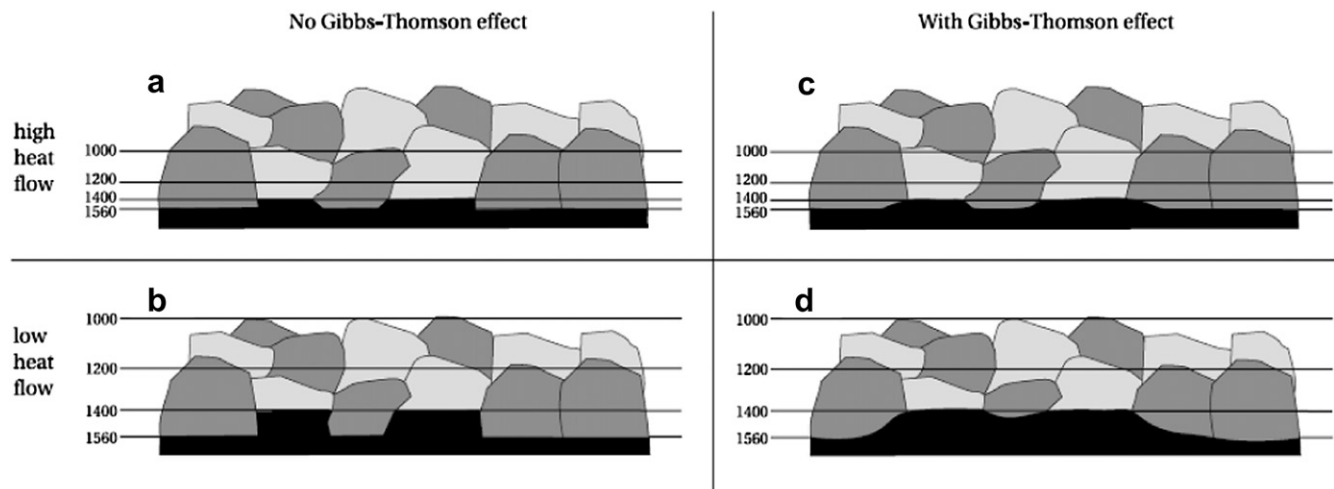


Fig. 15. Roughness dependence with power density. Idealized models of melting boundary in two mineral rock. Dark gray areas represent minerals melting at relatively high temperature (e.g. anorthite, 1560 °C), while lighter areas minerals with low melting temperature (e.g. diopside, 1400 °C). Black areas represent melt. The straight lines show isotherms in the wall rocks. (a,b): steep and gentle temperature gradient, respectively, with melting boundary strictly following the isotherms in each mineral. (c,d): same temperature gradients as (a,b) but the melt/solid boundaries are drawn in a more round-shaped fashion to account for the preferential melting of sharp corners and isolated asperities. In (a,b) the temperature gradient affects the only the asperity height in the profile topography, while in (c,d) it affects both the height and the asperity radius distribution. Higher heat flow results from high power densities, which are found either during the early phases of melting or under conditions of high normal stress and slip rate (from Nielsen et al., 2010a).

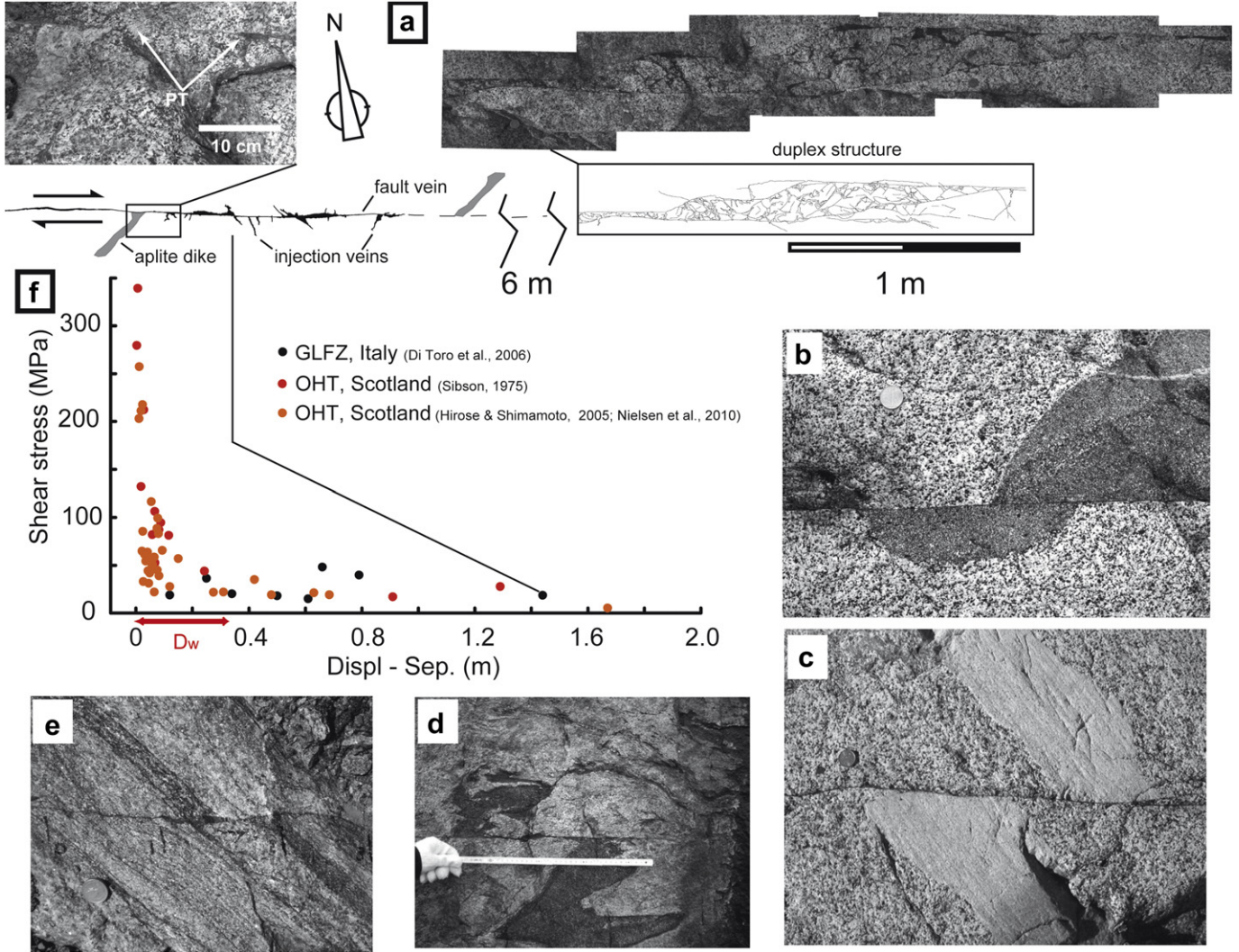


Fig. 16. Estimate of the slip weakening distance from exhumed faults. The average dynamic shear stress was estimated for (single-jerk) pseudotachylite-bearing faults with Eq. (3). The data are from the Outer Hebrides Thrust in Scotland (OHT, Sibson, 1975; Hirose and Shimamoto, 2005b; Nielsen et al., 2010b) and Gole Larghe Fault Zone (GLFZ, Di Toro and Pennacchioni, 2005a). (a) For large displacements faults (up to 1.4 m in the case of the GLFZ), the thickness was calculated from fault profiles (Fig. 11) as the ratio between the pseudotachylite area and the length of the fault segment (Di Toro et al., 2005a). Here, the presence of a continuous layer of pseudotachylite and the absence of cataclastites (also in the duplex structure about 6 m to the east) support the hypothesis of a single jerk. This field interpretation is further supported by microstructural studies (Pittarello et al., 2008). (b) Mafic enclave separated by pseudotachylite-bearing fault (GLFZ, Italy). (c) Aplitic dyke separated by pseudotachylite-bearing fault (GLFZ, Italy). (d) Structural marker separated by pseudotachylite-bearing fault (OHT, Scotland). (e) Foliation separated by pseudotachylite-bearing fault (OHT, Scotland). (f) Average shear stress data from faults with different slip amounts illustrate the progressive frictional decay with increasing slip. In the abscissa are reported separations and displacements as in the case of the OHT, only separations were determined. The slip weakening distance is between 0.1 and 0.4 m. In both the OHT and GLFZ, the host rock is granitoid in composition and faults were exhumed from 4 to 12 km depth (Di Toro and Pennacchioni, 2004).

stage, but at increasing slip distances, the evolution of roughness with increasing slip can be determined by microstructural analysis (Hirose and Shimamoto, 2003). A useful parameter to quantify roughness is the fractal dimension D (e.g. Turcotte, 1997), which is determined with the divider method used to describe coastlines (Mandelbrot, 1967). This, according to Hirose and Shimamoto (2003), increases from 1.0 at the peak friction to about 1.1 at steady-state. The increase in fractal dimension describes the increasing complexity of surface roughness due to selective melting and Gibbs–Thomson effects (Fig. 15). A higher fractal dimension seems to correspond to the achievement of “steady-state” conditions and could somehow constrain d_w , but this method has not been attempted on natural samples.

5.4. Energy partitioning of an earthquake

As previously discussed, it is presently impossible to evaluate the heat (which is related to the absolute level of shear stress

during seismic slip) and the surface energy from seismological data. For this reason, several attempts have been made recently to determine the surface energy from samples obtained from boreholes along active fault zones (Chelungpu Fault, Ma et al., 2006) or in exhumed faults (Punchbowl Fault, Chester et al., 2005; Gole Larghe Fault, 10 km depth, Pittarello et al., 2008). In all these cases, the surface energy is estimated by measuring the clast size distribution and the fracture density in the wall rocks produced during rupture propagation (Chester et al., 2005):

$$Us = (A_{SZ} + A_{DZ})\gamma \quad [Jm^{-2}] \quad (8)$$

where A_{SZ} and A_{DZ} are the new surface per unit fault area (A_{SZ} and A_{DZ} are dimensionless) produced in the slipping zone (SZ) and in the damage zone (DZ, the wall rocks), respectively, and γ is the specific surface energy ($1–10 J m^{-2}$ in silica-bearing minerals). It is critical to recognize if the fractures, microfractures, and new grains are associated with only a single seismic event, a very difficult task in

faults that do not bear pseudotachylites. In cases where more than one slip event occurred, the significance of the measured surface area, and of the estimated surface energy, should be discussed in detail. In this case, the estimated surface energy per unit fault area can be divided by the number of “type” earthquakes that might have propagated through the studied fault (Chester et al., 2005). The main result of these investigations to date (Chester et al., 2005; Ma et al., 2006) is that surface fracture energy is just a small fraction of the so-called fracture energy (the remnant being heat).

In the case of pseudotachylite-bearing faults, it might be possible to separately determine both heat and fracture surface energy from field and microstructural analysis of a fault segment (Pittarello et al., 2008). Heat can be calculated from the thickness of a pseudotachylite (Di Toro et al., 2005a,b):

$$Q = [H(1 - \phi) + Cp(T_m - T_{hr})] \rho w_{av} \left[\text{Jm}^{-2} \right] \quad (9)$$

whereas the surface fracture energy produced during rupture propagation can be determined from Eq. (8). In the case of frictional melting, fragmented clasts are assimilated into the melt. However, it is possible that grain sintering occurs to some degree (Togo and Shimamoto, in press). Finite Element Method (FEM) modeling (Pittarello et al., 2009) shows that the initial clast size distribution (so the fragmentation produced at the rupture tip during the early stages of slip and melting) may be preserved inside larger clasts aggregates, especially if located near the wall rocks or in thin veins, where cooling rates are very fast. The measured fragment distribution inside larger clast aggregates can be integrated across the whole slipping zone thickness assuming that all the rock passed through this ultracomminution stage before being melted. In a pseudotachylite-bearing fault segment from the Gole Larghe Fault Zone, Q was estimated as $\sim 27 \text{ MJ m}^{-2}$, whereas fracture surface energy was limited to less than 0.4 MJ m^{-2} (Pittarello et al., 2008). It follows that in the case of a fault segment exhumed from 10 km depth, frictional heat is probably the largest energy sink and at such depths earthquakes are mainly a thermal process. Moreover, earthquake rupture modeling for the same fault segment yielded a breakdown work of $8\text{--}67 \text{ MJ/m}^2$ (Di Toro et al., 2005b), suggesting that in this case, surface fracture energy (0.4 MJ/m^2) is a small fraction of the breakdown work. This result is consistent with seismological and theoretical work (Cocco and Tinti, 2008).

6. Extrapolation of laboratory results to natural conditions – how well do laboratory friction experiments simulate earthquake ruptures along natural faults?

As explained in the Introduction, linking results from laboratory experiments and observations on exhumed fault zones is an extremely promising strategy for developing realistic models of earthquakes and on the mechanics of faulting in general. However, this is also a very challenging task, and issues stem from the change of scale and reference framework implicit when going from the laboratory to a large-scale model of a natural fault zone. Ben-Zion and Sammis (2003) evidenced how different aspects of a fault zone may be alternatively described in different frameworks: (i) as a continuous, smooth surface embedded in a continuous solid (continuum-Euclidean framework), (ii) as a shear zone composed of a heterogeneous granular material (granular framework), or (iii) as a collection of rough objects with a branching geometry, showing an increasing complexity as the observation scale decreases (fractal framework). Only in the first case geometrical, morphological and material properties vary continuously and smoothly, and only in this case fundamental continuum mechanics quantities, like stress and strain, can be defined. Hence, a straightforward extrapolation to natural faults of constitutive relations and

other properties defined in the lab will be possible only when the continuum-Euclidean framework can be used, and strong limitations will appear in the other two cases.

Even if we choose the simple continuum-Euclidean description framework, going from the lab to nature requires changes of scale and reference frames. Faults in structural geology and earthquake seismology are typically viewed in a Lagrangian frame of reference where deformation is described by tracking the flow of material coordinates from an initial to a deformed state. High speed laboratory rock friction experiments, on the other hand, are by-and-large one-dimensional physical models where fault slip is idealized as occurring at a point along a fault (Fig. 13a). This set-up is akin to a Eulerian frame of reference, where deformation is described in the current spatial state and no attempt is made to track material particles through space. Instead of varying spatially, the frictional parameter varies at a stationary point with time, slip, velocity, and, in some cases, normal stress while sliding rock material flows through the reference point. The advantage of this latter set-up is that experiments can simulate very large strains, in terms of the amount of slip accumulated on the interface, and the entire slip history at a point on a theoretical earthquake fault, from the passage of the rupture front to the passage of the trailing edge of the rupture, can be simulated, for example, by varying the slip velocity throughout an experiment (e.g. Sone and Shimamoto, 2009, and Fig. 13a). However, this model set-up necessitates the idealization of the “laboratory fault” as a flat plane with similar material properties along the length of the entire fault.

Attributing material properties defined in this kind of laboratory framework to natural faults, and using experimental results in numerical models is possible if the natural fault is represented in the continuum-Euclidean framework (Ben-Zion and Sammis, 2003), as in this case a continuous description (requiring some averaging) of heterogeneous material and geometrical properties is possible at the relevant length and time scales. In the following we discuss problems related to (1) the geometrical/topological heterogeneity and complexity of natural faults (as compared to their simplicity in experiments), (2) the role of material heterogeneity, and (3) the spatial finiteness of natural faults and/or fault rupture patches, which contrasts with the absence of a shear rupture tip in high velocity friction experiments. All three of these factors can result to various extents in stress heterogeneities along the fault complicating the extrapolation of laboratory results to natural faults.

6.1. Effects of fault geometry

Natural fault surfaces are not planar and show a finite thickness – hence the term fault “surface” and “zone” is used instead of fault “plane”, and generally show different kinds of geometrical complexity: (1) a waviness or roughness along a single fault segment that, under some assumptions discussed in the following, can still be modeled as a continuous-Euclidean surface, (2) a “network” complexity that arises due to the interconnection of different fault segments with a certain characteristic length, (3) a “granular” complexity defined as in Ben-Zion and Sammis (2003), which again may be relevant only at a certain length scale, and finally (4) “roughness” or “network” complexities which do not show a characteristic scale, but are replicated self-similarly at all scales, hence should be described as fractals. Examples of the four kinds of complexity, relevant to earthquake mechanics, are respectively: (1) fault surface waviness/roughness, either limited to certain wavelengths or which do not show a characteristic length but decays with wavelength (self-affine roughness); (2) structures such as stepovers, jogs, sidewall ripouts (very often observed in pseudotachylite-bearing faults), etc.; (3) layers of fault gouge or

other heterogeneous fault rocks occurring very often along large mature faults, and; (4) truly self-similar fault surface roughness (extended at all scales) and self-similar fault networks.

In the last case, for strictly self-similar objects or collections of objects, very fundamental quantities cannot be defined, such as the stress and strain tensor. If faults really belonged to this class of objects, as was proposed in many contributions particularly in the '80s (e.g. Power et al., 1987), extrapolating experimental results and implementing continuum mechanics models would not have been possible. However, recent published results indicate that faults do not show a truly self-similar roughness (see discussion below), hence modeling is possible, but still difficult. Considering the first three kinds of complexity, the stress field is expected to vary spatially and temporally along the fault (Berger and Johnson, 1980; Saucier et al., 1992; Chester and Fletcher, 1997; Chester and Chester, 2000; Griffith et al., 2009c, 2010), with complex feedbacks with material properties and constitutive equations (e.g. Griffith et al., 2010).

The third kind of geometrical complexity – the presence of a granular layer along the fault zone, is generally satisfactorily confronted by upscaling or homogenization techniques, which allow to obtain the average mechanical properties of the gouge layer. The fault is then described as a surface instead of a layer.

The second kind of heterogeneity, related to the presence of stepovers, branching faults, sidewall ripouts, etc., has been considered in a rich bibliography dealing with stress inhomogeneity, stress transfer and earthquake triggering in a fault network (e.g. Segall and Pollard, 1980; Stein, 1999; King et al., 1994; Toda et al., 2005). This kind of approach is possible with a generalization of the continuum-Euclidean framework, where each fault is seen as a continuous surface in a continuous volume. Hence, only a finite number of fault segments can be considered and fractal fault networks, with a large number of very small structures, cannot be considered. The complexity of this kind of models, in any case, allowed to develop only quasi-static models so far.

Finally, considering the first kind of geometrical complexity, we find that in most cases the waviness or roughness of natural faults is replicated across such a wide range of wavelengths (from microns to kilometers) that faults can be described as self-affine fractal surfaces, where roughness decays with wavelength according to a power law with a Hurst exponent <1 (e.g. Lee and Bruhn, 1996; Candela et al., 2009; Bistacchi et al., 2011). This means that faults show a more pronounced roughness at small wavelengths, or that small wavelength asperities are comparably "steeper" than large-scale ones. This conclusion is in accordance to the common observation that fault surfaces are irregular when seen from a close distance, but tend to appear as straight lines when seen in a satellite image or drawn on a map. This observation justifies the very general application of the continuum-Euclidean framework, because faults tend to be smooth at the largest scales.

As a historical note, it must be noted that a quantitative assessment of this observation is quite recent and is due to the availability of precise measurement methodologies, such as LIDAR and photogrammetry (e.g. Sagy et al., 2007; Candela et al., 2009; Bistacchi et al., 2011). Older works, carried out with profilometers (e.g. Power et al., 1987; Lee and Bruhn, 1996), indicated a self-similar behavior for fault roughness, where roughness would have been replicated identically at every length scale (contradicting the above-mentioned observation). Where the older and newer works agree, is in detecting the anisotropic character of fault surfaces, which are smoother parallel to the slip direction due to generalized "wear" processes (e.g. Power et al., 1987; Lee and Bruhn, 1996).

Still considering the "single fault surface" continuous-Euclidean framework, fault roughness can be included in models up to a certain spatial resolution, which is the spatial resolution of the

mesh used in the model. In this kind of model, roughness causes local variations in the stress and displacement fields, so that the deformation pattern may deviate significantly from that expected for a straight fault (e.g. Berger and Johnson, 1980; Saucier et al., 1992; Chester and Fletcher, 1997; Chester and Chester, 2000; Griffith et al., 2010). In the following we summarize some examples of the complex feedbacks that arise in these models.

Static resistance to slip of a rough fault (Fig. 17a) is higher than that of its smooth counterpart in elastic, brittle-elastic or elasto-plastic models with a steady friction coefficient (Nielsen and Knopoff, 1998; Dieterich and Smith, 2009; Brodsky et al., 2011). In this case, the interlocking asperities should be deformed, or strong dilatancy should develop so that slip can occur (this is well known and extensively exploited in engineering rock mechanics, e.g. Barton and Choubey, 1977). Since dilatancy is not likely to occur at high confining stresses, elastic models hypothesize a "flattening" of asperities (Fig. 17b), resulting in an increase of normal stress as a reaction to this elastic deformation (e.g. Schmittbuhl et al., 2006), which in turn results in an increased bulk tangential strength. On the other hand, brittle or plastic models require a decapitation or ploughing of asperities (Fig. 17c) which results in an evolution of the fault's mechanical properties with accumulating slip, and produces a fault gouge layer according to some wear law (e.g. Power et al., 1987).

Considering dynamic fracture propagation, Okubo and Dieterich (1984) showed experimental evidence for lower rupture velocities, larger critical slip weakening distances, and larger fracture energies for slip on rough (rms roughness = 80 μm) versus smooth (rms roughness = 0.2 μm) fault surfaces. Clearly, non-planarity on rough or "wavy" fault surfaces exerts an important control on the parameters affecting dynamic fault friction and thus the energy budget of earthquakes.

With somehow different results, Griffith et al. (2010) studied the effects of fault non-planarity on the distribution of both slip and off-fault damage in a melt-lubricated wavy fault. They show that the effect of geometric barriers (waviness) on retarding slip is at least partially counteracted by (1) opening and (2) enhancement of temperature-related weakening mechanisms due to elevated normal stress in contractional bends (Fig. 17d). Weakening is accelerated in restraining bends, where normal stresses are enhanced. This is consistent with field observations of multiple weakening mechanisms acting during individual ruptures along a single fault entirely contained in a single, effectively homogeneous rock body (Kirkpatrick and Shipton, 2009). Weakening and increased slip in restraining bends are transferred to releasing bends as larger opening displacements (Griffith et al., 2010). Because the walls of the fault are no longer in contact, friction effectively drops to zero in the latter segments. With fault weakening in both contractional and extensional bends, it is more reasonable to extrapolate experimental results regarding frictional weakening to natural faults, at least for relatively small faults that can be described as single Euclidean surfaces, as extreme weakening at a few points along a fault should be nearly equivalent to homogeneous weakening across an entire fault. If anything, since laboratory friction tests are typically performed at normal stresses far below those expected at asperities at seismogenic depths, laboratory friction tests may actually underestimate the overall weakening behavior of non-planar faults at depth, although further work needs to be done to confirm this assertion.

6.2. Effects of material heterogeneity

Material properties (e.g. elastic modulus, permeability, melt temperature, mineral and chemical composition, etc.) may vary along fault strike, or, particularly in the case of large displacement faults, across the fault interface, due to juxtaposition of different

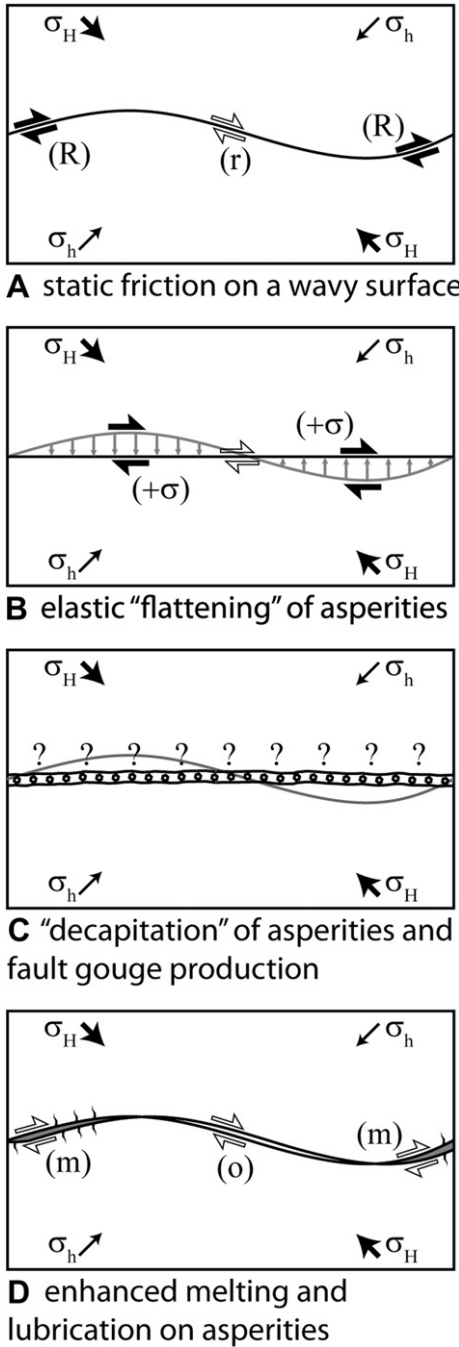


Fig. 17. The effect of fault surface waviness on fault strength. (a) In a simplified static reference model, normal stress is enhanced in restraining bends (R) and reduced in releasing bends (r), resulting in a proportional fault strength variation. (b) In models based on elastic "flattening" of asperities, normal stress is enhanced ($+σ$) proportionally to asperity elevation. (c) In models based on brittle/plastic deformation of asperities, a fault gouge layer is produced, and the mechanical properties of the fault then depend on properties of the gouge. (d) In models including frictional melting, a generalized weakening is observed, depending on enhanced melting (m) in restraining bends and opening in releasing bends (o). In all sketches maximum ($σ_H$) and minimum ($σ_h$) regional background principal stresses for a strike-slip environment are represented.

lithostratigraphic units (e.g. Graymer et al., 2005). In addition, material heterogeneity may be a result of lithologic variability, or due to structurally-induced heterogeneity in the form of micro-cracks, pulverized rocks (Section 4.4 and Reches and Dewers, 2005), or large, discrete, intergranular fractures (Griffith et al., 2009c). Material heterogeneity may result in a variation of frictional

properties as well as variable distributions of individual stress components along the fault (e.g. De Paola et al., 2008; Collettini et al., 2009). For example, at a small scale the polycrystalline nature of rocks results in enormously heterogeneous materials in terms of melting temperature and indentation hardness (Spray, 1992). For seismic slip rates on such rocks, this can result in enhanced roughness development due to preferential melting of lower melting point minerals such as biotite (Nielsen et al., 2010a). The roughness of the melting surface decreases with increasing melting rate, a quantity depending on the heat production rate (see Section 5.3 and Fig. 15). Therefore, in cases where friction melting is the primary weakening mechanism, one might expect smoother fault surfaces in contractional bends of a fault where fault-normal stress is more compressive than in extensional bends (Griffith et al., 2010).

6.3. Spatially varying friction: the effects of fault and fault rupture patch finiteness

The increased resistance to slip simulated by fault models with spatially varying friction is related to physical processes acting along the fault. Cooke (1997) suggests that the physical processes leading to varying friction on natural faults may include frictional wear of the sliding surfaces (e.g. Power et al., 1987; Sagy et al., 2007), decreased fault gouge grain size with increasing slip (Morrow and Byerlee, 1989; Gu and Wong, 1994) or increased gouge thickness (Biegel et al., 1989). Increased resistance to slip may also be related to inelastic deformation in the host rock (e.g. Cowie and Scholz, 1992) or microstructural weakening (or strengthening) processes acting within the faults (e.g. Palmer and Rice, 1973). It is clear that regardless the model of spatially varying friction or traction, the slip magnitude may vary considerably along otherwise planar faults. The effect that resulting local slip (or slip rate) gradients, or gradients in normal stress have on the effective frictional behavior of faults is unclear, for, as is the case with non-planar faults, the spatially constant slip rate boundary conditions present in laboratory friction simulations differs significantly.

Cases in which the friction or traction variations are concentrated at the tip of faults or moving slip patches fall into the general class of "cohesive endzone" crack models (Dugdale, 1960; Barenblatt, 1962; Ida, 1972; Palmer and Rice, 1973; Rudnicki, 1980). Cohesive endzone models simulate (1) changes in frictional strength of faults (or moving slip patches) in finite zones near their tips and (2) spatial gradients in the local stress fields by applying either linear or non-linear traction distributions along the fault plane which act to resist the driving stress, thereby eliminating physically impossible infinite stress concentrations at the crack tip which are a prominent feature of Linear Elastic Fracture Mechanics models. Depending on the formation of the cohesive endzone model, the length of the endzone (roughly the dimension of the process zone) can be directly related to measurable parameters defining the friction constitutive law, most notably the slip weakening distance, d_w (e.g. Rice, 1980). The increased resistance near fault terminations in endzone models typically results in slip distributions with a bell-shaped curve; however, asymmetries in the slip distribution may also be achieved by applying a linearly varying stress distribution along the fault (e.g. Bürgmann et al., 1994). It is important to note that for the case of friction gradients, the endzone size and exact nature (i.e. slope) of the gradient exerts an important control on the stress field near the endzone (Martel, 1997; Willemse and Pollard, 1998).

6.4. Influence on scaling experiments to nature

Each of the three factors listed above can induce spatial variability in slip, slip rate, weakening mechanisms, and tractions acting

on natural faults. Clearly, taking such spatial heterogeneity into account in the laboratory is not currently feasible. Recent advances in numerical simulation techniques are beginning to allow the incorporation of heterogeneity in the form of non-planar geometries (e.g. Dunham et al., 2011a,b) and weakening behaviors (e.g. Noda and Lapusta, 2010). In addition, a better understanding of the dependence of friction constitutive behavior on normal stress (e.g. Nielsen et al., 2010b; Niemeijer et al., 2011) will allow laboratory and field studies of earthquake rupture to be more intimately linked.

To date, the bulk of numerical simulations concerning the influence of friction on natural (non-planar) faults have been of the quasi-static variety as described above (e.g. Lovely et al., 2009; Griffith et al., 2010). Dynamic simulations have been limited either to straight synthetic or highly idealized straight natural faults (e.g. Andrews, 1976; Day, 1982; Olsen et al., 1997). The development of codes capable of dynamic simulations of frictional slip on non-planar faults, incorporating laboratory friction laws, is an active area of research (Dunham et al., 2011a,b) and should provide critical insights into the efficacy of scaling laboratory-derived friction laws to natural faults. Preliminary results of such simulations indicate that ruptures become extremely sensitive to fault roughness and exhibit significant fluctuations in rupture velocity (Dunham et al., 2011a,b), apparently consistent with experimental observations (Okubo and Dieterich, 1984).

7. Future challenges and open questions

Despite (or perhaps thanks to) significant technological advances in the fields of experimental geology (emergence of HVRF apparatuses), field geology (LIDAR, photogrammetry) and numerical modeling (increased computer power), there are many questions and problems that need to be tackled, some of which have been mentioned in the previous sections. In the following, we will discuss some issues that we believe will be important to resolve in order to obtain a better understanding of earthquake mechanics.

7.1. From the field geology side

From Section 4, it is clear that it remains a challenge to recognize fossil seismic ruptures in outcrops of exhumed fault zones. Apart from the occurrence of pseudotachylites, the most promising indicator of seismic slip is represented by clast aggregates, either formed by clay minerals or by carbonates. Recognition of aggregated clasts in rocks that experienced seismic slip does not preclude the possibility that these grains formed at lower velocities as well. A way to clarify this point is to perform laboratory experiments that can help in mapping out the stress, velocity and ambient (e.g. presence of fluids, ambient temperature) conditions under which such grains should occur and thus help in constraining the conditions of formation. Furthermore, chemical studies of fault rocks and careful consideration of the thermodynamics of the possible chemical reactions can constrain the peak temperatures reached in this kind of process. It is unclear, however, over what time period the signature of a thermal event (due to seismic slip) can be preserved in natural fault rocks and how these signatures might be reset or offset. Field-based geology studies might constrain several physical fault zone properties which are relevant for theoretical modeling of weakening processes (and for their occurrence in nature). For instance, models of thermal pressurization are limited by the poor knowledge of the coseismic permeability in the wall rocks: the analysis of sealed microfractures (e.g. density of fluid inclusion trails) might yield some constraints on this.

Despite being central in field-based studies of exhumed fault zones, finding evidence for fossil seismic ruptures is not the only concern in this kind of study. Actually, when the likelihood of

seismic behavior has been assessed, many more parameters should be collected in a detailed and quantitative way in order to form an overall picture of the earthquake process and of the “environmental” conditions in its source zone. The most important parameters are related to (1) base physical variables (P , T , etc.), (2) the stress field (regional background and local heterogeneities), (3) rock properties (composition, mechanical properties, chemical reactions), (4) presence or absence of fluids (composition, pressure and pressure variations, fluid-rock interactions), (5) fault zone geometry and architecture (see Section 6), and (6) fracture networks at all scales, including pulverization.

Parameters listed from points 1 to 4 can be reconstructed by means of structural and microstructural analysis, petrology (P , T , metamorphic and metasomatic reactions), paleostress field inversion (the necessity of obtaining reliable background stress data may revamp this kind of studies around important fault zones), laboratory experiments on fault rocks and their less deformed protoliths, and geochemical investigations, with emphasis on those regarding fluid–rock interaction (e.g. Mittempergher et al., 2009; De Paola et al., 2011b), but also including geochronological studies that may be very important in defining the regional tectonic and environmental conditions around a fault zone at the time of its activity (e.g. Pennacchioni et al., 2006).

Parameters listed at points 5 and 6 generally require special conditions to be studied. Fault zones are generally characterized by poor exposures, since they are very often highly fractured and altered, so they tend to be the site of enhanced weathering and correspond to areas covered by debris, occurring along valleys and depressions. Not many very good fault exposures (clean and continuous for kilometers, so at a length scale comparable to that of a moderate in magnitude earthquake) are available around the world, and some of the best have been extensively studied (see the examples of the Gole Larghe Fault Zone in Italy, or of the Fort Foster Brittle Zone in Maine). Other opportunities of detailed studies come from fault zones that have been drilled during mining or tunneling projects (Pretorius Fault, Heesakker et al., 2011a,b; Sprechenstein-Mules Fault, Bistacchi et al., 2010). In this case, the availability of different crosscutting mining shafts and boreholes, and in some case of outcrops some hundred meters above the boreholes, allows for a 3D reconstruction of fault zone architecture, which cannot be achieved in deep drilling projects on active faults, where data are collected essentially in 1D.

In all these examples, the focus has been placed mainly on the study of fundamental structural parameters, like fracture patterns, distribution and nature of fault rocks, measurement of slip and possibly slip gradients and heterogeneities, etc. In the last years, the availability of advanced surveying techniques (differential GPS, Lidar, photogrammetry) allowed to define all these parameters more and more quantitatively, and to effectively measure fault roughness (see Section 6). However, sometimes, the very abundant information requires some classification scheme to summarize the field data. This has been done for instance by Bistacchi et al. (2010) for fracturing in damage zones, represented in 3-dimensional models with the DI (Damage Index) parameter.

7.2. From the experimental side

Models of thermal pressurization predict that this is an efficient dynamic weakening mechanism under most wet crustal conditions. However, a poorly defined parameter in these models is the permeability of the actively slipping zone and the surrounding wall rock during dynamic slip. In fact, dynamic measurements of fault-parallel and fault-perpendicular permeability are scarce (one recent example can be found in Tanikawa et al., in press) and most of the existing data were acquired at low sliding velocities (e.g.

Zhang et al., 1999; Wibberley and Shimamoto, 2003; Faoro et al., 2009), mainly because of technical difficulties. Since the permeability structure and anisotropy of permeability of a fault zone undergoing active slip will most likely change drastically as a result of the intense stress field at the rupture tip, porosity increase, chemical reactions and pore fluid pressurization, potentially leading to hydrofracturing, experimental studies are necessary to investigate these effects. Obviously this kind of study should then be confronted with field observations of the kind considered above.

An even more challenging task deals with the fact that several dynamic weakening mechanisms have been discussed in this paper, but we still have limited possibilities to isolate individual weakening mechanisms in experiments to better understand the microphysics that underlie them. This will be necessary to be able to model the processes and reliably extrapolate laboratory results to natural conditions. If it proves to be impossible to isolate each weakening mechanism, the dominant weakening mechanism should be identified in a particular set of conditions and microphysical modeling is then required to extrapolate to natural conditions. Deformation maps will need to be constructed to identify the dominant mechanisms under fixed conditions of lithology, fluid pressure and composition, temperature, stress, slip, slip rate, acceleration and normal stress.

At the moment, it seems unlikely that a single equation can be found that reliably reproduces the details of friction evolution for the variety of weakening mechanisms. However, the fact that friction decays exponentially with slip at seismic slip rate, independently of the weakening mechanism involved, seems promising for a future finding of a general equation for friction evolution during earthquakes.

As high speed friction technology continues to advance, several important limitations of earlier studies might be tackled in the near future. Of these, the extension of previous work to higher normal stresses that approach natural conditions is in the process of being fulfilled (e.g. Niemeijer et al., 2011). Unfortunately, experiments on fault gouges are still limited to relatively low normal stresses (<3 MPa), due to the difficulty to confine samples without having too much contribution of the confining medium to the measured friction (and with the issue of the very large temperatures achieved at the interface between the confining medium and the sample). Other technological improvements that have been made or are likely to be made in the near future include adding a pore fluid system with controlled pore fluid pressure (and composition), the ability to confine specimens to better replicate natural stress conditions (e.g. to investigate the effect of mean stress), the possibility to run experiments imposing the shear stress (i.e. torque) rather than the slip rate to the samples (this will better replicate natural conditions), the application of a constant shear stress (torque) boundary condition instead of displacement, addition of environmental chambers that allow gas emissions from the sample to be measured and furnaces that heat the samples to temperatures typical at seismogenic depths. As all these technological advances are made, more high precision data will become available under a wide variety of deformation conditions and lithologies which will help in identifying the dominant weakening mechanisms during earthquake rupture.

7.3. Integration of field and laboratory data

We have discussed earlier how laboratory experiments might be used to identify microstructural and chemical signatures that geologists might look for in exhumed fault zones to identify fossil seismic slip. However, the ultimate goal is to use laboratory data to develop microphysical models that can be applied to large-scale numerical models of fault zones whose geometry and fault zone architecture is

based on field observations. Unfortunately, large-scale numerical models require significant computer power and the constitutive equations that govern the properties of the fault zone at each point can thus not be too complex. For instance, the melt lubrication model of Nielsen et al. (2008, 2010a,b) can only be solved numerically and is thus too demanding to be used in large-scale models. In the same way, geometrical complexity should be limited, and, whilst large wavelength roughness is not a big problem (self-affine roughness decays with wavelength), short wavelength roughness can be included only up to a certain spatial resolution. Can we simplify such models without losing the details of the microphysical processes? One possibility is to cast microphysical models into a rate-and-state frictional framework, since these equations have already been widely used in large-scale dynamic models. As such, we would need to describe the RSF parameters a , b and d_c (and possibly b_1 and d_{c2}) in terms of the microphysical model, so that we can reliably predict their values and variability under natural conditions.

Acknowledgments

We would like to thank Nicola De Paola and Nick Beeler for their criticisms and constructive comments, which helped to improve the manuscript. The authors remain responsible for the views expressed in this work. The authors contributed to each section specifically as follows: AN (Sections 1–4 and 7), GDT (Sections 1, 4, 5 and 7), WAG (Section 6), AB (Sections 3 and 6), SS (Section 4), SN (Sections 3 and 5). All authors contributed to the general review of manuscript before submission. This research was funded by the European Research Council Starting Grant Project No. 205175 and by Netherlands Organisation for Scientific Research (NWO) through VENI grant No. 863.09.013 (AN).

References

- Abercrombie, R.E., Rice, R.J., 2005. Can observations of earthquake scaling constrain slip weakening? *Geophysical Journal International* 162, 406–424.
- Abercrombie, R., McGarr, A., Di Toro, G., Kanamori, H., 2006. Earthquakes: Radiated Energy and the Physics of Faulting. In: *Geophysical Monograph*, vol. 170. American Geophysical Union, Washington D.C., USA.
- Agosta, F., Aydin, A., 2006. Architecture and deformation mechanism of a basin-bounding normal fault in Mesozoic platform carbonates, central Italy. *Journal of Structural Geology* 28 (8), 1445–1467.
- Agrinier, P., Deutsch, A., Schärer, U., Martínez, I., 2001. Fast back-reactions of shock-released CO₂ from carbonates: an experimental approach. *Geochimica et Cosmochimica Acta* 65 (15), 2615–2632.
- Allen, J.L., 2005. A multi-kilometer pseudotachylite system as an exhumed record of earthquake rupture geometry at hypocentral depths (Colorado, USA). *Tectonophysics* 402 (1–4), 37–54.
- Anders, M.H., Aharonov, E., Walsh, J.J., 2000. Stratification of granular media at the base of large slide blocks: implications for mode of emplacement. *Geology* 28, 971–974.
- Anders, M.H., Fouke, B.W., Zerkle, A.L., Tavarnelli, E., Alvarez, W., Harlow, G.E., 2010. The role of calcining and basal fluidization in the long runout of carbonate slides: an example from the Heart Mountain slide block, Wyoming and Montana, U.S.A. *Journal of Geology* 118, 577–599.
- Andersen, T.B., Mair, K., Austrheim, H., Podladchikov, Y.Y., Vrijmoed, J.C., 2008. Stress-release in exhumed intermediate-deep earthquakes determined from ultramafic pseudotachylite. *Geology* 36, 995–998.
- Andrews, D.J., 1976. Rupture propagation with finite stress in antiplane strain. *Journal of Geophysical Research* 81 (20), 3575–3582.
- Andrews, D.J., 2005. Rupture dynamics with energy loss outside the slip zone. *Journal of Geophysical Research* 110 (B1), B01307.
- Bakun, W.H., Aagaard, B., Dost, B., Ellsworth, W.L., Hardebeck, J.L., Harris, R.A., Ji, C., Johnston, M.J.S., Langbein, J., Lienkaemper, J.J., Michael, A.J., Murray, J.R., Nadeau, R.M., Reasenberg, P.A., Reichle, M.S., Roeloffs, E.A., Shakal, A., Simpson, R.W., Waldhauser, F., 2005. Implications for prediction and hazard assessment from the 2004 Parkfield Earthquake – Parkfield. *Nature* 437, 969–974.
- Barenblatt, G.I., 1962. The mathematical theory of equilibrium cracks in brittle fracture. *Advances in Applied Mechanics* 7, 55–129.
- Barker, S.L.L., 2005. Pseudotachylite-generating faults in Central Otago, New Zealand. *Tectonophysics* 397, 211–223.
- Barton, N., Choubey, V., 1977. The shear strength of rock joints in theory and practice. *Rock Mechanics and Rock Engineering* 10 (1–2), 1–54. doi:10.1007/BF01261801.

- Beeler, N.M., Tullis, T.E., 1996. Self-healing slip pulse in dynamic rupture models due to velocity dependent strength. *Bulletin of the Seismological Society of America* 86, 1130–1148.
- Beeler, N.M., Tullis, T.E., Weeks, J.D., 1994. The roles of time and displacement in the evolution effect in rock friction. *Geophysical Research Letters* 21, 1987–1990.
- Beeler, N.M., Tullis, T.E., Goldsby, D.L., 2008. Constitutive relationships and physical basis of fault strength due to flash heating. *Journal of Geophysical Research* 113 (B01401). doi:10.1029/2007JB004988.
- Beeler, N.M., 2006. Inferring earthquake source properties from laboratory observations and the scope of lab contributions to source physics. In: Abercrombie, R., McGarr, A., Di Toro, G., Kanamori, H. (Eds.), *Earthquakes: Radiated Energy and the Physics of Faulting*, vol. 170. American Geophysical Union, Washington D.C, pp. 121–134.
- Ben-Zion, Y., Sammis, C.G., 2003. Characterization of fault zones. *Pure and Applied Geophysics* 160 (3), 677–715.
- Ben-Zion, Y., Shi, Z.Q., 2005. Dynamic rupture on a material interface with spontaneous generation of plastic strain in the bulk. *Earth and Planetary Science Letters* 236, 486–496.
- Berger, P., Johnson, A.M., 1980. First-order analysis of deformation of a thrust sheet moving over a ramp. *Tectonophysics* 70 (3–4), T9–T24.
- Beutner, E.C., Gerbi, G.P., 2005. Catastrophic emplacement of the Heart Mountain block slide, Wyoming and Montana, USA. *Geological Society of America Bulletin* 117 (5/6), 724–735.
- Biegel, R.L., Sammis, C.G., Dieterich, J.H., 1989. The frictional properties of a simulated gouge having a fractal particle distribution. *Journal of Structural Geology* 11 (7), 827–846.
- Bistacchi, A., Massironi, M., Menegon, L., 2010. Three-dimensional characterization of a crustal-scale fault zone: the Pusteria and Sprechenstein Fault system (Eastern Alps). *Journal of Structural Geology* 32 (12), 2022–2041.
- Bistacchi, A., Griffith, W.A., Smith, S.A., Di Toro, G., Jones, R., Nielsen, S., 2011. Fault roughness at seismogenic depths from LIDAR and photogrammetric analysis. *Pure and Applied Geophysics* 168, 2345–2363.
- Bizzarri, A., Cocco, M., 2003. Slip-weakening behavior during the propagation of dynamic ruptures obeying rate- and state-dependent friction laws. *Journal of Geophysical Research* 108 (B8). doi:10.1029/2002JB002198.
- Boatwright, J., 2007. The persistence of directivity in small earthquakes. *Bulletin of the Seismological Society of America* 97, 1850–1861.
- Bos, B., Peach, C.J., Spiers, C.J., 2000. Slip behavior of simulated gouge-bearing faults under conditions favoring pressure solution. *Journal of Geophysical Research* 105 (B7), 16669–16718.
- Boullier, A.-M., Ohtani, T., Fujimoto, K., Ito, H., Dubois, M., 2001. Fluid inclusions in pseudotachylites from the Nojima Fault, Japan. *Journal of Geophysical Research* 106 (B10), 21965–21977.
- Boullier, A.M., Yeh, E.-C., Boutareaud, S., Song, S.-R., Tsai, C.-H., 2009. Microscale anatomy of the 1999 Chi-Chi earthquake fault zone. *Geochemistry Geophysics Geosystems* 10 (3), Q03016. doi:10.1029/2008GC002252.
- Boullier, A.M., 2011. Fault-zone geology: lessons from drilling through the Nojima and Chelungpu Faults. In: Fagereng, Å., Toy, V.G., Rowland, J.V. (Eds.), *Geology of the Earthquake Source: a Volume in Honour of Rick Sibson*. Geological Society, London, Special Publications, vol. 359, pp. 17–37. doi:10.1144/SP359.2.
- Boutareaud, S., Calugaru, D.-G., Han, R., Fabbri, O., Mizoguchi, K., Tsutsumi, A., Shimamoto, T., 2008. Clay-clast aggregates: a new textural evidence for seismic fault sliding? *Geophysical Research Letters* 35 (5), L05302.
- Boutareaud, S., Boullier, A.-M., Andréani, M., Calugaru, D.-G., Beck, P., Song, S.-R., Shimamoto, T., 2010. Clay clast aggregates in gouges: new textural evidence for seismic faulting. *Journal of Geophysical Research* 115 (B2), B02408.
- Brantut, N., Schubnel, A., Rouzaud, J.N., Brunet, F., Shimamoto, T., 2008. High-velocity frictional properties of a clay-bearing fault gouge and implications for earthquake mechanics. *Journal of Geophysical Research* 113 (B10), B10401.
- Brantut, N., Schubnel, A., Corvisier, J., Sarout, J., 2010. Thermochemical pressurization of faults during coseismic slip. *Journal of Geophysical Research* 115 (B5), B05314.
- Brantut, N., Han, R., Shimamoto, T., Findling, N., Schubnel, A., 2011. Fast slip with inhibited temperature rise due to mineral dehydration: evidence from experiments on gypsum. *Geology* 39 (1), 59–62.
- Brodsky, E.E., Rowe, C.D., Meneghini, F., Moore, J.C., 2009. A geological fingerprint of low-viscosity fault fluids mobilized during an earthquake. *Journal of Geophysical Research* 114, B01303. doi:10.1029/2008JB005633.
- Brodsky, E.E., Gilchrist, J.G., Sagy, A., Colletini, C., 2011. Faults smooth gradually as a function of slip. *Earth and Planetary Science Letters* 302 (1–2), 185–193.
- Brune, J.N., 2001. Fault normal dynamic loading and unloading: an explanation for “non-gouge” rock powder and lack of fault-parallel shear bands along the San Andreas Fault. *EOS, Transactions, American Geophysical Union* 82 (Abstract).
- Bürgmann, R., Pollard, D.D., Martel, S.J., 1994. Slip distributions on faults: effects of stress gradients, inelastic deformation, heterogeneous host-rock stiffness, and fault interaction. *Journal of Structural Geology* 16 (12), 1675–1690.
- Candela, T., Renard, F., Bouchon, M., Brouste, A., Marsan, D., Schmittbuhl, J., Voisin, C., 2009. Characterization of fault roughness at various scales: implications of three-dimensional high resolution topography measurements. *Pure and Applied Geophysics* 166 (10), 1817–1851.
- Carlslaw, H.S., Jaeger, J.C., 1959. *Conduction of Heat in Solids*. Oxford University Press, USA.
- Chang, L., Zhang, Z., Zhang, H., Schlarb, A.K., 2006. On the sliding wear of nanoparticle filled polyamide 66 composites. *Composites Science and Technology* 66 (16), 3188–3198.
- Chester, F.M., Chester, J.S., 2000. Stress and deformation along wavy frictional faults. *Journal of Geophysical Research* 105 (B10), 23421–23430.
- Chester, J.S., Fletcher, R.C., 1997. Stress distribution and failure in anisotropic rock near a bend on a weak fault. *Journal of Geophysical Research* 102 (B1), 693–708.
- Chester, J.S., Chester, F.M., Kronenberg, A.K., 2005. Fracture surface energy of the Punchbowl Fault, San Andreas System. *Nature* 437, 133–136.
- Chioldini, C., Cioni, R., 1989. Gas geochemistry for hydrothermal systems and its application to some Italian geothermal areas. *Applied Geochemistry* 4 (5), 465–472.
- Cirella, A., Piatanesi, M., Cocco, E., Tinti, L., Scognamiglio, A., Michelini, A., Lomax, E., Boschi, 2009. Rupture history of the 2009 L'Aquila (Italy) earthquake from non-linear joint inversion of strong motion and GPS data. *Geophysical Research Letters* 36, L19304. doi:10.1029/2009GL039795.
- Cocco, M., Tinti, E., 2008. Scale dependence in the dynamics of earthquake propagation: evidence from seismological and geological observations. *Earth and Planetary Science Letters* 273, 123–131.
- Cocco, M., Spudich, P., Tinti, E., 2006. On the mechanical work absorbed on faults during earthquake ruptures. In: Abercrombie, R., McGarr, A., Di Toro, G., Kanamori, H. (Eds.), *Earthquakes: Radiated Energy and the Physics of Faulting*. Geophysical Monograph Series, vol. 170. American Geophysical Union, Washington, D.C, pp. 237–254.
- Cocco, M., Tinti, E., Marone, C., Piatanesi, A., 2009. Scaling of slip weakening distance with final slip during dynamic earthquake rupture. In: Fukuyama, Eiichi (Ed.), *Fault-zone Properties and Earthquake Rupture Dynamics*. International Geophysics Series. Elsevier, pp. 163–186.
- Collettini, C., De Paola, N., Faulkner, D.R., 2009. Insights on the geometry and mechanics of the Umbria–Marche earthquake (Central Italy) from the integration of field and laboratory data. *Tectonophysics* 476 (1–2), 99–109.
- Cooke, M.L., 1997. Fracture localization along faults with spatially varying friction. *Journal of Geophysical Research* 102 (B10), 22425–22434.
- Cowan, D.S., 1999. Do faults preserve a record of seismic slip? A field geologist's opinion. *Journal of Structural Geology* 21 (8–9), 995–1001.
- Cowie, P.A., Scholz, C.H., 1992. Physical explanation for the displacement-length relationship of faults using a post-yield fracture mechanics model. *Journal of Structural Geology* 14 (10), 1133–1148.
- D'Amico, S., Koper, K.D., Herrmann, R.B., Akinci, A., Malagnini, L., 2010. Imaging the rupture of the Mw 6.3 April 6, 2009 L'Aquila, Italy earthquake using back-projection of teleseismic P-waves. *Geophysical Research Letters* 37, L03301. doi:10.1029/2009GL042156.
- Dahlen, F.A., 1977. The balance of energy in earthquake faulting. *Geophysical Journal of Royal Astronomical Society* 48, 239–261.
- Day, S.M., 1982. Three-dimensional finite difference simulation of fault dynamics: rectangular faults with fixed rupture velocity. *Bulletin of the Seismological Society of America* 72 (3), 705–727.
- De Paola, N., Collettini, C., Faulkner, D.R., Trippetta, F., 2008. Fault zone architecture and deformation processes within evaporitic rocks in the upper crust. *Tectonics* 27, TC4017. doi:10.1029/2007TC002230.
- De Paola, N., Hirose, T., Mitchell, T., Di Toro, G., Viti, C., Shimamoto, T., 2011a. Fault lubrication and earthquake propagation in thermally unstable rocks. *Geology* 39 (1), 35–38.
- De Paola, N., Chiodini, G., Hirose, T., Cardellini, C., Caliro, S., Shimamoto, T., 2011b. The geochemical signature caused by earthquake propagation in carbonate-hosted faults. *Earth and Planetary Science Letters* 310, 225–232.
- Del Gaudio, P., Di Toro, G., Han, R., Nielsen, S., Shimamoto, T., Cavallo, A., 2009. Frictional melting of peridotite and seismic slip. *Journal of Geophysical Research* 114, B06306. doi:10.1029/2008JB005990.
- Di Toro, G., Pennacchioni, G., 2004. Superheated friction-induced melts in zoned pseudotachylites within the Adamello tonalites (Italian Southern Alps). *Journal of Structural Geology* 26 (10), 1783–1801.
- Di Toro, G., Pennacchioni, G., 2005. Fault plane processes and mesoscopic structure of a strong-type seismogenic fault in tonalites (Adamello batholith, Southern Alps). *Tectonophysics* 402 (1–4), 55–80.
- Di Toro, G., Goldsby, D.L., Tullis, T.E., 2004. Friction falls towards zero in quartz rock as slip velocity approaches seismic rates. *Nature* 427, 436–439.
- Di Toro, G., Pennacchioni, G., Teza, G., 2005a. Can pseudotachylites be used to infer earthquake source parameters? An example of limitations in the study of exhumed faults. *Tectonophysics* 402 (1–4), 3–20.
- Di Toro, G., Nielsen, S., Pennacchioni, G., 2005b. Earthquake rupture dynamics frozen in exhumed ancient faults. *Nature* 436, 1009–1012.
- Di Toro, G., Hirose, T., Nielsen, S., Pennacchioni, G., Shimamoto, T., 2006a. Natural and experimental evidence of melt lubrication of faults during earthquakes. *Science* 311, 647–649.
- Di Toro, G., Hirose, T., Nielsen, S., Shimamoto, T., 2006b. Relating high-velocity rock friction experiments to coseismic slip. In: Abercrombie, R., McGarr, A., Di Toro, G., Kanamori, H. (Eds.), *Earthquakes: Radiated Energy and the Physics of Faulting*, vol. 170. American Geophysical Union, Washington D.C, pp. 121–134.
- Di Toro, G., Pennacchioni, G., Nielsen, S., Eiichi, F., 2009. Pseudotachylites and earthquake source mechanics. In: Fukuyama, E. (Ed.), *International Geophysics*, vol. 94. Academic Press, pp. 87–133.
- Di Toro, G., Niemeijer, A., Tripoli, A., Nielsen, S., Di Felice, F., Scarlato, P., Spada, G., Alessandrini, R., Romeo, G., Di Stefano, G., Smith, S., Spagnuolo, E., Mariano, S., 2010. From field geology to earthquake simulation: a new state-of-the-art tool to investigate rock friction during the seismic cycle (SHIVA). *Rendiconti Lincei*, 1–20.
- Di Toro, G., Han, R., Hirose, T., De Paola, N., Nielsen, S., Mizoguchi, K., Ferri, F., Cocco, M., Shimamoto, T., 2011. Fault lubrication during earthquakes. *Nature* 471, 494–498. doi:10.1038/nature09838.

- Dieterich, J.H., Smith, D.E., 2009. Nonplanar faults: mechanics of slip and off-fault damage. In: Ben-Zion, Y., Sammis, C.G. (Eds.), Mechanics, Structure and Evolution of Fault Zones. Pageoph Topical Volumes. Birkhäuser, Basel, pp. 1799–1815.
- Dieterich, J.H., 1978. Time-dependent friction and the mechanics of stick-slip. *Pure and Applied Geophysics* 116, 790–806.
- Dieterich, J.H., 1979. Modeling of rock friction 1. Experimental results and constitutive equations. *Journal of Geophysical Research* 84 (B5), 2162–2168.
- Dieterich, J.H., 1992. Earthquake nucleation on faults with rate-and-state-dependent strength. *Tectonophysics* 211 (1–4), 115–134.
- Dieterich, J., 1994. A constitutive law for rate of earthquake production and its application to earthquake clustering. *Journal of Geophysical Research* 99 (B2), 2601–2618.
- Doan, M.L., Gary, G., 2009. Rock pulverization at high strain rate near the San Andreas Fault. *Nature Geoscience* 2, 709–712.
- Dor, O., Ben-Zion, Y., Rockwell, T.K., Brune, J., 2006a. Pulverized rocks in the Mojave section of the San Andreas Fault Zone. *Earth and Planetary Science Letters* 245, 642–654.
- Dor, O., Rockwell, T.K., Ben-Zion, Y., 2006b. Geological observations of damage asymmetry in the structure of the San Jacinto, San Andreas and Punchbowl faults in Southern California: a possible indicator for preferred rupture propagation direction. *Pure and Applied Geophysics* 163, 301–349.
- Dor, O., Yıldırım, C., Rockwell, T.K., Ben-Zion, Y., Emre, O., Sisk, M., Duman, T.Y., 2008. Geological and geomorphologic asymmetry across the rupture zones of the 1943 and 1944 earthquakes on the North Anatolian Fault: possible signals for preferred earthquake propagation direction. *Geophysical Journal International* 173, 483–504.
- Dor, O., Chester, J.S., Ben-Zion, Y., Brune, J.N., Rockwell, T.K., 2009. Characterization of damage in sandstones along the Mojave section of the San Andreas Fault: implications for the shallow extent of damage generation. *Pure and Applied Geophysics* 166, 1747–1773.
- Dugdale, D.S., 1960. Yielding of steel sheets containing slits. *Journal of the Mechanics and Physics of Solids* 8 (2), 100–104.
- Dunham, E.M., Belanger, D., Cong, L., Kozdon, J.E., 2011a. Earthquake ruptures with strongly rate-weakening friction and off-fault plasticity: 1. Planar faults. *Bulletin of the Seismological Society of America* 101, 2296–2307. doi:10.1785/020100075.
- Dunham, E.M., Belanger, D., Cong, L., Kozdon, J.E., 2011b. Earthquake ruptures with strongly rate-weakening friction and off-fault plasticity: 2. Nonplanar faults. *Bulletin of the Seismological Society of America* 101, 2308–2322. doi:10.1785/020100076.
- Ellsworth, W.L., Hickman, S.H., Zoback, M.D., 2000. Seismology in the source: the San Andreas Fault Observatory at Depth (SAFOD). *Seismological Research Letters* 71, 252 (abstract).
- Erismann, T., Heuberger, H., Preuss, E., 1977. Der Bimsstein von Köfels (Tirol), ein Bergsturz-„Frictionit“. *Mineralogy and Petrology* 24 (1), 67–119.
- Erismann, T., 1979. Mechanisms of large landslides. *Rock Mechanics and Rock Engineering* 12 (1), 15–46.
- Faoro, I., Niemeijer, A., Marone, C., Ellsworth, D., 2009. Influence of shear and deviatoric stress on the evolution of permeability in fractured rock. *Journal of Geophysical Research* 114, B01201. doi:10.1029/2007JB005372.
- Ferri, F., Di Toro, G., Hirose, T., Shimamoto, T., 2010. Evidences of thermal pressurization in high velocity friction experiments on smectite-rich gouges. *Terra Nova*. doi:10.1111/j.1365-3121.2010.00955.x.
- Fialko, Y., Khazan, Y., 2005. Fusion by earthquake fault friction: stick or slip? *Journal of Geophysical Research* 110, B12407. doi:10.1029/2005JB003869.
- Fisher, T.E., 1988. Triboochemistry. *Annual Review of Materials Science* 18, 303–323.
- Fox, P.G., 1975. Mechanically initiated chemical reactions in solids. *Journal of Materials Science* 10, 340–360.
- Freund, L.B., 1998. Dynamic Fracture Mechanics. Cambridge University Press, Cambridge.
- Friedman, M., Logan, J.M., Rigert, J.A., 1974. Glass-indurated quartz gouge in sliding-friction experiments on sandstone. *Geological Society of America Bulletin* 85 (6), 937–942.
- Fukuyama, E., Madariaga, R., 1998. Rupture dynamics of a planar fault in a 3D elastic medium: rate- and slip-weakening friction. *Bulletin of the Seismological Society of America* 88 (1), 1–17.
- Fukuyama, E., Mikumo, T., Olsen, K.B., 2003. Estimation of the critical slip-weakening distance: theoretical background. *Bulletin of the Seismological Society of America* 93, 1835–1840.
- Galai, H., Pijolat, M., Nahdi, K., Trabelsi-Ayadi, M., 2007. Mechanism of growth of MgO and $CaCO_3$ during a dolomite partial decomposition. *Solid State Ionics* 178, 1039–1047.
- Giger, S.B., Cox, S.F., Tenthorey, E., 2008. Slip localization and fault weakening as a consequence of fault gouge strengthening – Insights from laboratory experiments. *Earth and Planetary Science Letters* 276 (1–2), 73–84.
- Goldsby, D.L., Tullis, T.E., 2002. Low frictional strength of quartz rocks at subseismic slip rates. *Geophysical Research Letters* 29 (17). doi:10.1029/2002GL015240.
- Goldsby, D.L., Tullis, T.E., 2011. Flash heating leads to low frictional strength of crustal rocks at earthquake slip rates. *Geology* 39, 216–218.
- Goren, L., Aharonov, E., Anders, M.H., 2010. The long runout of the Heart Mountain landslide: a chemo-thermo-poro-elastic mechanism. *Journal of Geophysical Research*. doi:10.1029/2009JB007113.
- Graymer, R.W., Ponce, D.A., Jachens, R.C., Simpson, R.W., Phelps, G.A., Wentworth, C.M., 2005. Three-dimensional geologic map of the Hayward Fault, northern California: correlation of rock units with variations in seismicity, creep rate, and fault dip. *Geology* 33, 521–524.
- Griffith, W.A., Di Toro, G., Pennacchioni, G., Pollard, D.D., 2008. Thin pseudotachylites in faults of the Mt. Abbot quadrangle, Sierra Nevada: physical constraints for small seismic slip events. *Journal of Structural Geology* 30 (9), 1086–1094.
- Griffith, W.A., Rosakis, A., Pollard, D., Ko, C.W., 2009a. Dynamic rupture experiments elucidate tensile crack development during propagating earthquake ruptures. *Geology* 37, 795–798.
- Griffith, W.A., Di Toro, G., Pennacchioni, G., Pollard, D.D., Nielsen, S., 2009b. Static stress drop associated with brittle slip events on exhumed faults. *Journal of Geophysical Research* 114, B02402.
- Griffith, W.A., Sanz, P.F., Pollard, D.D., 2009c. Influence of outcrop scale fractures on the effective stiffness of fault damage zone rocks. In: Ben-Zion, Y., Sammis, C. (Eds.), Mechanics, Structure and Evolution of Fault Zones. Pageoph Topical Volumes. Birkhäuser, Basel, pp. 1595–1627.
- Griffith, W.A., Nielsen, S., Di Toro, G., Smith, S.A.F., 2010. Rough faults, distributed weakening, and off-fault deformation. *Journal of Geophysical Research* 115 (B8), B08409.
- Gu, Y., Wong, T.-F., 1994. Development of shear localization in simulated quartz gouge: effect of cumulative slip and gouge particle size. *Pure and Applied Geophysics* 143 (1/2), 387–423.
- Guatteri, M., Spudich, P., 1998. Coseismic temporal changes of slip direction: the effect of absolute stress on dynamic rupture. *Bulletin of the Seismological Society of America* 88 (3), 777–789.
- Hamada, Y., Hirono, T., Ikebara, M., Soh, W., Song, S.-R., 2009. Estimated dynamic shear stress and frictional heat during the 1999 Taiwan Chi-Chi earthquake: a chemical kinetics approach with isothermal heating experiments. *Tectonophysics* 469, 73–84.
- Han, R., Shimamoto, T., Hirose, T., Ree, J.-H., Ando, J.-i., 2007a. Ultralow friction of carbonate faults caused by thermal decomposition. *Science* 316 (5826), 878–881.
- Han, R.H., Shimamoto, T., Ando, J.I., Ree, J.H., 2007b. Seismic slip record in carbonate-bearing fault zones: an insight from high-velocity friction experiments on siderite gouge. *Geology* 35 (12), 1131–1134.
- Han, R., Hirose, T., Shimamoto, T., 2010. Strong velocity weakening and powder lubrication of simulated carbonate faults at seismic slip rates. *Journal of Geophysical Research* 115 (B03412). doi:10.1029/2008JB006136.
- Hanks, T.C., 1977. Earthquake stress drops, ambient tectonic stresses and stresses that drive plate motions. *Pure and Applied Geophysics* 143, 441–458.
- Harris, R.A., Simpson, R.W., 1998. Suppression of large earthquakes by stress shadows: a comparison of Coulomb and rate-and-state failure. *Journal of Geophysical Research* 103 (B10), 24439–24451.
- Hayashi, N., Tsutsumi, A., 2010. Deformation textures and mechanical behavior of a hydrated amorphous silica formed along an experimentally produced fault in chert. *Geophysical Research Letters* 37 (12), L12305.
- Heaton, T.H., 1990. Evidence for and implications of self-healing pulses of slip in earthquake rupture. *Physics of the Earth and Planetary Interiors* 64 (1), 1–20.
- Heesakker, V., Murphy, S., Lockner, D.A., Reches, Z., 2011a. Earthquake rupture at focal depth: part 1: structure of the Pretorius Fault, TauTona mine, South Africa. *Pure and Applied Geophysics* 168, 2395–2425.
- Heesakker, V., Murphy, S., Reches, Z., 2011b. Earthquake rupture at focal depth: Part 2: the 2004 M2.2 earthquake along the Pretorius Fault. *Pure and Applied Geophysics* 168, 2427–2449.
- Heshmat, H., 1991. The Rheology and Hydrodynamics of dry powder lubrication. *Tribology Transactions* 34 (3), 433–439.
- Heshmat, H., 1995. The quasi-hydrodynamic mechanism of powder Lubricationâ€”Part III: on theory and rheology of triboparticulates. *Tribology Transactions* 38 (2), 269–276.
- Hirono, T., Hamada, Y., 2010. Specific heat capacity and thermal diffusivity and their temperature dependencies in a rock sample from adjacent to the Taiwan Chelungpu Fault. *Journal of Geophysical Research* 115, B05313. doi:10.1029/2009JB006816.
- Hirono, T., Lin, W., Yeh, E.-C., Soh, W., Hashimoto, Y., Sone, H., Matsubayashi, O., Aoike, K., Ito, H., Kinoshita, M., Murayama, M., Song, S.-R., Ma, K.-F., Hung, J.-H., Wang, C.-Y., Tsai, Y.-B., 2006. High magnetic susceptibility of fault gouge within Taiwan Chelungpu Fault: nondestructive continuous measurements of physical and chemical properties in fault rocks recovered from Hole B, TCDP. *Geophysical Research Letters* 33, L15303. doi:10.1029/2006GL026133.
- Hirono, T., Yokoyama, T., Hamada, Y., Tanikawa, W., Mishima, T., Ikebara, M., Famin, V., Tanizumi, M., Lin, W., Soh, W., Song, S.-R., 2007. A chemical kinetic approach to estimate dynamic shear stress during the 1999 Taiwan Chi-Chi earthquake. *Geophysical Research Letters* 34 (19), L19308.
- Hirose, T., Bystricky, M., 2007. Extreme dynamic weakening of faults during dehydration by coseismic shear heating. *Geophysical Research Letters* 34 (14), L14311.
- Hirose, T., Shimamoto, T., 2003. Fractal dimension of molten surfaces as a possible parameter to infer the slip-weakening distance of faults from natural pseudotachylites. *Journal of Structural Geology* 25 (10), 1569–1574.
- Hirose, T., Shimamoto, T., 2005a. Growth of molten zone as a mechanism of slip weakening of simulated faults in gabbro during frictional melting. *Journal of Geophysical Research* 110, B05202. doi:10.1029/2004JB003207.
- Hirose, T., Shimamoto, T., 2005b. Slip-weakening distance of faults during frictional melting as inferred from experimental and natural pseudotachylites. *Bulletin of the Seismological Society of America* 95 (5), 1666–1673.
- Ida, Y., 1972. Cohesive force across the tip of a longitudinal-shear crack and Griffith's specific surface energy. *Journal of Geophysical Research* 77 (20), 3796–3805.
- Ide, S., Takeo, M., 1997. Determination of the constitutive relation of fault slip based on wave analysis. *Journal of Geophysical Research* 102, 27,379–27,392.

- Imanishi, K., Ellsworth, W.L., 2006. Source scaling relationships of microearthquakes at Parkfield, CA, determined using the SAFOD pilot hole seismic array. In: Abercrombie, R., McGarr, A., Di Toro, G., Kanamori, H. (Eds.), *Earthquakes: Radiated Energy and the Physics of Faulting*. Geophysical Monograph Series, vol. 170. American Geophysical Union, Washington, D.C, pp. 81–90.
- Ishikawa, T., Tanimizu, M., Nagaishi, K., Matsuoka, J., Sakaguchi, M., Hirono, T., Mishima, T., Tanikawa, W., Lin, W., Kikuta, H., Soh, W., Song, S.-R., 2008. Coseismic fluid-rock interactions at high temperatures in the Chelungpu Fault. *Nature Geoscience* 1 (10), 679–683.
- Kame, N., Rice, J.R., Dmowska, R., 2003. Effects of prestress state and rupture velocity on dynamic fault branching. *Journal of Geophysical Research—Solid Earth* 108 (B5).
- Kanamori, H., Anderson, D.L., 1975. Theoretical basis of some empirical relations in seismology. *Bulletin of the Seismological Society of America* 65, 1073–1095.
- Kanamori, H., Brodsky, E.E., 2004. The physics of earthquakes. *Reports on Progress in Physics* 67 (8), 1429.
- Kanamori, H., Heaton, T., 2000. Microscopic and macroscopic physics of earthquakes. In: Rundle, J., Turcotte, D., Klein, W. (Eds.), *Geocomplexity and the Physics of Earthquakes*. Geophysical Monograph, vol. 20. American Geophysical Union, D.C, pp. 127–141.
- Kanamori, H., Rivera, L., 2006. Energy partitioning during an earthquake. In: Abercrombie, R., McGarr, A., Di Toro, G., Kanamori, H. (Eds.), *Earthquakes: Radiated Energy and the Physics of Faulting*. Geophysical Monograph Series, vol. 170. American Geophysical Union, Washington, D.C, pp. 3–13.
- Karner, S.L., Marone, C., 2001. Frictional restrengthening in simulated fault gouge: effect of shear load perturbations. *Journal of Geophysical Research* 106 (B9), 19319–19337.
- Karner, S.L., Marone, C., Evans, B., 1997. Laboratory study of fault healing and lithification in simulated fault gouge under hydrothermal conditions. *Tectonophysics* 277, 41–55.
- King, G.C.P., Stein, R.S., Lin, J., 1994. Static stress changes and the triggering of earthquakes. *Bulletin of the Seismological Society of America* 84, 935–953.
- Kirkpatrick, J.D., Shipton, Z.K., 2009. Geologic evidence for multiple slip weakening mechanisms during seismic slip in crystalline rock. *Journal of Geophysical Research* 114 (B12), B12401.
- Kirkpatrick, J.D., Shipton, Z.K., Evans, J.P., Micklithwaite, S., Lim, S.J., McKillop, P., 2008. Strike-slip fault terminations at seismogenic depths: the structure and kinematics of the Glacier Lakes Fault, Sierra Nevada United States. *Journal of Geophysical Research* 113 (B4), B04304.
- Kirkpatrick, J.D., Shipton, Z.K., Persano, C., 2009. Pseudotachylites; rarely generated, rarely preserved or rarely reported? *Bulletin of the Seismological Society of America* 99, 382–388.
- Kitajima, H., Chester, J.S., Chester, F.M., Shimamoto, T., 2010. High-speed friction of disaggregated ultracataclasite in rotary shear: characterization of frictional heating, mechanical behavior, and microstructure evolution. *Journal of Geophysical Research* 115 (B8), B08408.
- Kohli, A.H., Goldsby, D.L., Hirth, G., Tullis, T.E., 2011. Flash weakening of serpentinite at near-seismic slip rates. *Journal of Geophysical Research* 116, B03202. doi:10.1029/2010JB007833.
- Kostrov, B., Das, S., 1988. *Principles of Earthquake Source Mechanics*. Cambridge University Press, London.
- Kuo, L.-W., Song, S.-R., Huang, L., Yeh, E.-C., Chen, H.-F., 2011. Temperature estimates of coseismic heating in clay-rich fault gouges, the Chelungpu fault zones, Taiwan. *Tectonophysics* 502, 315–327.
- Kuroki, H., Ito, H.M., Takayama, H., Yoshida, A., 2004. 3-D simulation of the occurrence of slow slip events in the Tokai region with a rate- and state-dependent friction law. *Bulletin of the Seismological Society of America* 94 (6), 2037–2050.
- Lachenbruch, A.H., Sass, J.H., 1980. Heat flow and energetics of the San Andreas Fault Zone. *Journal of Geophysical Research* 85, 6185–6222.
- Lachenbruch, A.H., 1980. Frictional heating, fluid pressure and the resistance to fault motion. *Journal of Geophysical Research* 85 (B11), 6097–6112.
- Lee, J.-J., Bruhn, R.L., 1996. Structural anisotropy of normal fault surfaces. *Journal of Structural Geology* 18 (8), 1043–1059.
- Lee, W.H., Kanamori, H., Jennings, P.C., Kisslinger, C., 2002. *Earthquake and Engineering Seismology*. Academic Press, Amsterdam.
- Lewis, M.A., Peng, Z., Ben-Zion, Y., Vernon, F.L., 2005. Shallow seismic trapping structure in the San Jacinto Fault Zone near Anza, California. *Geophysical Journal International* 162, 867–881.
- Lin, A., Shimamoto, T., 1998. Selective melting processes as inferred from experimentally generated pseudotachylites. *Journal of Asian Earth Sciences* 16 (5–6), 533–545.
- Lin, A., Chen, C., Liu, C., Lee, C., Lin, C., Lin, P., Wen, S., Ouchi, T., 2001. Frictional fusion due to coseismic slip landsliding during the 1999 Chi-Chi (Taiwan) ML 7.3 earthquake. *Geophysical Research Letters* 28, 4011–4014.
- Lin, A., 1996. Injection veins of crushing-originated pseudotachylite and fault gouge formed during seismic faulting. *Engineering Geology* 43, 213–224.
- Lin, A., 2008. *Fossil Earthquakes: The Formation and Preservation of Pseudotachylites*. Springer.
- Liu, Y., Rice, J.R., 2005. Aseismic slip transients emerge spontaneously in three-dimensional rate and state modeling of subduction earthquake sequences. *Journal of Geophysical Research* 110 (B8), B08307.
- Lovely, P.J., Pollard, D.D., Mutlu, O., 2009. Regions of reduced static stress drop near fault tips for large strike-slip earthquakes. *Bulletin of the Seismological Society of America* 99 (3), 1691–1704.
- Lucier, A.M., Zoback, M.D., Heesakkers, V., Reches, Z., Murphy, S.K., 2008. Constraining the far-field in situ stress state near a deep South African gold mine. *International Journal of Rock Mechanics and Mining Sciences* 46 (3), 555–567. doi:10.1016/j.ijrmms.2008.09.005.
- Ma, K.-F., Brodsky, E.E., Mori, J., Ji, C., Song, T.-R.A., Kanamori, H., 2003. Evidence for fault lubrication during the 1999 Chi-Chi, Taiwan earthquake (Mw7.6). *Geophysical Research Letters* 30, 1244. doi:10.1029/2002GL015380.
- Ma, K.-F., Tanaka, H., Song, S.-R., Wang, C.-Y., Hung, J.-H., Tsai, Y.-B., Mori, J., Song, Y.-F., Yeh, E.-C., Soh, W., Sone, H., Kuo, L.-W., Wu, H.-Y., 2006. Slip zone and energetics of a large earthquake from the Taiwan Chelungpu-fault Drilling Project. *Nature* 444 (7118), 473–476.
- Maddock, R.H., Grocott, J., Van Nes, M., 1987. Vesicles, amygdales and similar structures in fault-generated pseudotachylites. *Lithos* 20, 419–432.
- Magloughlin, J.F., Spray, J.G., 1992. Frictional melting processes and products in geological materials: introduction and discussion. *Tectonophysics* 204 (3–4), 197–204.
- Mair, K., Marone, C., 1999. Friction of simulated fault gouge for a wide range of velocities and normal stresses. *Journal of Geophysical Research* 104 (B12), 28899–28914.
- Malagnini, L., Nielsen, S., Mayeda, K., Boschi, E., 2010. Energy radiation from intermediate- to large-magnitude earthquakes: implications for dynamic fault weakening. *Journal of Geophysical Research* 115, B06319. doi:10.1029/2009JB006786.
- Mandelbrot, B.B., 1967. How long is the coast of Britain? *Science* 156, 636–638.
- Marone, C., Kilgore, B., 1993. Scaling of the critical slip distance for seismic faulting with shear strain in fault zones. *Nature* 362, 618–621.
- Marone, C., 1998. Laboratory-derived friction laws and their application to seismic faulting. *Annual Review of Earth and Planetary Science* 26, 643–696.
- Martel, S.J., 1997. Effects of cohesive zones on small faults and implications for secondary fracturing and fault trace geometry. *Journal of Structural Geology* 19 (6), 835–847.
- Masch, L., Wenk, R.H., Preuss, E., 1985. Electron microscopy of hyalomylonites – Evidence for frictional melting in landslides. *Tectonophysics* 115, 131–160.
- Mayeda, K., Walter, W.R., 1996. Moment, energy, stress drop, and source spectra of western United States earthquakes from regional coda envelopes. *Journal of Geophysical Research* 101, 11,195–11,208.
- McGarr, A., Spottiswoode, S.M., Gay, N.C., 1975. Relationship of mine tremors to induced stresses and to rock properties in the focal region. *Bulletin of the Seismological Society of America* 65, 981–993.
- McKenzie, D., Brune, J.N., 1972. Melting on fault planes during large earthquakes. *Geophysical Journal of the Royal Astronomical Society* 29 (1), 65–78.
- Meneghini, F., Di Toro, G., Rowe, D.C., Moore, J.C., Tsutsumi, A., Yamaguchi, A., 2010. Record of mega-earthquakes in subduction thrusts: the black fault rocks of Pasagshak Point (Kodiak Island, Alaska). *Bulletin of the Geological Society of America* 122, 1280–1297. doi:10.1130/B30049.1.
- Miller, S.A., Collettini, C., Chiaraluce, L., Cocco, M., Barchi, M., Kaus, B.J.P., 2004. Aftershocks driven by a high-pressure CO₂ source at depth. *Nature* 427, 724–727.
- Mitchell, T.M., Ben-Zion, Y., Shimamoto, T., 2011. Pulverized fault rocks and damage asymmetry along the Arima-Takatsuki tectonic line, Japan: fault structure, damage distribution and textural characteristics. *Earth and Planetary Science Letters* 308 (3–4), 284–297.
- Mittemperger, S., Pennacchioni, G., Di Toro, G., 2009. Effects of fault orientation and fluid infiltration on fault rock assemblages at seismogenic depths. *Journal of Structural Geology* 31, 1511–1524.
- Mizoguchi, K., Hirose, T., Shimamoto, T., Fukuyama, E., 2006. Moisture-related weakening and strengthening of a fault activated at seismic slip rates. *Geophysical Research Letters* 33 (16), L16319.
- Mizoguchi, K., Hirose, T., Shimamoto, T., Fukuyama, E., 2007. Reconstruction of seismic faulting by high-velocity friction experiments: an example of the 1995 Kobe earthquake. *Geophysical Research Letters* 34 (L01308). doi:10.1029/2006GL027931.
- Mizoguchi, K., Takahashi, M., Tanikawa, W., Masuda, K., Song, S.-R., Soh, W., 2008. Frictional strength of fault gouge in Taiwan Chelungpu Fault obtained from TCDP Hole B. *Tectonophysics* 460 (1–4), 198–205.
- Mizoguchi, K., Hirose, T., Shimamoto, T., Fukuyama, E., 2009a. Fault heals rapidly after dynamic weakening. *Bulletin of the Seismological Society of America* 99 (6), 3470–3474.
- Mizoguchi, K., Hirose, T., Shimamoto, T., Fukuyama, E., 2009b. High-velocity frictional behavior and microstructure evolution of fault gouge obtained from Nojima Fault, southwest Japan. *Tectonophysics* 471 (3–4), 285–296.
- Monzawa, N., Otsuki, K., 2003. Commutation and fluidization of granular fault materials: implications for fault slip behavior. *Tectonophysics* 367, 127–143.
- Morrow, C.A., Byerlee, J.D., 1989. Experimental studies of compaction and dilatancy during frictional sliding on faults containing gouge. *Journal of Structural Geology* 11 (7), 815–825.
- Nielsen, S., Carlson, J.M., 2000. Rupture pulse characterization: self-healing, self-similar expanding solutions in a continuum model of fault dynamics. *Bulletin of the Seismological Society of America* 90, 1480–1497.
- Nielsen, S.B., Knopoff, L., 1998. The equivalent strength of geometrical barriers to earthquakes. *Journal of Geophysical Research* 103 (B5), 9953–9965.
- Nielsen, S., Di Toro, G., Hirose, T., Shimamoto, T., 2008. Frictional melt and seismic slip. *Journal of Geophysical Research* 113, B01308. doi:10.1029/2007JB005122.
- Nielsen, S., Di Toro, G., Griffith, W.A., 2010a. Friction and roughness of a melting rock interface. *Geophysical Journal International* 182 (1), 299–310.
- Nielsen, S., Mosca, P., Giberti, G., Di Toro, G., Hirose, T., Shimamoto, T., 2010b. On the transient behavior of frictional melt during seismic slip. *Journal of Geophysical Research* 115 (B10), B10301.

- Niemeijer, A.R., Spiers, C.J., 2006. Velocity dependence of strength and healing behaviour in simulated phyllosilicate-bearing fault gouge. *Tectonophysics* (Deformation Mechanisms, Microstructure and Rheology of Rocks in Nature and Experiment) 427 (1–4), 231–253.
- Niemeijer, A.R., Spiers, C.J., 2007. A microphysical model for strong velocity weakening in phyllosilicate-bearing fault gouges. *Journal of Geophysical Research* 112, B10405. doi:10.1029/2007JB005008.
- Niemeijer, A., Marone, C., Elsworth, D., 2008. Healing of simulated fault gouges aided by pressure solution: results from rock analogue experiments. *Journal of Geophysical Research* 113, B04204. doi:10.1029/2007JB005376.
- Niemeijer, A., Marone, C., Elsworth, D., 2010. Frictional strength and strain weakening in simulated fault gouge: competition between geometrical weakening and chemical strengthening. *Journal of Geophysical Research* 115 (B10), B10207.
- Niemeijer, A., Di Toro, G., Nielsen, S., Di Felice, F., 2011. Frictional melting of gabbro under extreme experimental conditions of normal stress, acceleration and sliding velocity. *Journal of Geophysical Research* 116, B07404. doi:10.1029/2010JB008181.
- Noda, H., Lapusta, N., 2010. Three-dimensional earthquake sequence simulations with evolving temperature and pore pressure due to shear heating: effect of heterogeneous hydraulic diffusivity. *Journal of Geophysical Research* 115, B12314. doi:10.1029/2010JB007780.
- O'Hara, K., 2004. Paleo-stress estimates on ancient seismogenic faults based on frictional heating of coal. *Geophysical Research Letters* 31, L03601. doi:10.1029/2003GL018890.
- Okubo, P., Dieterich, J., 1984. Effects of physical fault properties on frictional instabilities produced on simulated faults. *Journal of Geophysical Research* 89 (B7), 5817–5827.
- Olsen, K.B., Madariaga, R., Archuleta, R.J., 1997. Three-dimensional dynamic simulation of the 1992 Landers earthquake. *Science* 278 (5339), 834–838.
- Otsuki, K., Monzawa, N., Nagase, T., 2003. Fluidization and melting of fault gouge during seismic slip: identification in the Nojima Fault Zone and implications for focal earthquake mechanism. *Journal of Geophysical Research* 108 (B4). doi:10.1029/2001JB001711.
- Palmer, A.C., Rice, J.R., 1973. The growth of slip surfaces in the progressive failure of over-consolidated clay. *Proceedings of the Royal Society of London. Series A, Mathematical and Physical Sciences* 332 (1591), 527–548.
- Pennacchioni, G., Di Toro, G., Brack, P., Menegon, L., Villa, I.M., 2006. Brittle-ductile-brittle deformation during cooling of tonalite (Adamello, Southern Italian Alps). *Tectonophysics* 427 (1–4), 171–197.
- Pittarello, L., Di Toro, G., Bizzarri, A., Pennacchioni, G., Hadizadeh, J., Cocco, M., 2008. Energy partitioning during seismic slip in pseudotachylite-bearing faults (Gole Larghe Fault, Adamello, Italy). *Earth and Planetary Science Letters* 269, 131–139.
- Pittarello, L., Teza, G., Di Toro, G., Pennacchioni, G., 2009. 3-D FEM-based thermal modeling of frictional melt cooling and constraints on microstructures in pseudotachylite vein. In: Eos, Trans., AGU 90(52) Fall Meeting Suppl. Abstract T23C-1934, American Geophysical Union Annual Meeting, San Francisco.
- Poliakov, A.N.B., Dmowska, R., Rice, J.R., 2002. Dynamic shear rupture interactions with fault bends and off-axis secondary faulting. *Journal of Geophysical Research* 107 (B11), 2295.
- Power, W.L., Tullis, T.E., Brown, S.R., Boitnott, G.N., Scholz, C.H., 1987. Roughness of natural fault surfaces. *Geophysical Research Letters* 14 (1), 29–32.
- Rapoport, L., Leshchinsky, V., Lvovsky, M., Lapsker, I., Volovik, Y., Feldman, Y., Popovitz-Biro, R., Tenne, R., 2003. Superior tribological properties of powder materials with solid lubricant nanoparticles. *Wear* 255 (7–12), 794–800.
- Reches, Z.E., Dewers, T.A., 2005. Gouge formation by dynamic pulverization during earthquake rupture. *Earth and Planetary Science Letters* 235 (1–2), 361–374.
- Reches, Z.E., Lockner, D.A., 2010. Fault weakening and earthquake instability by powder lubrication. *Nature* 467 (7314), 452–455.
- Reches, Z.E., 2006. Building a natural earthquake laboratory at focal depth. *Scientific Drilling* 3, 30–33.
- Reimold, W.U., 1998. Exogenic and endogenic breccias: a discussion of major problematics. *Earth Sciences Reviews* 43, 25–47.
- Rempel, A.W., Rice, J.R., 2006. Thermal pressurization and onset of melting in fault zones. *Journal of Geophysical Research* 111 (B09314). doi:10.1029/2006JB004314.
- Rempel, A.W., Weaver, S.L., 2008. A model for flash weakening by asperity melting during high-speed earthquake slip. *Journal of Geophysical Research* 113 (B11), B11308.
- Rempel, A.W., 2006. The effects of flash weakening and damage on the evolution of fault strength and temperature. In: Abercrombie, R., McGarr, A., Di Toro, G., Kanamori, H. (Eds.), *Earthquakes: Radiated Energy and the Physics of Faulting*, vol. 170. American Geophysical Union, Washington D.C. pp. 263–270.
- Rice, J.R., Tse, S.T., 1986. Dynamic motion of a single degree of freedom system following a rate and state dependent friction law. *Journal of Geophysical Research* 91 (B1), 521–530.
- Rice, J.R., Sammis, C.G., Parsons, R., 2005. Off-fault secondary failure induced by a dynamic slip-pulse. *Bulletin of the Seismological Society of America* 95 (1), 109–134.
- Rice, J.R., 1980. The mechanics of earthquake rupture. In: Dziewonski, A.M., Boschi, E. (Eds.), *Physics of the Earth's Interior*. Italian Physical Society, North-Holland, New York, pp. 555–649.
- Rice, J.R., 1999. Flash heating at asperity contacts and rate-dependent friction. *EOS, Transactions, American Geophysical Union* 80 (46), F681. Fall Meet. Suppl.
- Rice, J.R., 2006. Heating and weakening of faults during earthquake slip. *Journal of Geophysical Research* 111 (B05311). doi:10.1029/2005JB004006.
- Rockwell, T., Sisk, M., Girty, G., Dor, O., Wechsler, N., Ben-Zion, Y., 2009. Chemical and physical characteristics of pulverized Tejon lookout granite adjacent to the San Andreas and Garlock Faults: implications for earthquake physics. *Pure and Applied Geophysics* 166, 1725–1746.
- Roig Silva, C., Goldsby, D.L., Di Toro, G., Tullis, T.E., 2004. The role of silica content in dynamic fault weakening due to gel lubrication. In: Southern California Earthquake Center Annual Meeting, Proceedings and Abstracts, vol. XIV, p. 150.
- Rosakis, A.J., Samudrala, S., Coker, D., 2000. Intersonic shear crack growth along weak planes. *Materials Research Innovation* 3, 236–243. doi:10.1007/s100190050009.
- Rowshandel, B., 2006. Incorporating source rupture characteristics into ground-motion hazard analysis models. *Seismological Research Letters* 77, 708–722.
- Rubin, A.M., 2008. Episodic slow slip events and rate-and-state friction. *Journal of Geophysical Research* 113 (B11), B11414.
- Rudnicki, J.W., 1980. Fracture mechanics applied to the earth's crust. *Annual Review of Earth and Planetary Sciences* 8 (1), 489–525.
- Ruina, A., 1983. Slip instability and state variable friction laws. *Journal of Geophysical Research* 88 (B12), 10,359–10,370.
- Sagy, A., Brodsky, E.E., Axen, G.J., 2007. Evolution of fault-surface roughness with slip. *Geology* 35 (3), 283–286.
- Sakaguchi, A., Chester, F., Curewitz, D., Fabbri, O., Goldsby, D., Kimura, G., Li, C.-F., Masaki, Y., Screamton, E.J., Tsutsumi, A., Ujiie, K., Yamaguchi, A., 2011. Seismic slip propagation to the up-dip end of plate boundary subduction interface faults: vitrinite reflectance geothermometry on IODP NanTroSEIZE cores. *Geology* 39, 395–398.
- Sammis, C.G., Steacy, S.J., 1994. The micromechanics of friction in a granular layer. *Pure and Applied Geophysics* 142 (3/4), 778–794.
- Samtani, M., Dollimore, D., Alexander, K.S., 2002. Comparison of dolomite decomposition kinetics with related carbonates and the effect of procedural variables on its kinetic parameters. *Thermochimica Acta* 392–393, 135–145.
- Samudrala, O., Huang, Y., Rosakis, A.J., 2002. Subsonic and intersonic shear rupture of weak planes with a velocity weakening cohesive zone. *Journal of Geophysical Research* 107 (B8), 2170.
- Saucier, F., Humphreys, E., Weldon II, R., 1992. Stress near geometrically complex strike-slip faults: application to the San Andreas Fault at Cajon Pass, Southern California. *Journal of Geophysical Research* 97 (B4), 5081–5094.
- Schmittbuhl, J., Chambon, G., Hansen, A., Bouchon, M., 2006. Are stress distributions along faults the signature of asperity squeeze? *Geophysical Research Letters* 33. doi:10.1029/2006GL025952.
- Scholz, C.H., 2002. *The Mechanics of Earthquakes and Faulting*. Cambridge University Press, Cambridge.
- Segall, P., Pollard, D.D., 1980. Mechanics of discontinuous faults. *Journal of Geophysical Research* 85, 4337–4350.
- Segall, P., Rice, J.R., 1995. Dilatancy, compaction and slip instability of a fluid-infiltrated fault. *Journal of Geophysical Research* 100 (B11), 22155–22171.
- Shand, S.J., 1914. On tachylite veins and assimilation phenomena in the granite of Parijs (Orange Free State). *Geological Society of London Proceedings* 964, 10–11.
- Shand, S.J., 1916. The pseudotachylite of Parijs (Orange free State), and its relation to 'Trap-Shotten Gneiss' and 'Flinty Crush-rock'. *Quarterly Journal of the Geological Society* 72 (1–4), 198–221.
- Shaw, D.J., 1980. *Introduction to Colloid and Surface Chemistry*. Butterworths, London.
- Shimamoto, T., Tsutsumi, A., 1994. A new rotary-shear high-speed friction testing machine its basic design and scope of research. *Journal of the Tectonic Research Group of Japan* 39, 65–78 (in Japanese with English abstract).
- Sibson, R.H., Toy, V.G., 2006. The habitat of fault-generated pseudotachylite: presence vs. absence of friction-melt. In: Abercrombie, R., McGarr, A., Di Toro, G., Kanamori, H. (Eds.), *Earthquakes: Radiated Energy and the Physics of Faulting*. Geophysical Monograph Series, vol. 170. American Geophysical Union, Washington, D.C. pp. 153–166.
- Sibson, R.H., 1973. Interactions between temperature and pore-fluid pressure during earthquake faulting and a mechanism for partial or total stress relief. *Nature-Physical Science*, *Nature* 243, 66–68.
- Sibson, R.H., 1975. Generation of pseudotachylite by ancient seismic faulting. *Geophysical Journal of the Royal Astronomical Society* 43 (3), 775–794.
- Sibson, R.H., 1977. Fault rocks and fault mechanisms. *Journal of the Geological Society of London* 133, 191–213.
- Sibson, R., 1980. Power dissipation and stress levels on faults in the upper crust. *Journal of Geophysical Research* 85 (B11), 6239–6247.
- Sibson, R.H., 2003. Thickness of the seismic slip zone. *Bulletin of the Seismological Society of America* 93 (3), 1169–1178.
- Smith, S.A.F., Holdsworth, R.E., Colletti, C., 2008. Recognizing the seismic cycle along ancient faults: CO₂-induced fluidization of breccias in the footwall of a sealing low-angle normal fault. *Journal of Structural Geology* 30, 1034–1046.
- Smith, S.A.F., Billi, A., Di Toro, G., Spiess, R., 2011. Principal slip zones in limestone: microstructural characterization and implications for the seismic cycle (Tre Monti Fault, central Apennines, Italy). *Pure and Applied Geophysics* 168 (12), 2365–2393.
- Snoke, A.W., Tullis, J., Todd, V.R., 1998. *Fault-Related Rocks: a Photographic Atlas*. Princeton Univ. Press, Princeton, N.J.
- Somerville, P.G., Smith, N., Graves, R., Abrahamson, N.A., 1997. Modification of empirical strong ground motion attenuation relations to include the amplitude and duration effects of rupture directivity. *Seismological Research Letters* 68, 199–212.
- Sone, H., Shimamoto, T., 2009. Frictional resistance of faults during accelerating and decelerating earthquake slip. *Nature Geoscience*. doi:10.1038/Ngeo637.

- Spray, J.G., 1987. Artificial generation of pseudotachylite using friction welding apparatus: simulation of melting on a fault plane. *Journal of Structural Geology* 9 (1), 49–60.
- Spray, J.G., 1992. A physical basis for the frictional melting of some rock forming minerals. *Tectonophysics* 204, 205–221.
- Spray, J.G., 1995. Pseudotachylite controversy: fact or friction? *Geology* 23 (12), 1119–1122.
- Spray, J.G., 1997. Superfaults. *Geology* 25 (7), 579–582.
- Spray, J.G., 2010. Frictional melting processes in planetary materials: from hyper-velocity impact to earthquakes. *Annual Review of Earth and Planetary Sciences* 38 (1), 221–254.
- Spudich, P., Chiou, B.S.J., 2008. Directivity in NGA earthquake ground motions: analysis using isochrone theory. *Earthquake Spectra* 24, 279–298.
- Stein, R.S., 1999. The role of stress transfer in earthquake occurrence. *Nature* 402, 605–609.
- Sulem, J., Famin, V., 2009. Thermal decomposition of carbonates in fault zones: slip weakening and temperature limiting effects. *Journal of Geophysical Research* 114, B03309.
- Swanson, M.T., 1988. Pseudotachylite-bearing strike-slip duplex structures in the Fort Foster Brittle Zone, S. Maine. *Journal of Structural Geology* 10, 813–828.
- Swanson, M.T., 1992. Fault structure, wear mechanisms and rupture processes in pseudotachylite generation. *Tectonophysics* 204, 223–242.
- Swanson, M.T., 2006. Pseudotachylite-bearing strike-slip faults in mylonitic host rocks, Fort Foster Brittle Zone, Kittery, Maine. In: Abercrombie, R., McGarr, A., Di Toro, G., Kanamori, H. (Eds.), *Geophysical Monograph Series*, vol. 170. American Geophysical Union, Washington, D.C., pp. 167–179.
- Tanikawa, W., Mukoyoshi, H., Tadai, O., in press. Experimental investigation of the influence of slip velocity and temperature on permeability during and after high-velocity fault slip. *Journal of Structural Geology*. doi:10.1016/j.jsg.2011.08.013.
- Tenthorey, E., Cox, S.F., 2006. Cohesive strengthening of fault zones during the interseismic period: an experimental study. *Journal of Geophysical Research* 111 (B09202). doi:10.1029/2005JB004122.
- Tinti, E., Spudich, P., Cocco, M., 2005. Earthquake fracture energy inferred from kinematic rupture models on extended faults. *Journal of Geophysical Research* 110 (B12), B12303.
- Tinti, E., Cocco, M., Fukuyama, E., Piatanesi, A., 2009. Dependence of slip weakening distance (Dc) on final slip during dynamic rupture of earthquakes. *Geophysical Journal International* 177, 1205–1220.
- Tisato, N., Di Toro, G., De Rossi, N., Quaresimin, M., Candela, T., in press. Experimental investigation of flash weakening in limestones. *Journal of Structural Geology*. doi:10.1016/j.jsg.2011.11.017.
- Toda, S., Stein, R.S., Richards-Dinger, K., Bozkurt, S., 2005. Forecasting the evolution of seismicity in southern California: animations built on earthquake stress transfer. *Journal of Geophysical Research*, B05S16. doi:10.1029/2004JB003415.
- Togo, T., Shimamoto, T., in press. Energy partition for grain crushing in quartz gouge during subseismic to seismic fault motion: an experimental study. *Journal of Structural Geology*. doi:10.1016/j.jsg.2011.12.014.
- Tsutsumi, A., Shimamoto, T., 1997. High-velocity frictional properties of gabbro. *Geophysical Research Letters* 24 (6). doi:10.1029/97GL00503.
- Tullis, T.E., Goldsby, D.L., 2003. Flash melting of crustal rocks at almost seismic slip rates. *EOS, Transactions, American Geophysical Union* 84 (46). Fall Meet. Suppl., Abstract S51B-05.
- Tullis, T.E., 2008. Friction of rock at earthquake slip rates. In: Kanamori, H. (Ed.), *Of the Treatise of Geophysics, Earthquake Seismology*, vol. 4. Elsevier, Amsterdam.
- Turcotte, D.L., 1997. *Fractals and Chaos in Geology and Geophysics*, second ed. Cambridge University Press, New York, USA.
- Ujiie, K., Tsutsumi, A., 2010. High-velocity frictional properties of clay-rich fault gouge in a megasplay fault zone, Nankai subduction zone. *Geophysical Research Letters* 37 (24), L24310.
- Ujiie, K., Yamaguchi, A., Kimura, G., Toh, S., 2007. Fluidization of granular material in a subduction thrust at seismogenic depths. *Earth and Planetary Science Letters* 259, 307–318. doi:10.1016/j.epsl.2007.04.049.
- Ujiie, K., Yamaguchi, A., Taguchi, S., 2008. Stretching of fluid inclusions in calcite as an indicator of frictional heating on faults. *Geology* 36, 111–114.
- Venkataraman, A., Beroza, C.G., Boatwright, J., 2006. A brief review of techniques used to estimate radiated energy. In: Abercrombie, R., McGarr, A., Di Toro, G., Kanamori, H. (Eds.), *Earthquakes: Radiated Energy and the Physics of Faulting*. *Geophysical Monograph Series*, vol. 170. American Geophysical Union, Washington, D.C., pp. 15–24.
- Warr, L.N., Cox, S.J., 2001. Clay mineral transformations and weakening mechanisms along the Alpine Fault, New Zealand. In: Holdsworth, R.E. (Ed.), *The Nature and Significance of Fault Zone Weakening*. Geological Society of London, Special Publications, London, pp. 85–101.
- Wenk, H.R., Johnson, L.R., Ratschbacher, L., 2000. Pseudotachylites in the eastern peninsular ranges of California. *Tectonophysics* 321, 253–277.
- Wenk, H.R., 1978. Are pseudotachylites products of fracture or fusion? *Geology* 16, 507–511.
- Wibberley, C.A.J., Shimamoto, T., 2003. Internal structure and permeability of major strike-slip fault zones: the Median Tectonic Line in Mie Prefecture, Southwest Japan. *Journal of Structural Geology* 25, 59–78.
- Wibberley, C.A.J., Graham, Y., Di Toro, G., 2008. Recent advances in the understanding of fault zone internal structure: a review. In: Wibberley, C.A.J., Kurz, W., Imber, J., Holdsworth, R.E., Collettini, C. (Eds.), *The Internal Structure of Fault Zones – Implications for Mechanical and Fluid Flow Properties*. Special Volume of the Geological Society of London, vol. 299, pp. 5–33.
- Willemse, E.J.M., Pollard, D.D., 1998. On the orientation and patterns of wing cracks and solution surfaces on the tips of a sliding flaw or fault. *Journal of Geophysical Research* 103 (B2), 2427–2438.
- Wilson, B., Dewers, T., Reches, Z., Brune, J., 2005. Particle size and energetics of gouge from earthquake rupture zones. *Nature* 434, 749–752.
- Wornyo, E.Y.A., Jasti, V.K., Higgs, C.F., Iii, 2007. A review of dry Particulate lubrication: powder and granular materials. *Journal of Tribology* 129 (2), 438–449.
- Yoshida, S., Kato, N., 2003. Episodic aseismic slip in a two-degree-of-freedom block-spring model. *Geophysical Research Letters* 30 (13), 1681.
- Yuan, F., Prakash, V., 2008. Slip weakening in rocks and analog materials at coseismic slip rates. *Journal of the Mechanics and Physics of Solids* 56, 542–560.
- Yuan, F., Prakash, V., Tullis, T., 2011. Origin of pulverized rocks during earthquake fault rupture. *Journal of Geophysical Research* 116, B06309. doi:10.1029/2010JB007721.
- Zhang, S., Tullis, T.E., Scruggs, V.J., 1999. Permeability anisotropy and pressure dependency of permeability in experimentally sheared gouge materials. *Journal of Structural Geology* 21 (7), 795–806.
- Zheng, G., Rice, J., 1998. Conditions under which velocity weakening friction allows a self-healing versus a cracklike mode of rupture. *Bulletin of the Seismological Society of America* 88, 1466–1483.
- Ziv, A., Rubin, A.M., 2003. Implications of rate-and-state friction for properties of aftershock sequence: quasi-static inherently discrete simulations. *Journal of Geophysical Research* 108 (B1). doi:10.1029/2001JB001219.